

FOSR-TR- 85-1232

②

*DTIC
all one
report
with appendix*

FUNDAMENTAL PROPERTIES OF SOILS
FOR COMPLEX DYNAMIC LOADINGS

FINAL REPORT

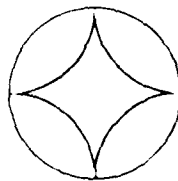
"Development of a Three Invariant
Constitutive Model"

AD-A164 206

DTIC
SELECTED
FEB 11 1986
S D

Approved for public release;
distribution unlimited.

DTIC FILE COPY



APPLIED
RESEARCH
ASSOCIATES, INC.

Engineering and Applied Science

88 2 11 033

②

FUNDAMENTAL PROPERTIES OF SOILS
FOR COMPLEX DYNAMIC LOADINGS

FINAL REPORT

"Development of a Three Invariant
Constitutive Model"

by

Douglas H. Merkle
William C. Dass

22 April 1985

Applied Research Associates, Inc.
4300 San Mateo NE, Suite A220
Albuquerque, NM 87110

DTIC
ELECTE
FEB 11 1986
S D D

Prepared for

Air Force Office of Scientific Research
Bolling Air Force Base
Washington, DC 20332

DISTRIBUTION STATEMENT A

**Approved for public release;
Distribution Unlimited**

Contract No. F49620-80-C-0088

**AIR FORCE OFFICE OF SCIENTIFIC RESEARCH (AFOSR)
NOTICE OF SPANISH TRANSLATION**

This report
approved for
Distribution
with the
Chief, Technical Information Division

AD-A164206

REPORT DOCUMENTATION PAGE				Form Approved OMB No. 0704-0188 Exp. Date Jun 30, 1986	
1a REPORT SECURITY CLASSIFICATION UNCLASSIFIED		1b RESTRICTIVE MARKINGS			
2a SECURITY CLASSIFICATION AUTHORITY		3 DISTRIBUTION / AVAILABILITY OF REPORT			
2b DECLASSIFICATION / DOWNGRADING SCHEDULE		Approved for public release; distribution unlimited			
4 PERFORMING ORGANIZATION REPORT NUMBER(S) 5230		5 MONITORING ORGANIZATION REPORT NUMBER(S) AFOSR-TR- 85 - 1 2 3 2			
6a NAME OF PERFORMING ORGANIZATION Applied Research Associates, Inc.		6b OFFICE SYMBOL (if applicable)	7a NAME OF MONITORING ORGANIZATION Air Force Office of Scientific Research/NA		
6c ADDRESS (City, State, and ZIP Code) 4300 San Mateo Blvd. NE Suite A220 Albuquerque, NM 87110		7b ADDRESS (City, State, and ZIP Code) Bolling AFB, DC 20332			
8a NAME OF FUNDING / SPONSORING ORGANIZATION AFOSR		8b OFFICE SYMBOL (if applicable) NA	9. PROCUREMENT INSTRUMENT IDENTIFICATION NUMBER Contract F49620-80-C-0088		
8c ADDRESS (City, State, and ZIP Code) Bolling AFB, DC 20332		10 SOURCE OF FUNDING NUMBERS			
		PROGRAM ELEMENT NO 61102F	PROJECT NO 2307	TASK NO C1	WORK UNIT ACCESSION NO
11 TITLE (Include Security Classification) FUNDAMENTAL PROPERTIES OF SOILS FOR COMPLEX DYNAMIC LOADINGS: Development of a Three Invariant Constitutive Model (U)					
12 PERSONAL AUTHOR(S) Merkle, Douglas Hall; and Dass, William Christopher					
13a TYPE OF REPORT Final		13b TIME COVERED FROM 800801 TO 840731		14 DATE OF REPORT (Year, Month, Day) 850422	15 PAGE COUNT 609
16 SUPPLEMENTARY NOTATION					
17 COSATI CODES			18 SUBJECT TERMS (Continue on reverse if necessary and identify by block number)		
FIELD	GROUP	SUB-GROUP	effective stress, soil dynamics, stress-strain behavior, shear strength, material modeling		
19 ABSTRACT (Continue on reverse if necessary and identify by block number)					
<p>The objective of the study reported herein was to develop a general soil stress-strain model which can be used to solve a wide range of soil dynamics problems of interest to the Air Force. The approach used was to review existing soil constitutive models used to predict the response of soil masses to complex dynamic loads, and then formulate a new model for that purpose. Eight existing soil dynamic stress-strain models were studied, including exercising them along common stress and strain paths for comparison. The models were: linear elastic, linear viscoelastic, hyperbolic, Pyke cyclic simple shear, elastic-perfectly plastic, modified AFWL engineering, effective stress cap, and Lade. Each model is discussed and reviewed. The discussion of each model includes: motivation, assumptions, basic equations, parameter determination, and computed behavior. Based on the above review, the Lade model was selected as the best point of departure for developing a new soil stress-strain model for complex dynamic loading, because of its accuracy and flexibility in representing soil stress-strain behavior, ease of parameter determination, and ease of developing intuition for parameter</p>					
20 DISTRIBUTION / AVAILABILITY OF ABSTRACT <input type="checkbox"/> UNCLASSIFIED/UNLIMITED <input checked="" type="checkbox"/> SAME AS RPT <input type="checkbox"/> DTIC .SERS			21 ABSTRACT SECURITY CLASSIFICATION UNCLASSIFIED		
22a NAME OF RESPONSIBLE INDIVIDUAL Lt. Col. Lawrence D. Hokanson		22b TELEPHONE (Include Area Code) (202) 767-4935		22c OFFICE SYMBOL AFOSR/NA	

SECURITY CLASSIFICATION OF THIS PAGE

ABSTRACT (continued)

physical significance and accuracy. The same five attributes discussed for each existing model were examined for the new ARA-conic model, so called because its principal mathematical surfaces are conic sections. The computer code used to exercise all nine soil constitutive models under eleven stress and strain paths is called the Soil Element Model (SEM). It can be incorporated in large finite difference or finite element codes for analyzing the response of soil masses to complex dynamic loads.

The ARA-conic model performs well over a wide range of loading conditions, many departing considerably from those used to determine the model parameters. The parameters are determined in a straightforward manner, and the model reflects the influence of the intermediate principal stress on shear strength through a shear failure surface involving three independent stress invariants: the first total stress invariant and the second and third deviator stress invariants. For this reason the model is also called a three invariant model. Measured shear strengths in both compression and extension can be matched exactly, and the mathematical formulation of the shear failure surface is such that the shear strength for any value of the intermediate principal stress can be computed directly without trial and error. The ARA-conic model also exhibits dilatancy, generates only positive plastic work, and has a provision for strain softening in shear.

TABLE OF CONTENTS

<u>Section</u>	<u>Title</u>	<u>Page</u>
1.0	INTRODUCTION	1
2.0	SOIL CONSTITUTIVE MODEL REQUIREMENTS	5
	2.1 The Nature of Soil	5
	2.2 Soil Stress-Strain Characteristics	6
	2.3 The Soil Element Model	18
	2.4 Computational Exercises for Model Comparisons	21
	2.4.1 Test Descriptions	21
	2.4.2 Test Data	26
3.0	EXISTING MODELS	32
	3.1 Introduction	32
	3.2 Evaluation Summary	33
	3.3 Individual Evaluation	33
	3.4 Comparative Evaluation	56
4.0	ARA CONIC MODEL	71
	4.1 Introduction	71
	4.2 Individual Evaluation	73
	4.3 Comparative Evaluation	76
5.0	SUMMARY	88
	REFERENCES	92
	APPENDICES	
	A. ANALYSIS OF STRESS	97
	B. CAYLEY-HAMILTON INVARIANT FORMULATIONS	119
	C. OCTAHEDRAL PLANE PLOTS	125
	D. BASIC EQUATIONS OF ELASTOPLASTICITY	137

Accession For	
NTIS CRA&I	<input checked="" type="checkbox"/>
DTIC TAB	<input type="checkbox"/>
Unannounced	<input type="checkbox"/>
Justification	
By	
Distribution/	
Availability Codes	
Dist	Avail and/or Special
A-1	

TABLE OF CONTENTS (concluded)

<u>Section</u>	<u>Title</u>	<u>Page</u>
E.	VECTOR REPRESENTATION OF A GENERAL STRESS OR STRAIN STATE	149
F.	INCREMENTAL FLEXIBILITY MATRIX FOR STRESS CONTROL	156
G.	INCREMENTAL STIFFNESS MATRIX FOR STRAIN CONTROL	162
H.	INCREMENTAL DEFORMATION MODE LOGIC FOR STRESS CONTROL	168
I.	INCREMENTAL DEFORMATION MODE LOGIC FOR STRAIN CONTROL	178
J.	ELASTIC STRESS-STRAIN EQUATIONS	192
K.	SPECIAL EQUATIONS FOR THE TRIAXIAL TEST	199
L.	TRANSIENT RESPONSE OF A THREE ELEMENT VISCOELASTIC MODEL	209
M.	YOUNG'S MODULUS FOR A HYPERBOLIC STRESS-STRAIN CURVE	216
N.	A HYPERBOLIC EXPRESSION FOR POISSON'S RATIO	225
O.	HYPERBOLIC MODEL FOR CYCLIC SIMPLE SHEAR	230
P.	YIELD SURFACE VIOLATION CORRECTION FOR AN ELASTIC-PERFECTLY PLASTIC MODEL	234
Q.	AFWL ENGINEERING MODEL INCREMENTAL PLASTIC RESPONSE	241
R.	DRAINED CAP MODEL AND COMPUTATIONAL ALGORITHM	246
S.	UNDRAINED CAP MODEL AND COMPUTATIONAL ALGORITHM	271
T.	LADE MODEL CROSS SECTIONS AND PARAMETER DETERMINATION	274
U.	ARA CONIC MODEL CROSS SECTIONS AND PARAMETER DETERMINATION	286
V.	EVALUATION OF EXISTING MODELS	301
W.	DEVELOPMENT OF THE ARA CONIC MODEL	549

LIST OF FIGURES

<u>Number</u>	<u>Title</u>	<u>Page</u>
2.1	Influence of Effective Stress Path on Stress-Strain Curve Nonlinearity	7
2.2	Compressive Stress-Strain Curve Exhibiting Yielding Due to Grain Crushing at Interparticle Contacts	9
2.3	Drained Stress-Strain Curves for Loose and Dense Samples of the Same Sand, Under the Same Constant Confining Pressure	11
2.4	Drained Stress-Strain Curves for a Sand at the Same Initial Void Ratio, Under High and Low Constant Confining Pressures	12
2.5	Drained Stress-Strain Curves for Normally Consolidated and Overconsolidated Samples of the Same Clay, Under the Same Constant Confining Pressure	13
2.6	Drained Stress-Strain Curves for a Clay at the Same Initial Void Ratio, Under High and Low Constant Confining Pressures	14
2.7	Effect of $\bar{\sigma}_2$ on the Strength of Standard Ottawa Sand	15
2.8	Effect of $\bar{\sigma}_2$ on the Strength of Ham River Sand	16
2.9	Soil Element Model Basic Logic and Options	20
2.10	Soil Element Model Exercises	22
2.11	WES Axisymmetric Strain Paths	25
2.12	Lade Axisymmetric Strain Paths	27
2.13	Three-Dimensional Strain Path	28
2.14	Gradation and Index Test Results for Remolded CARES-Dry Sand and Remolded Nellis Baseline Sand	29
3.1	Elastic Model Exercise-Isotropic Comp.-Pressure vs. Volumetric Strain	35
3.2	Elastic Model Exercise-Triaxial Comp. (CTC)-Stress Difference vs. Strain Difference	37
3.3	Visco Model Exercise-Uniaxial Strain-Pressure vs. Volumetric Strain	38

LIST OF FIGURES (continued)

<u>Number</u>	<u>Title</u>	<u>Page</u>
3.4	Visco Model Exercise-Uniaxial Strain-Stress Difference vs. Strain Difference	39
3.5	Hyperbolic Model Exercise-Triaxial Comp. (CTC)-Stress Difference vs. Axial Strain	41
3.6	Hyperbolic Model Exercise-Triaxial Comp. (CTC)-Pressure vs. Volumetric Strain	42
3.7	Pyke Model Exercise-Cyclic Shear-Shear Stress vs. Shear Strain	44
3.8	Elpla Model Exercise-Triaxial Comp. (CTC)-Stress Difference vs. Axial Strain	45
3.9	Elpla Model Exercise-Triaxial Comp. (CTC)-Pressure vs. Volumetric Strain	46
3.10	AFWL Model Exercise-Triaxial Comp. (CTC)-Stress Difference vs. Axial Strain	48
3.11	AFWL Model Exercise-Triaxial Comp. (CTC)-Pressure vs. Volumetric Strain	49
3.12	Cap Model Exercise-Triaxial Comp. (CTC)-Stress Difference vs. Axial Strain	51
3.13	Cap Model Exercise-Triaxial Comp. (CTC)-Pressure vs. Volumetric Strain	52
3.14	Lade Model Exercise-Triaxial Comp. (CTC)-Stress Difference vs. Axial Strain	54
3.15	Lade Model Exercise-Triaxial Comp. (CTC)-Pressure vs. Volumetric Strain	55
3.16	Elastic Model Exercise-Uniaxial Strain (UXC)-Total Axial Stress vs. Axial Strain	57
3.17	Visco Model Exercise-Uniaxial Strain (UXC)-Total Axial Stress vs. Axial Strain	58
3.18	Hyperbolic Model-Uniaxial Strain (UXC)-Total Axial Stress vs. Axial Strain	59
3.19	Elpla Model Exercise-Uniaxial Strain (UXC)-Total Axial Stress vs. Axial Strain	60

LIST OF FIGURES (continued)

<u>Number</u>	<u>Title</u>	<u>Page</u>
3.20	AFWL Model Exercise-Uniaxial Strain (UXC)-Total Axial Stress vs. Axial Strain	61
3.21	Cap Model Exercise-Uniaxial Strain (UXC)-Total Axial Stress vs. Axial Strain	62
3.22	Lade Model Exercise-Uniaxial Strain (UXC)-Total Axial Stress vs. Axial Strain	63
3.23	Elastic Model Behavior Summary (S3C=7.1 MPa)-SDIFF/P/EV/EA Analysis	64
3.24	Hyperbolic Model Behavior Summary (S3C=7.1 MPa)-SDIFF/P/EV/EA Analysis	65
3.25	Elastic-Plastic Model Behavior Summary (S3C=7.1 MPa)-SDIFF/P/EV/EA Analysis	66
3.26	AFWL Eng. Model Behavior Summary (S3C=7.1 MPa)-SDIFF/P/EV/EA Analysis	67
3.27	Cap Model Behavior Summary (S3C=7.1 MPa)-SDIFF/P/EV/EA Analysis	68
3.28	Lade Model Behavior Summary (S3C=7.1 MPa)-SDIFF/P/EV/EA Analysis	69
4.1	ARA Model Exercise-Triaxial Comp. (CTC)-Stress Difference vs. Axial Strain	74
4.2	ARA Model Exercise-Triaxial Comp. (CTC)-Pressure vs. Volumetric Strain	75
4.3	ARA Model Exercise-Uniaxial Strain (UXC)-Total Axial Stress vs. Axial Strain	77
4.4	Model Comparison-Const. S3C=7MPa Triax.-SDIFF/P/EV/EA Analysis	78
4.5	Model Comparison-RTC/E S3C=7MPa Triax.-SDIFF/P/EV/EA Analysis	79
4.6	Model Comparison-Pure Shear (S3C=7.1E6)	81
4.7	Model Comparison-Uniaxial Strain Compression-SDIFF/P/EV/E11/S11 Analysis	82

LIST OF FIGURES (concluded)

<u>Number</u>	<u>Title</u>	<u>Page</u>
4.8	Model Comparison-Uniaxial Strain Extension-SDIFF/P/EV/E11/S11 Analysis	83
4.9	Model Comparison-WES Axisym Epath3C-SDIFF/P/EV/EDIFF Analysis	84
4.10	Model Comparison-True Triaxial Strain Path-Principal Stress Path	86
4.11	Model Comparison-True Triaxial Strain Path-Pressure vs. Volumetric Strain	87

LIST OF TABLES

<u>Number</u>	<u>Title</u>	<u>Page</u>
2.1	REPRESENTATIVE DATA FOR REMOLDED CARES-DRY SAND	30
3.1	PERFORMANCE OF EIGHT EXISTING SOIL STRESS-STRAIN MODELS WITH RESPECT TO TEN EVALUATION CRITERIA	34

1.0 INTRODUCTION

This report documents the results of research accomplished under Air Force Office of Scientific Research contract F49620-80-C-0088, "Fundamental Properties of Soils for Complex Dynamic Loadings," during the period 1 August 1980 through 31 July 1984. Three annual technical reports have been issued under this contract: [Dass, Bratton and Higgins (1981); Dass, Merkle and Bratton (1983); Merkle and Dass (1983)]. The objective of the study reported herein was to develop a general soil stress-strain model which can be used to solve a wide range of soil dynamics problems of interest to the Air Force. These problems include prediction of ground shock loads on and shock isolation system attachment point motions within current and future generation ICBM missile silos and launch control centers, under threat nuclear attack conditions. Another problem of interest is the design of structures hardened against conventional weapons, earthquake resistant structures, pavement subbases for concentrated dynamic loads, and vibrating machine foundations. The approach used was to review existing soil constitutive models used to predict the response of soil masses to complex dynamic loads, and then formulate a new model for that purpose.

In military hardened structure design, free field ground shock predictions are rarely an end in themselves. Generally, free field motions and/or stresses serve as inputs for structure medium interaction (SMI) analyses, frequently using a soil island approach. These yield ground shock loads on and interior motions of a surface

flush or buried hardened structure. Thus, although free field ground shock strain paths characteristic of a surface nuclear or conventional explosion are important for the design of a hardened structure, they are by no means the only strain paths a soil dynamic constitutive model must accommodate in a hardened structure analysis. Strain paths in the vicinity of a hardened structure, which are most affected by structure medium interaction, are no less important and much more diverse and complex than their free field counterparts.

Hardened structure ground shock response predictions are generally accomplished using finite difference or finite element numerical methods on large digital computers. Field tests are used to identify material and structural behavior modes which need to be modeled, and to assess the accuracy and reliability of calculated predictions. The calculation sequence is roughly as follows:

- a) Using previously calculated or prescribed stresses and body forces, calculate new accelerations from equations of motion.
- b) Calculate new velocities and displacements by integration, using the new accelerations.
- c) Calculate new strains from the new displacements, using strain-displacement equations.
- d) Calculate new stresses from the new strains, using soil dynamic constitutive equations.
- e) Repeat steps (a) through (d).

Details of the above calculation process are not of concern here, in particular whether the new displacements are obtained

explicitly or implicitly. What is important is that the new stresses are obtained from the new strains by using the soil stress-strain equations in a strain-controlled mode. The reason this is important is that the equations of plasticity theory, which are the basis for many soil stress-strain models, were originally formulated for use under stress-controlled conditions. Their use under strain-controlled conditions requires some reformulation, and careful consideration of their fundamental physical significance.

The requirements to be satisfied by a useful soil stress-strain model can be grouped under five headings:

- a) Theory--e.g. the model should not generate energy under cyclic loading, and inelastic deformation must dissipate energy, not create it;
- b) Phenomenology--e.g. the model should exhibit some hysteresis, as well as coupling between shear strain and volume strain;
- c) Computational efficiency--e.g. the strain increment required for numerical stability should be large enough to permit reasonable run times, and the model algorithms should be computationally efficient;
- d) Convenience--e.g. the model parameters should be easy to determine for someone other than the model originator;
- e) Accuracy--e.g. the model should correctly describe elemental response along stress or strain paths other than those used to determine the model parameters, and predictions of soil mass response to complex dynamic loads should be accurate and reliable.

With the above requirements in mind, eight existing soil dynamic stress-strain models were studied, including exercising them along common stress and strain paths for comparison. The models were:

- a) Linear elastic
- b) Linear viscoelastic
- c) Hyperbolic
- d) Pyke cyclic simple shear
- e) Elastic-perfectly plastic
- f) Modified AFWL engineering
- g) Effective stress cap
- h) Lade

The discussion of each model includes: motivation, assumptions, basic equations, parameter determination, and computed behavior. Based on the above review, the Lade model was selected as the best point of departure for developing a new soil stress-strain model for complex dynamic loading, because of its accuracy and flexibility in representing soil stress-strain behavior, ease of parameter determination, and ease of developing intuition for parameter physical significance and accuracy. The same five attributes discussed for each existing model were examined for the new ARA conic model, so called because its principal mathematical surfaces are conic sections.

Requirements for soil stress-strain models are discussed below in Section 2; the review of existing models is summarized in Section 3; and development of the ARA model is summarized in Section 4. Mathematical details are presented in Appendices A through W.

2.0 SOIL CONSTITUTIVE MODEL REQUIREMENTS

2.1 The Nature of Soil

Soil is a particulate material. Soil particles vary in size, shape, hardness and surface texture, and although they can be bonded together by mineral deposits, this is the exception rather than the rule. There are four primary consequences of the particulate nature of soil [Lambe and Whitman (1969:Chapter 2)]:

- a) Deformation of soil is partly the result of individual particle deformation, but primarily the result of interparticle sliding and rolling.
- b) Soil is inherently multiphase. The soil particles constitute the solid phase, and the remaining space is pore space. The pore space is filled by pore fluid, consisting of a gaseous phase (usually air) and a liquid phase (usually water). In dry soil the liquid phase is absent, and in saturated soil the gaseous phase is absent. The pore fluid chemically influences the nature of soil particle surfaces, including contact surfaces, and hence affects the process of interparticle force transmission and resistance.
- c) The pore fluid can flow through the pore space. Whether flowing or still, the pore fluid physically interacts with the soil particles, thus further influencing the process of interparticle force transmission and resistance.
- d) Sudden load changes are carried jointly by the soil skeleton and the pore fluid. The resulting change in pore pressure usually causes pore fluid flow, which alters the proportion of load

carried by the soil skeleton and the pore fluid, as well as changing the configuration of the soil skeleton.

Because soil deforms primarily by interparticle slip, soil strength is basically frictional in nature; and because pore fluid pressure reduces interparticle contact normal forces, the strength of a soil element is controlled by the difference between the total normal stress acting on the element and the value of the element pore pressure, i.e., by the effective stress. Due to the nature of soil formation and deposition processes, natural soil deposits are often inhomogeneous and inherently anisotropic, and soil profiles are frequently erratically discontinuous.

2.2 Soil Stress-Strain Characteristics

Soil stress-strain characteristics are a consequence of the particulate nature of soil and the processes by which soils are formed, deposited and subsequently altered in place. The following list of soil stress-strain characteristics is prioritized for construction of soil constitutive models to predict the behavior of soil masses under complex dynamic loads, such as explosions, earthquakes, and moving vehicles:

- a) Soil deformation and strength are governed by effective stress.
- b) Both volumetric and deviatoric stress-strain curves are nonlinear, even at small strains, and the type of nonlinearity is stress path dependent. Figure (2.1) shows the continuous transition from concavity to convexity with respect to the vertical strain axis of a plot of vertical effective stress versus vertical strain, measured in a drained triaxial test. The parameter controlling the shape of the stress-strain curve is the direction of the effective stress path. At mean

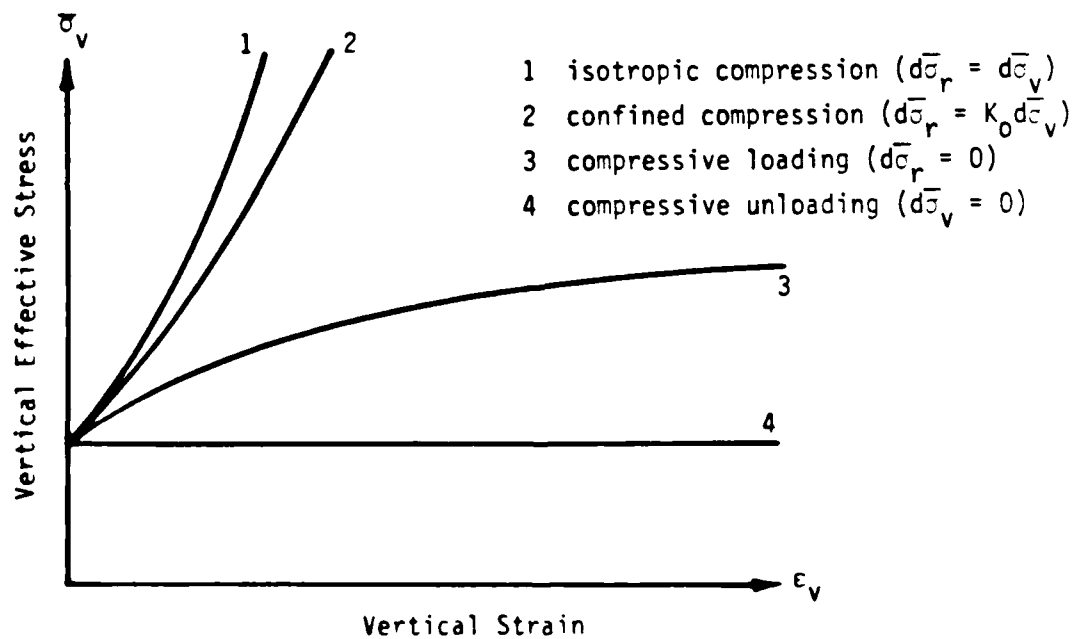
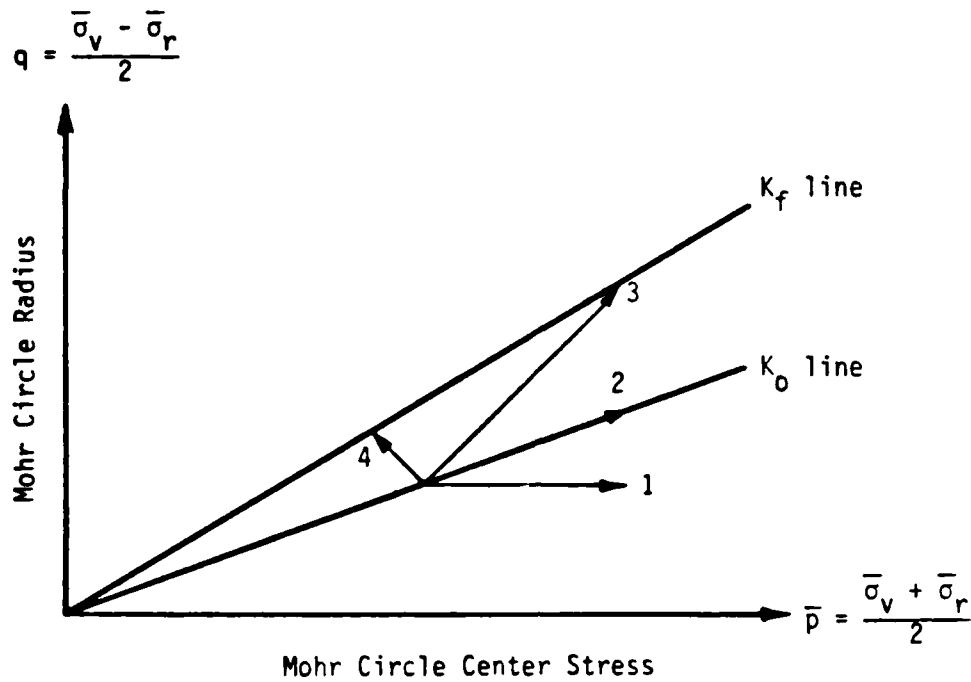


Figure 1 Influence of Effective Stress Path on Stress-Strain Curve Nonlinearity [after Lambe and Whitman (1969: 127, 129, 325)].

pressures above 500 psi some volumetric stress-strain curves exhibit a convex yield region due to grain crushing at highly stressed interparticle contact points, but at even higher mean pressure the volumetric stress-strain curve again becomes concave to the strain axis. Figure (2.2) illustrates the above behavior. A similar phenomenon is observed for one-dimensional compression curves at much lower stresses, due to interparticle slip followed by subsequent skeletal stiffening.

- c) Under drained conditions, shear strain and volumetric strain are coupled. This coupling is called dilatancy. Under undrained conditions the tendency of the soil skeleton to change volume is opposed by the relative incompressibility of the pore fluid, which develops an excess pore pressure sufficient to maintain the soil skeleton at constant, or near constant volume. It is vital that soil dilatancy be correctly modeled in order to obtain the correct pore pressure and effective stress under all loading conditions.
- d) At large shear strain a given soil approaches a residual or ultimate shear stress and void ratio which depend on the confining pressure, but are independent of the initial void ratio prior to shearing. The residual or ultimate shear stress and void ratio define the critical state at the given confining pressure [Casagrande (1936:262)].
- e) In approaching the critical state an initially dense or overconsolidated soil will attain a peak shear stress greater than the critical state value. The peak stress generally

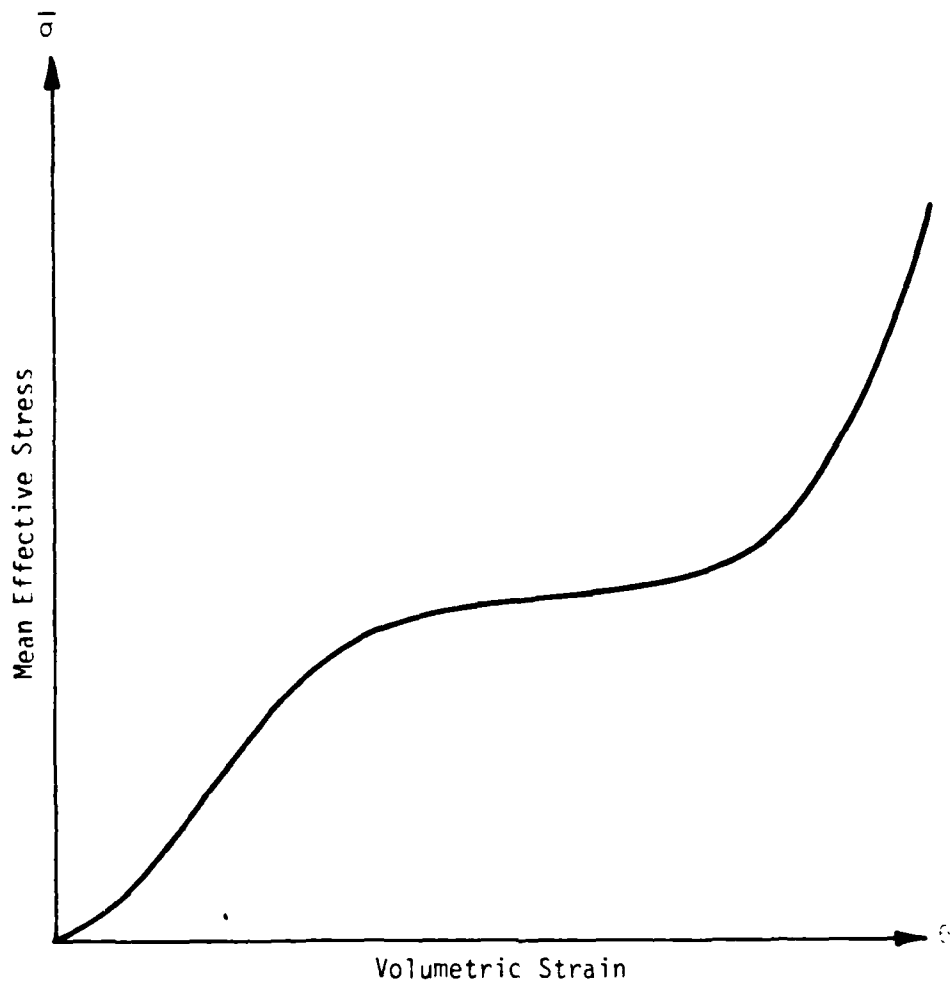


Figure 2.2 Compressive Stress-Strain Curve Exhibiting Yielding Due to Grain Crushing at Interparticle Contacts [after Lambe and Whitman (1969:298)].

corresponds closely to the maximum expansion rate. At larger shear strains in a strain-controlled test the shear stress decreases (strain softening) and the soil continues to expand at a decreasing rate until the critical state is attained. Both dense and loose soils show a tendency toward densification at small shear strains, due to particle rearrangement. Loose sands also initially compact, then expand as they approach the critical state, but normally consolidated clays compact throughout their approach to the critical state. Loose sands exhibit steadily increasing shear resistance as they approach the critical state; even normally consolidated clays can exhibit a peak shear resistance with subsequent strain softening as they approach the critical state. These basic soil stress-strain phenomena are illustrated in Figures (2.3), (2.4), (2.5) and (2.6).

- f) The intermediate principal effective stress can have a significant influence on both the peak and the ultimate friction angles. Figures (2.7) and (2.8) [Merkle (1971)] show representative soil strength data plotted in the octahedral plane. In those plots $\bar{\phi}$ is the Mohr-Coulomb friction angle, and μ is Lode's parameter. If $\bar{\sigma}_2$ had no influence on $\bar{\phi}$, the data points would all lie on a straight line of constant $\bar{\phi}$. Figures (2.7) and (2.8) show a sixty degree segment of a shear failure surface cross-section taken normal to the hydrostatic axis in principal stress space. The entire failure surface has six-fold symmetry, so only a sixty degree segment need be

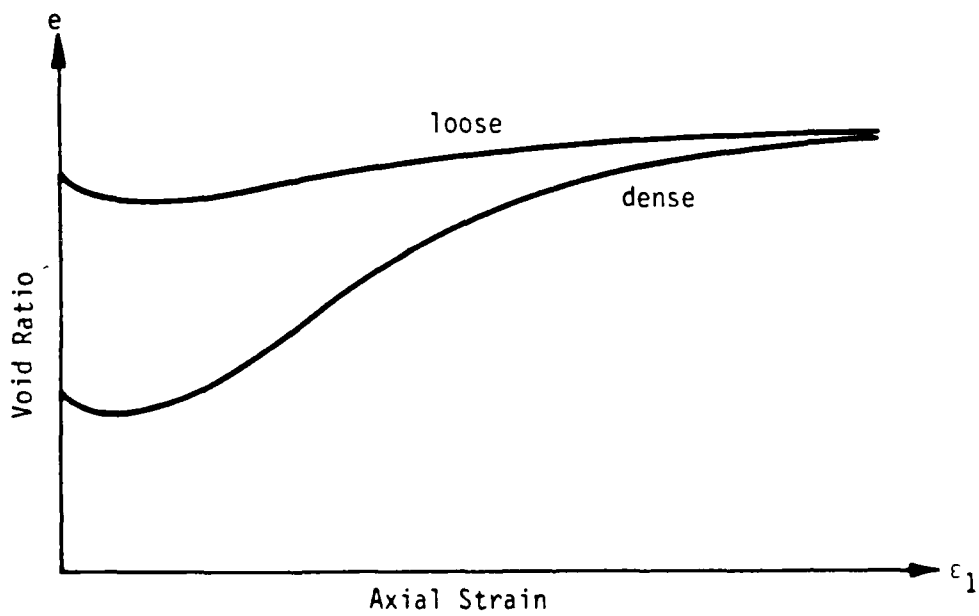
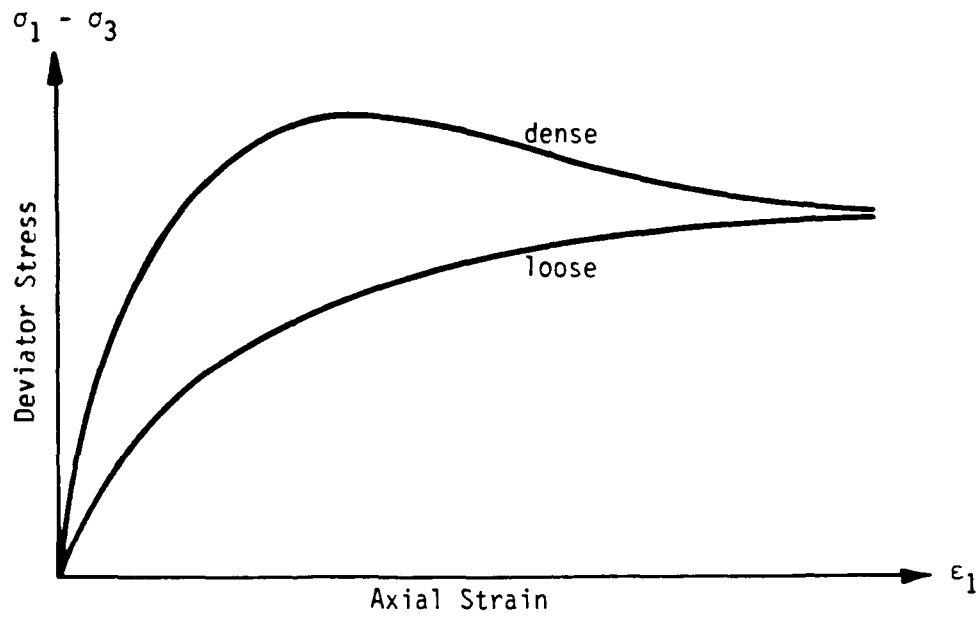


Figure 2.3 Drained Stress-Strain Curves for Loose and Dense Samples of the Same Sand, Under the Same Constant Confining Pressure [after Lambe and Whitman (1969:131)].

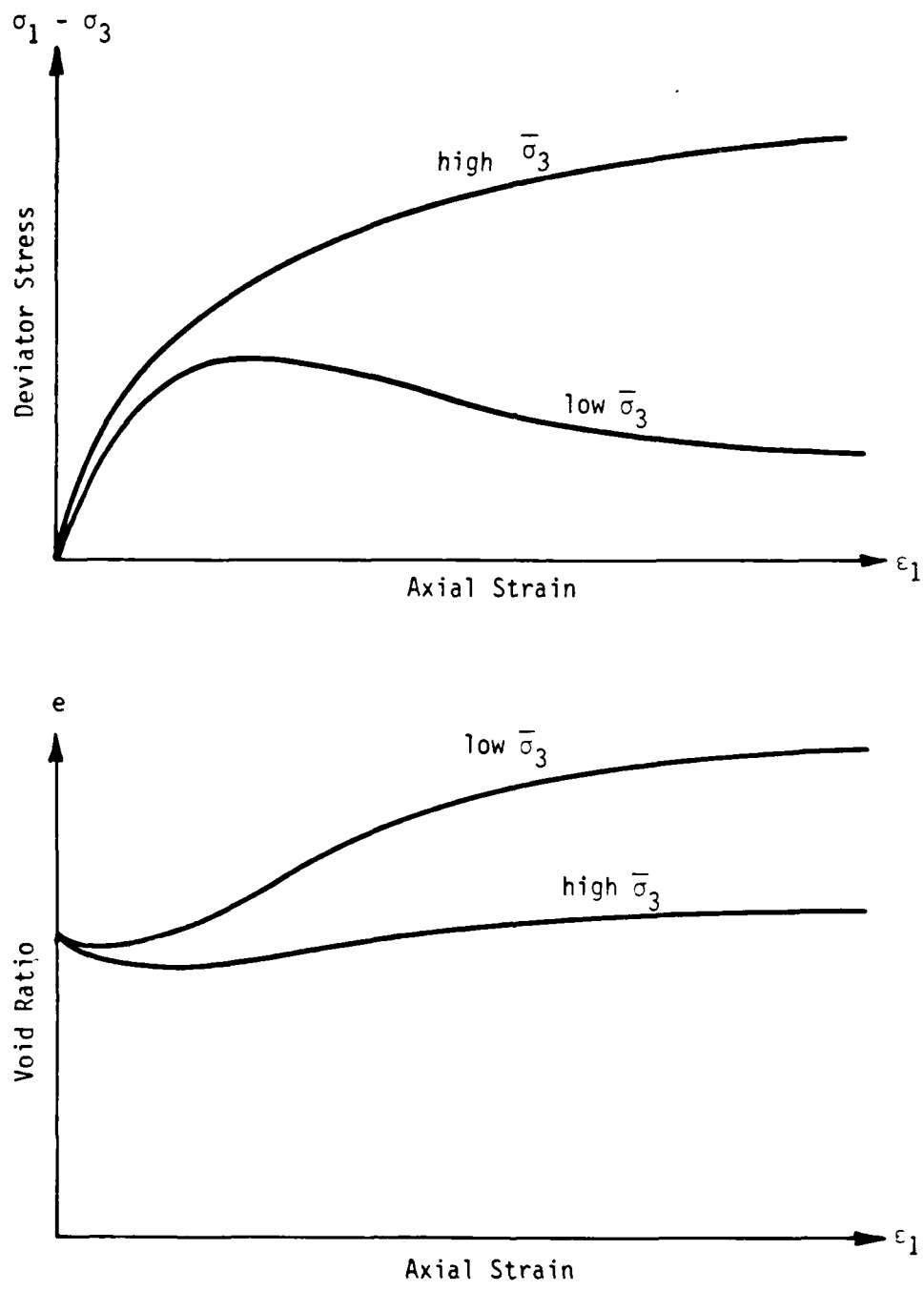


Figure 2.4. Drained Stress-Strain Curves for a Sand at the Same Initial Void Ratio, Under High and Low Constant Confining Pressures [after Lambe and Whitman (1969: 131)].

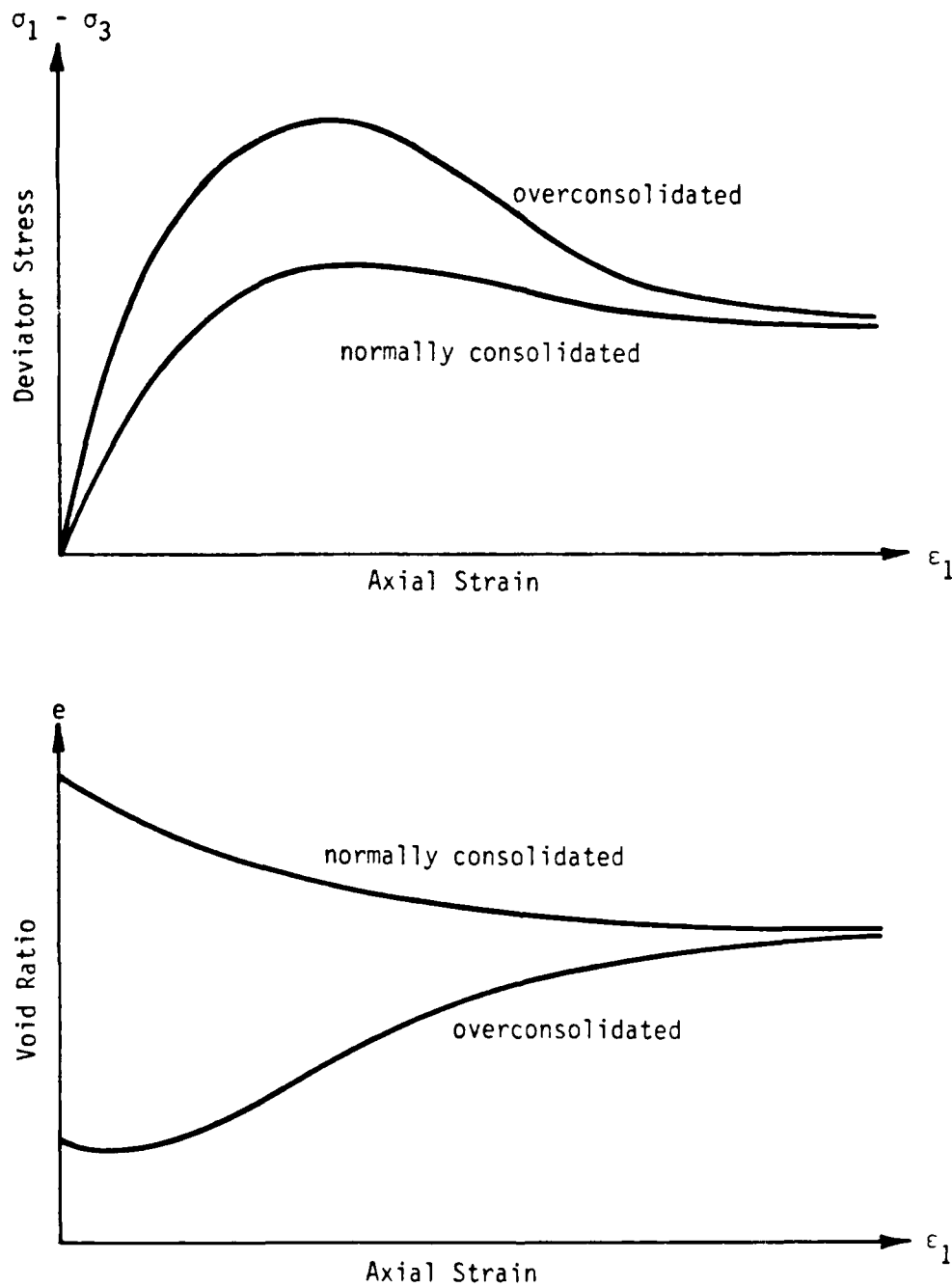


Figure 2.5. Drained Stress-Strain Curves for Normally Consolidated and Overconsolidated Samples of the Same Clay, Under the Same Constant Confining Pressure [after Lambe and Whitman (1969:302, 312)].

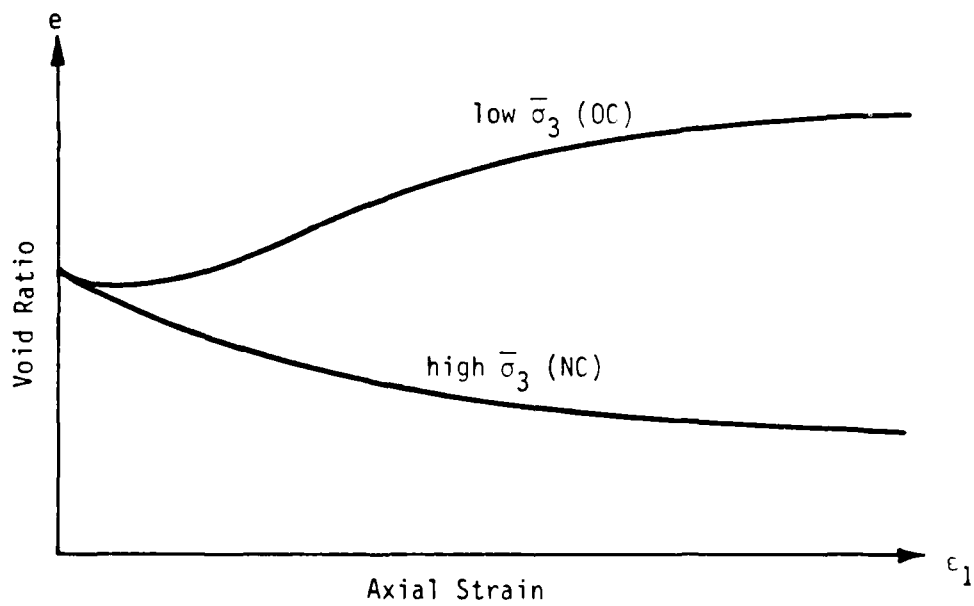
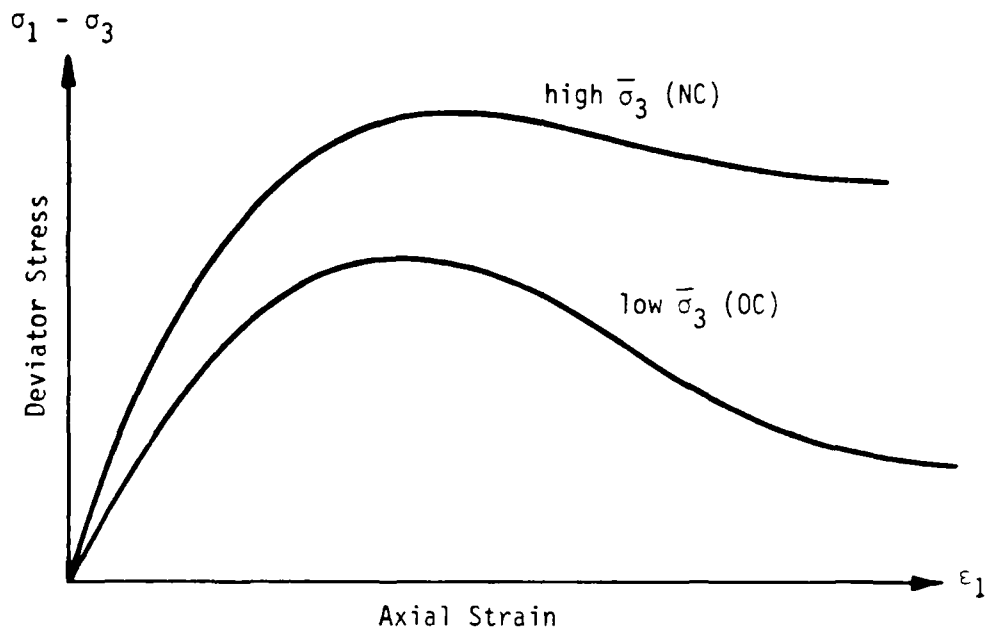


Figure 2.6. Drained Stress-Strain Curves for a Clay at the Same Initial Void Ratio, Under High and Low Constant Confining Pressures [after Lambe and Whitman (1969:302, 312)].

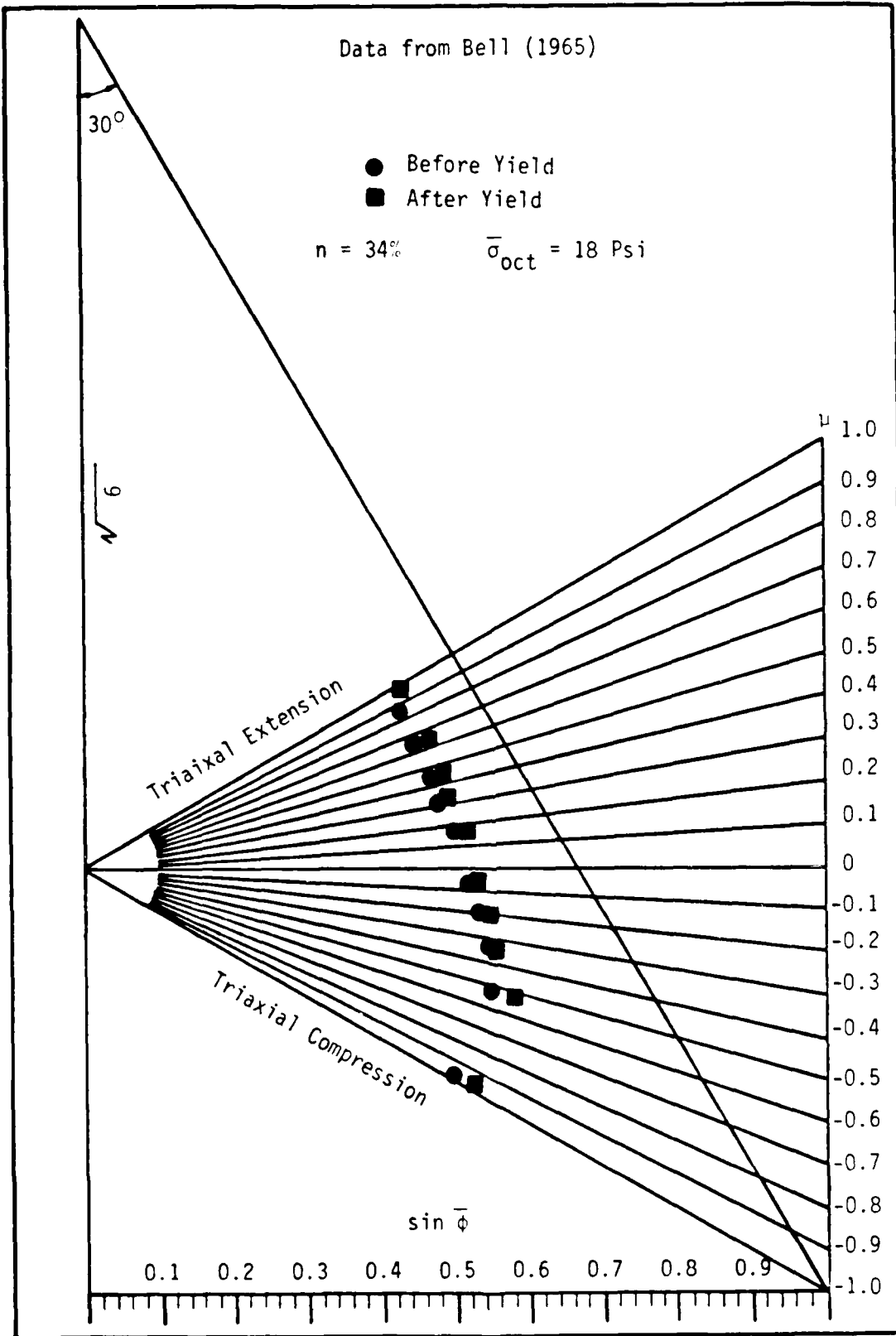


Figure 2.7. Effect of $\bar{\sigma}_2$ on the Strength of Standard Ottawa Sand.

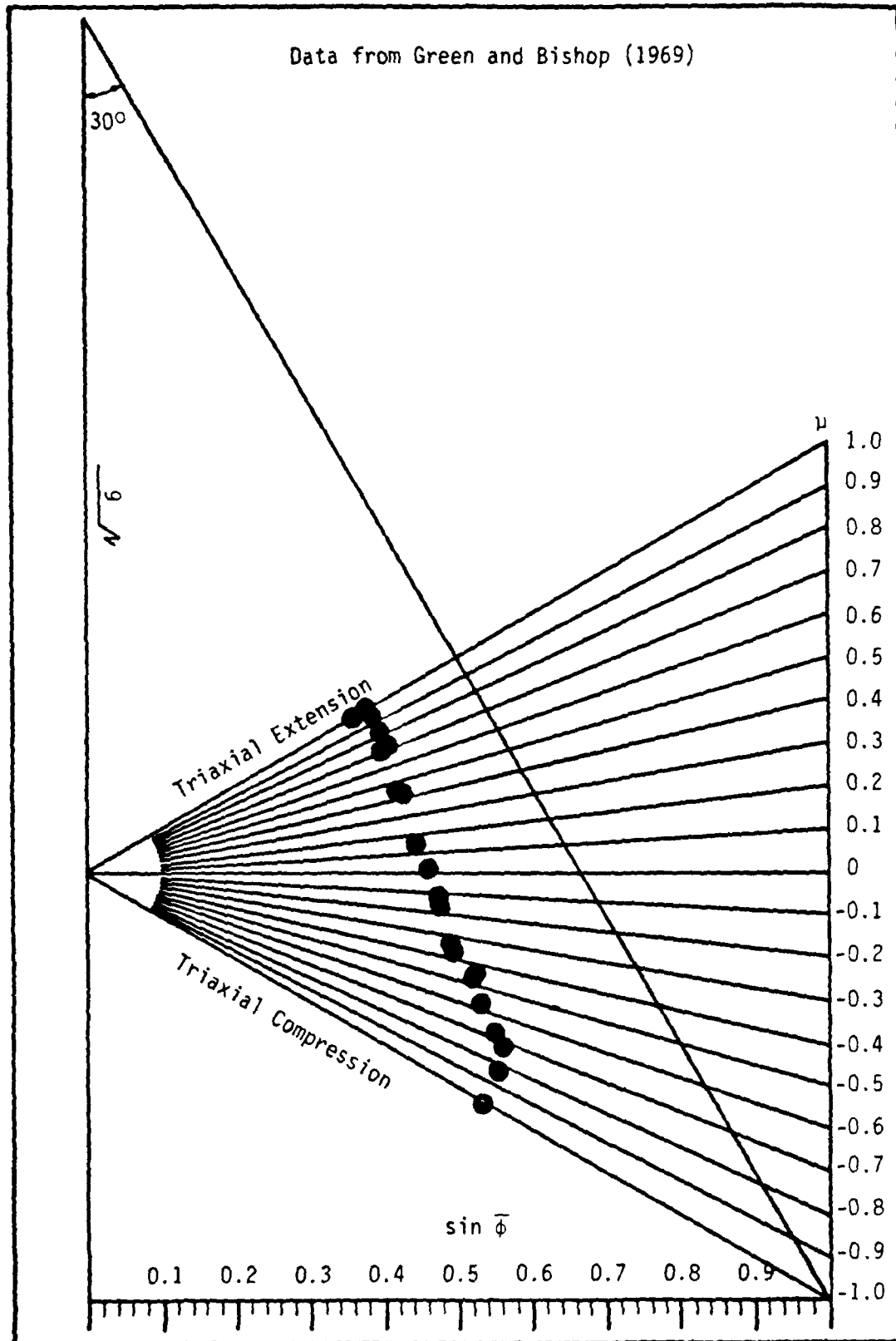


Figure 2.8. Effect of $\bar{\sigma}_2$ on the Strength of Ham River Sand,
 $n_j = 39.0\%$.

plotted to completely define the entire cross-section. The diverging lines extending from a point on the left hand vertical axis to the right hand vertical axis marked μ define values of Lode's parameter, which defines the relative position of the intermediate principal stress with respect to the major and minor principal stresses. A line from the top of the left hand vertical axis to a point on the bottom horizontal axis marked $\sin \bar{\phi}$ defines the value of the sine of the angle of obliquity. The distance of a point from the origin (the point from which the constant μ lines emanate) equals $\sqrt{3}$ times the ratio of the octahedral shear stress to the octahedral normal stress, for a material with no effective stress cohesion. (See Figure (C.4) and the accompanying explanation in Appendix C, and also [Merkle (1984)].)

- g) Because soil particles are generally not bonded together, soil tensile strength is primarily the result of particle interlocking, and is very small. Soil tensile failure causes stress redistribution in a loaded soil mass.
- h) Plastic (irrecoverable) volumetric and deviatoric strains are both generated from the onset of loading.
- i) Separate yield and plastic potential functions appear to be necessary for compression and shear, for a classical plasticity model. Plastic flow is frequently nonassociative, especially in shear.
- j) Soils exhibit the Baushinger effect, i.e., loading beyond the virgin yield point in one direction increases the elastic range

and yield point for unloading and reloading in that direction, but decreases the elastic range and yield point for subsequent loading in the opposite direction [Timoshenko (1956 II:412); Nadai (1950:20)].

- k) Soil stress-strain behavior can be strain rate dependent, both because the effective stress-strain behavior of the soil skeleton is strain rate dependent, and because of the time dependence of pore fluid flow and the associated pore pressure adjustment.
- l) Cyclic loading in compression and/or shear below a critical value produces a number of effects: initial densification; hysteresis; decreasing increments of permanent shear and volumetric strain with each cycle, leading eventually to stable hysteresis; stiffening; and decrease in damping.
- m) Natural soil deposits exhibit both inherent (depositional) and stress- (or strain-) induced anisotropy.
- n) Sample disturbance often makes the stress-strain behavior of a soil sample different in the laboratory from what it would have been in-situ.

The above characteristics significantly influence the response of a soil mass to complex dynamic loads associated with explosions, earthquakes and moving vehicles.

2.3 The Soil Element Model

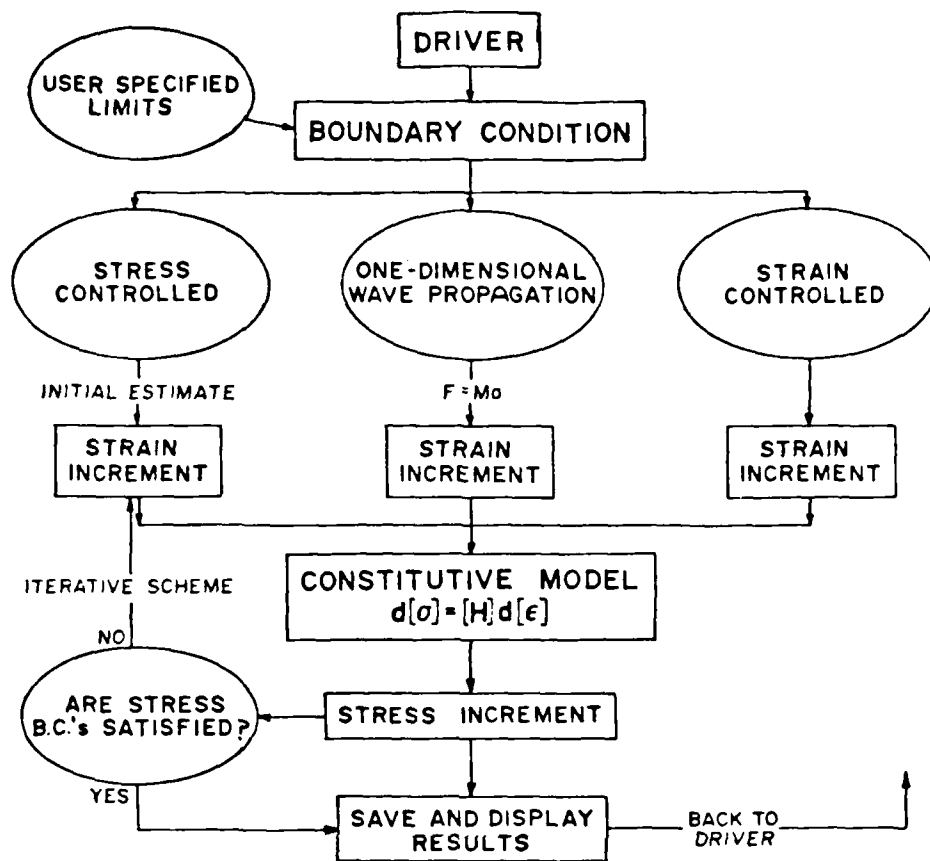
A computer code has been developed which can exercise any constitutive model over several stress and strain paths. The models incorporated in the Soil Element Model (SEM) are formulated to calculate

increments of stress, given strain increments, the current state of stress, and the stress-strain history at a point. The strain-control formulation was chosen because this is how most dynamic finite difference and finite element codes operate, and thus the models developed in the SEM would be immediately ready for use in these larger codes. Figure (2.9) shows a basic flow diagram for the code, and lists the primary options for boundary conditions and material models.

The single element mode of operation allows a model to be tested over a wide variety of stress-strain conditions. Most laboratory test boundary conditions have been incorporated. Triaxial compression/extension encompasses all tests which can be performed in a standard triaxial device, including K_0 uniaxial compression. Only strain-controlled (rigid platen) true triaxial tests can be simulated, however, as no multi-dimensional iterative scheme has yet been written for the program.

A one-dimensional finite difference processor for wave propagation studies was adapted from [Hart (1981)] and incorporated, directly using the SEM model routines. This boundary condition option allows the modeler to study the implementation of a given model and its computational features, such as efficiency and stability. Simple in-situ explosive tests, such as DISC TEST, CIST, and buried spheres can also be calculated using any of the implemented models. Note that the JWL high explosive material model [Lee, et al. (1968)] has been included specifically for these types of calculations. A post-processing option exists for Fourier transform analysis of the resultant time-histories.

The SEM is written in Fortran and can be used either in an interactive mode or in a batch mode. The full version of the code is



OPTIONS

BOUNDARY CONDITIONS

- ISOTROPIC COMPRESSION/CONSOLIDATION
- UNIAXIAL STRAIN
- TRIAXIAL COMPRESSION/EXTENSION
- SIMPLE SHEAR
- STRAIN CONTROLLED TRUE TRIAXIAL
- ARBITRARY STRAIN PATHS
- ONE-DIMENSIONAL WAVE PROPAGATION
 - PLANE STRAIN
 - AXISYMMETRIC
 - SPHERICAL

CONSTITUTIVE MODELS

- LINEAR ELASTIC
- LINEAR VISCOELASTIC
- HYPERBOLIC
- PYKE'S CYCLIC SHEAR
- ELASTIC-PERFECTLY PLASTIC
- AFWL ENGINEERING
- EFFECTIVE STRESS CAP
- LADE'S COHESIONLESS
- JWL (HE)
- ARA CONIC

Figure 2.9. Soil Element Model Basic Logic And Options.

operable on the Cray systems at the Air Force Weapons Laboratory and Los Alamos National Laboratory. A much-abridged version has been made operable on an Apple II-C personal computer. Future plans for the SEM include its use as the common material model processor for several large wave propagation codes. Such a common processor would yield advantages in parameter specification and comparability between results generated with different codes.

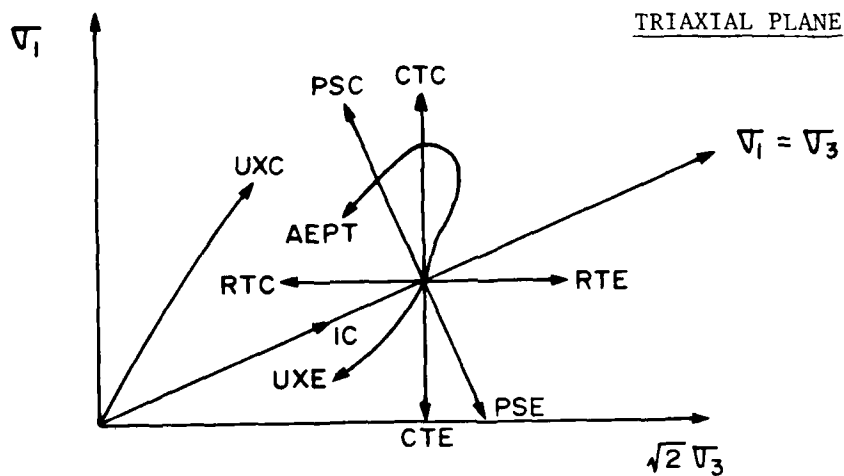
2.4 Computational Exercises for Model Comparisons

As a basis for comparing the stress-strain behavior produced by the constitutive models described in the following section, a common set of exercises has been run for each. The exercises consisted of laboratory test boundary conditions as shown in Figure (2.10), plus arbitrary strain path excursions. All exercises were calculated using the SEM.

2.4.1 Test Descriptions

Each exercise is described below as it would be performed in the laboratory:

a) The isotropic compression test (IC) subjects a cylindrical specimen to an equal all-around confining pressure. Typical measurements are changes of the specimen's height and diameter. Note that in the experiment, measurements are made only at a few specific locations and it becomes necessary to assume a complete deformation pattern to actually calculate volume strain. [Ehrgott (1971)] describes several possible assumptions for deformed shape, and the associated methods for calculating volume strain. For this report, actual laboratory data have been interpreted as if cylindrical specimens remained cylindrical during deformation.



- IC ISOTROPIC COMPRESSION
- CTC CONSTANT CELL PRESSURE TRIAXIAL COMPRESSION
- CTE CONSTANT CELL PRESSURE TRIAXIAL EXTENSION
- RTC REDUCED CELL PRESSURE TRIAXIAL COMPRESSION
- RTE INCREASED CELL PRESSURE TRIAXIAL EXTENSION
- PSC PURE SHEAR COMPRESSION
- PSE PURE SHEAR EXTENSION
- UXC UNIAXIAL STRAIN COMPRESSION
- UXE UNIAXIAL STRAIN EXTENSION
- AEPT AXISYMMETRIC STRAIN PATH

Figure 2.10. Soil Element Model Exercises.

b) The constant cell pressure triaxial compression test (CTC) is conducted after a desired equal all-around confining pressure has been reached via an IC test. While the lateral pressure is held constant, axial load is increased and measurements of the specimen's height and diameter changes are made.

c) The constant cell pressure triaxial extension test (CTE) is also conducted from an initial equal all-around confining pressure. While the lateral pressure is held constant, the axial pressure is decreased and height and diameter change measurements are made. Note that for this type of test, the axial piston is the same size as the specimen to allow control of axial stress independent of cell pressure.

d) The reduced cell pressure triaxial compression test (RTC) also starts from an initial equal all-around lateral pressure, but the axial load is held constant, while the confining pressure is reduced.

e) The increased cell pressure triaxial extension test (RTE) increases the lateral pressure from an initial equal all-around value, while the axial stress is maintained constant.

f) The pure shear compression test (PSC), as it is called here, is somewhat harder to perform in a standard triaxial cell because both the axial load and lateral pressure are varied from an initial IC state. Increase of axial load is proportional to decrease of lateral pressure to yield zero change in mean normal stress.

g) The pure shear extension test (PSE) starts from an initial equal all-around confining pressure. Lateral pressure is then increased and axial load is proportionally decreased to maintain constant mean normal stress.

h) The uniaxial strain compression test (UXC) can be run either in a uniaxial device (oedometer) or in a triaxial cell. In the uniaxial device, vertical pressure is applied to a wafer-shaped specimen that is physically restrained from deflecting radially. Applied axial stress and specimen height change are measured. When run in a triaxial cell the test is typically called a K_0 test. It is conducted by applying lateral pressure to a specimen until a slight inward movement of the diameter is detected. Axial load is then applied until the specimen returns to its original radial position. (Or, axial load can be applied until slight outward movement is observed, whereupon the lateral pressure is increased to zero out the radial strain.) Axial and lateral pressure are measured, along with specimen height and diameter changes.

i) The uniaxial strain extension test (UXE) is conducted in a triaxial cell from an initial equal all-around confining pressure. Axial stress is reduced while maintaining zero radial strain with respect to the specimen's diameter at the end of the IC phase.

Two types of strain path tests were calculated:

j) An axisymmetric strain path test (AEPT) is conducted in a standard triaxial test device. Following an initial hydrostatic loading a specified strain path is followed by controlling the vertical strain and manually adjusting the lateral confining pressure to yield the desired radial strain. (Note that lateral pressure could also be servo-controlled.) Measurements include axial and lateral stress, and specimen height and diameter changes.

Figure (2.11) shows two axisymmetric strain paths tested at WES [Akers (1983); Akers (1985)] and used for this exercise. They are denoted

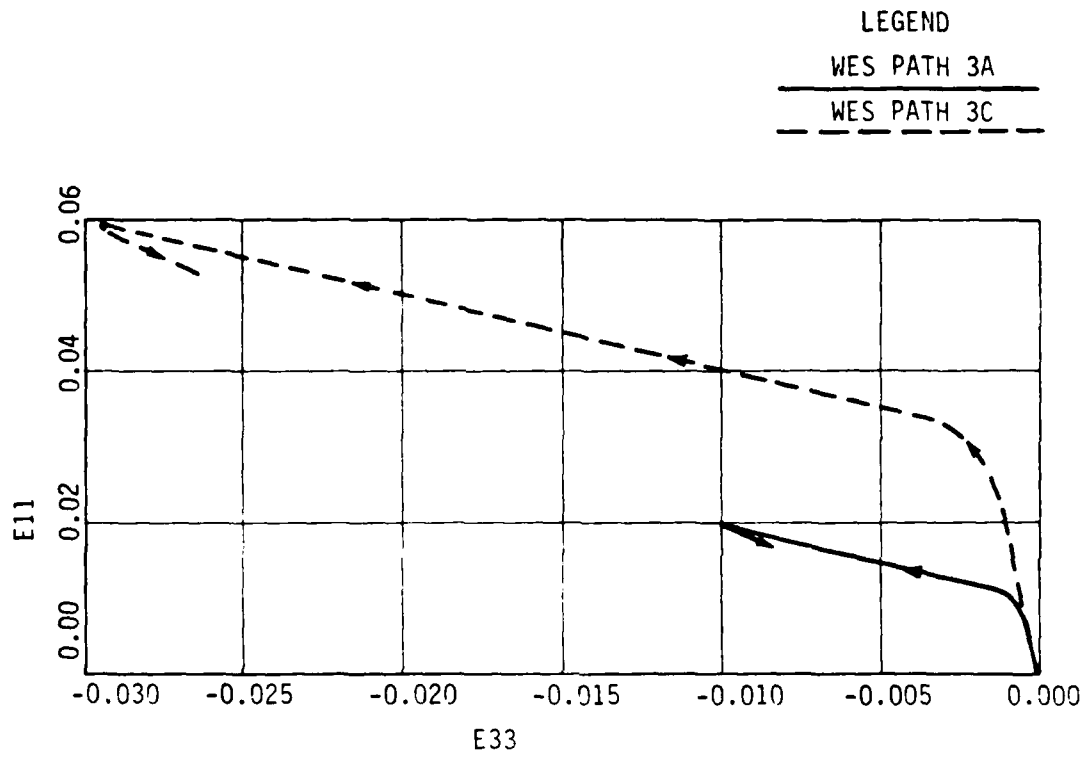


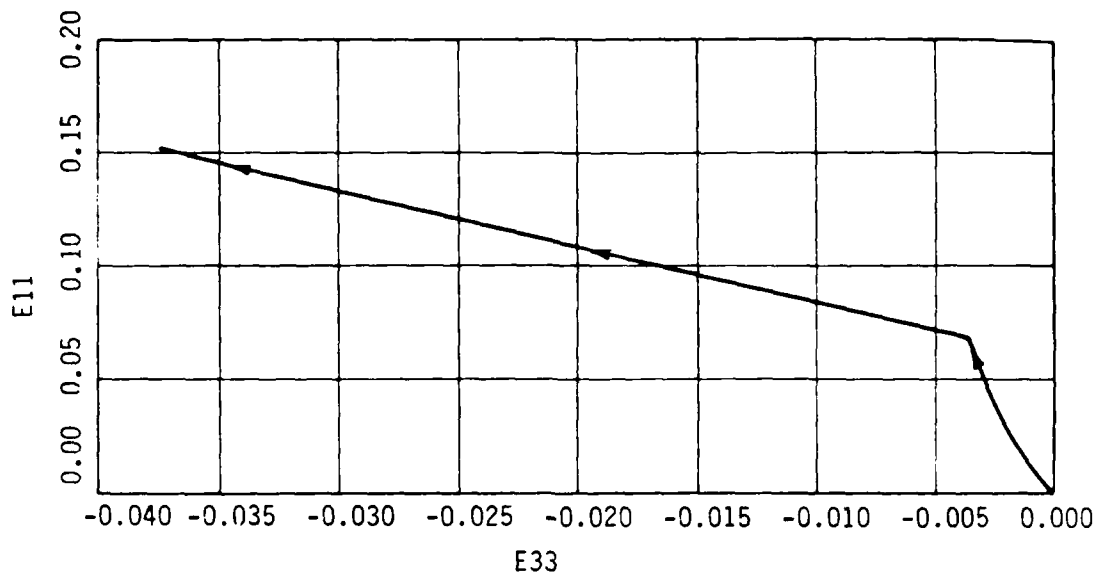
Figure 2.11. WES Axisymmetric Strain Paths

"WES Path 3A" and "WES Path 3C". Two paths tested by [Lade (1983)] were also used and are shown in Figure (2.12).

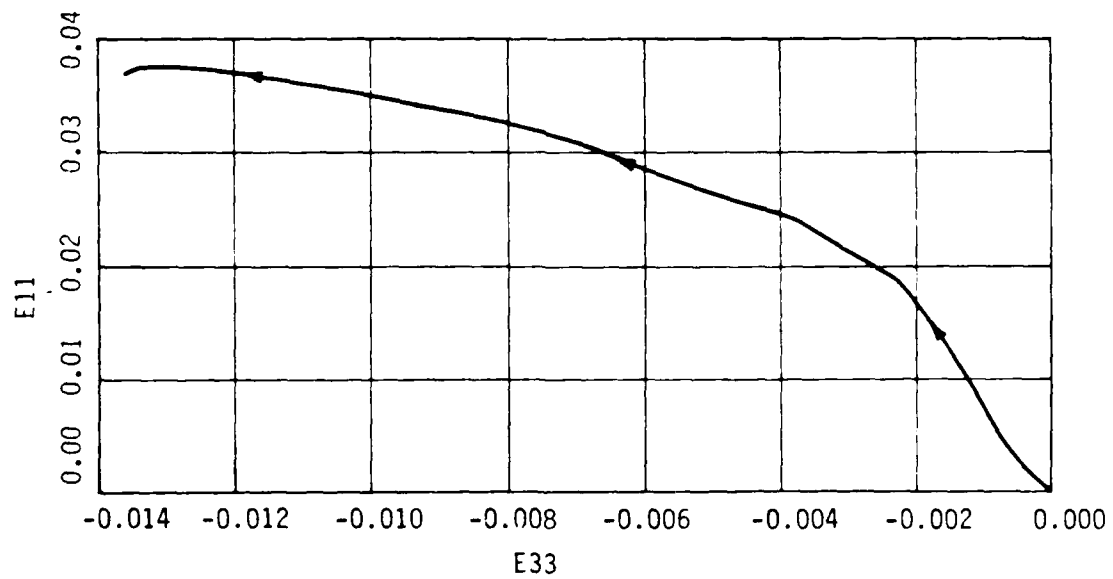
k) Arbitrary three-dimensional strain path tests (EPT) require a true-triaxial test device, because three independent strains must be applied. With a strain-controlled rigid platen device this can be accomplished directly; with a stress-controlled flexible platen device each applied stress must be servo- or manually controlled to yield correct strain increments. Figure (2.13) shows the 3-D strain path used for this exercise. It is Path 3A from [Ko and Meier (1983)], which they used for testing remolded Nellis baseline sand.

2.4.2 Test Data

So that all models could be fairly compared, each was fit to the same set of data from a single material. The material chosen was a dry alluvium obtained at the CARES DRY site near Yuma, Arizona. The material is a brown clayey sand (SC) which contains about 33 percent fines (clay and silt) by weight. Figure (2.14) shows results of gradation and index tests for this material. All test data used for this study, except those for true triaxial strain path 3A, are from tests on remolded samples, with the original material taken from near the surface. The majority of the tests were performed at the U.S. Army Engineer Waterways Experiment Station (WES), and are documented in [Cargile (1984)] and [Akers (1985)]. A small set of strain path experiments were also performed by [Lade (1983)] and these have been included in the exercises. From the many tests performed, a few have been identified as "most representative" of the behavior of CARES DRY alluvium. Table (2.1) lists the tests by number which were used for parameter fitting and comparison with SEM model



(a) PATH NO. 1



(b) PATH NO. 2

Figure 2.12. Lade Axisymmetric Strain Paths

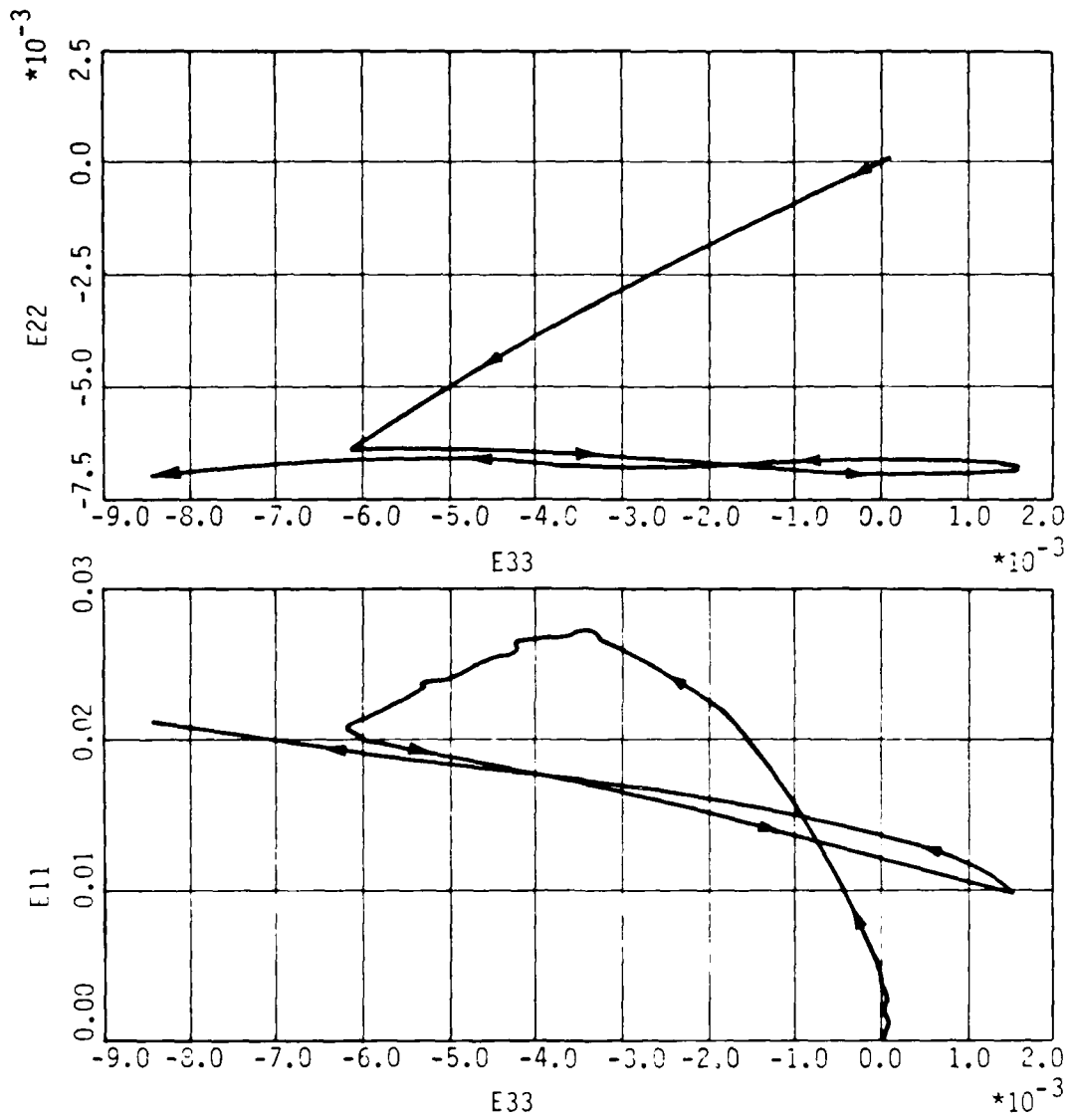
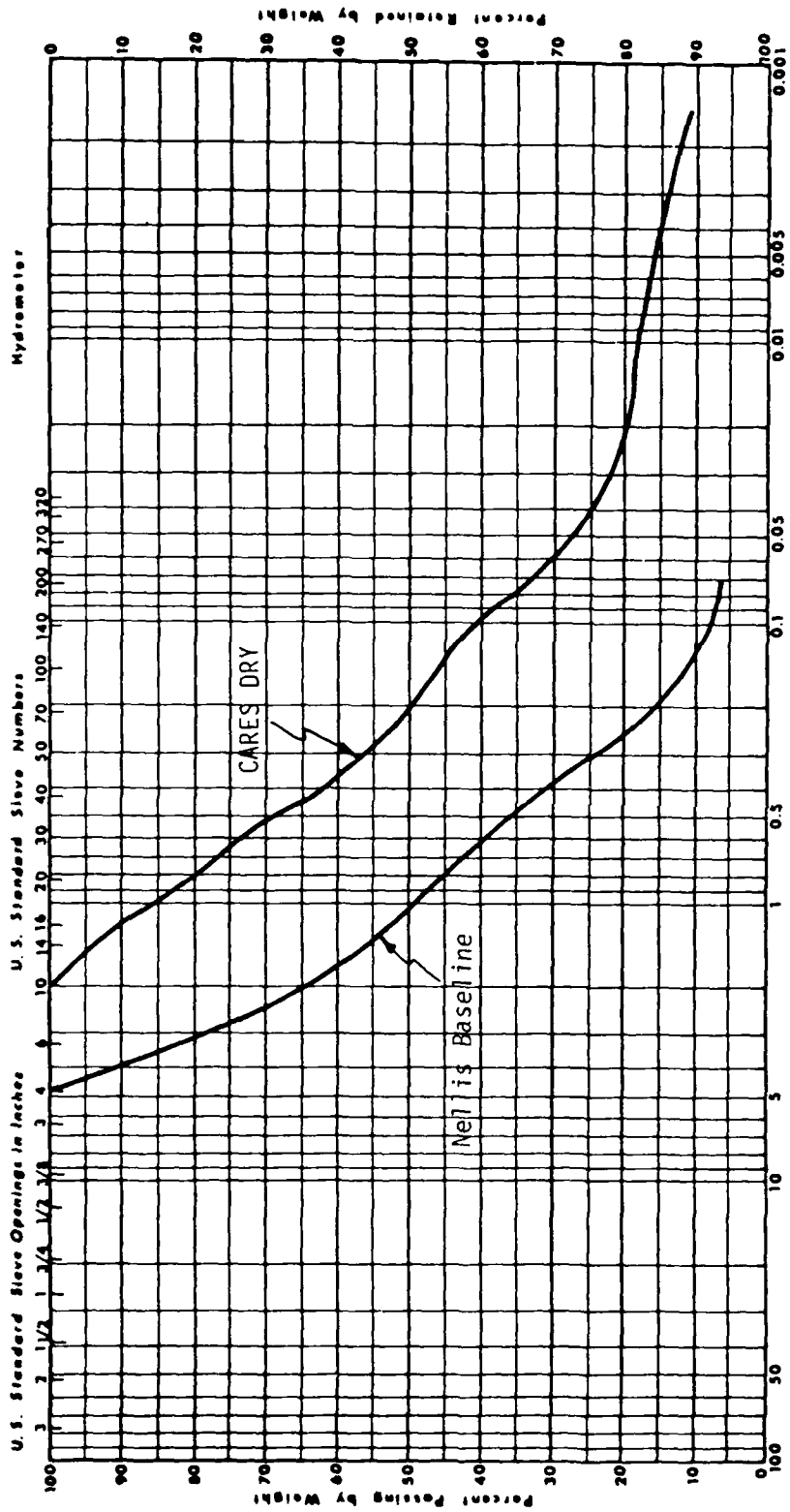


Figure 2.13. Three Dimensional Strain Path



Soil	GRAVEL			SAND			SILT or CLAY			
	Coarse	Fine		Coarse	Medium	Fine				
	Unified Soil Classification System - Corps of Engineers, U.S. Army						G_s	LL	PL	PI
CARES Dry							2.68	36	17	19
Net's Baseline							2.61	21	16	5

Figure 2.14. Gradation and Index Test Results For Remodeled CARES Dry Sand and Remodeled Baseline Sand.

TABLE 2.1. REPRESENTATIVE DATA FOR REMOLDED CARES-DRY SAND

Test Type	Confining Pressure (MPa)	Test Number	Dry Density (g/cc)
IC	---	RDC-IC-3	1.807
CTC	0.7	RDC-TXC-11	1.817
	1.4	RDC-TXC-1	1.809
	3.4	RDC-TXC-2	1.819
	7.0	RDC-TXC-4	1.816
	58.8	RDC-TXC-7	1.806
	100.0	RDC-TXC-16	1.844
CTE	1.8	RDC-TXE-12	1.808
	3.5	RDC-TXE-2	
	7.0	RDC-TXC-13	
UXC Dynamic	---	RDC-DUX-19	1.809
UXC K_0	---	RDC-KO-1	
UXE	1.8	RDC-ICKO-1	1.816
	3.5	RDC-ICKO-2	
	7.0	RDC-ICKO-3	
AEPT WES3A WES3C	6.9	RDC21	
	6.9	RDC32	
AEPT LADE PATH1 LADE PATH2	6.9	1-5	1.832
	6.9	1-3	1.777

calculations. Figure 2.14 also shows a particle size distribution curve for Nellis baseline sand, tested by Ko and Meier (1983) along true triaxial strain path 3A. The mechanical behavior of CARES DRY alluvium is similar to that of Nellis baseline sand. Consequently, prior to the availability of stress-strain data for CARES DRY alluvium, WES recommended approximating its stress-strain features by those of Nellis baseline sand.

Calculational exercises without any test data for comparison included the RTC, RTE, PSC, and PSE stress paths.

3.0 EXISTING MODELS

3.1 Introduction

The reason for reviewing existing soil stress-strain models was to identify their strengths and shortcomings under complex dynamic loading conditions of interest to the Air Force, such as those associated with explosions, earthquakes, and moving vehicles. The five principal types of requirements for a useful dynamic soil stress-strain model listed in Section 1.0, viz: theory, phenomenology, computational efficiency, convenience, and accuracy were considered, as were the fourteen key soil dynamic stress-strain characteristics discussed in Section 2.2, which fall under the phenomenology requirement heading above. The eight existing soil dynamic stress-strain models reviewed were:

- a) Linear elastic
- b) Linear viscoelastic
- c) Hyperbolic
- d) Pyke cyclic simple shear
- e) Elastic-perfectly plastic
- f) Modified AFWL engineering
- g) Effective stress cap
- h) Lade

Detailed results of the model reviews are contained in Appendix V, supported where necessary by mathematical derivations in Appendices A through U. The discussion of each model in Appendix V includes: motivation, assumptions, basic equations, parameter determination and computed behavior.

3.2 Evaluation Summary

Table 3.1 summarizes the evaluation of the eight existing soil stress-strain models with respect to ten criteria:

- a) ease of parameter determination
- b) influence of intermediate principal stress on shear strength
- c) exact match of measured shear strengths in triaxial compression and extension
- d) direct computation of shear strength for any value of Lode's parameter, without trial and error
- e) nonlinear, inelastic volumetric and deviatoric response even at small strains
- f) coupling of shear and volumetric strains even at small strains
- g) prediction of plastic strain increments only when the corresponding plastic work increment is positive
- h) nonassociative plastic flow rule for shear yield surface
- i) critical state at large shear strain
- j) strain softening

Of the eight models reviewed, the Lade model has the greatest number of favorable ratings.

3.3 Individual Evaluation

The main advantages of the linear elastic model are ease of parameter determination, and the availability of closed form solutions and proven, stable, numerical solution techniques. It does not accurately represent soil stress-strain behavior at strain levels larger than acoustic. For a linear elastic material, volumetric and deviatoric response are uncoupled. Thus, the computed relation between octahedral normal stress and volumetric strain shown in Figure (3.1) is unique and independent of

TABLE 3.1. PERFORMANCE OF EIGHT EXISTING SOIL STRESS-STRAIN MODELS WITH RESPECT TO TEN EVALUATION CRITERIA

	Linear Elastic	Linear Viscoelastic	Hyperbolic	Pyke Cyclic Simple Shear	Elastic-Perfectly Plastic	Modified Engineering	Effective Stress Cap	Lade
Ease of Parameter Determination	E	E	E	E	E	E	D	E
Influence of σ_2 on Shear Strength	N	N	N	N	Y	Y	Y	Y
Match TXC and TXE Shear Strength	N	N	N	N	N	N	N	N
Compute Shear Strength Directly	N	N	N	N	Y	Y	Y	N
Nonlinear, Inelastic Small ϵ Response	N	N	Y	Y	N	N	Y	Y
Dilatancy at Small Strains	N	N	N	N	N	N	N	Y
Dissipation Condition Satisfied	N	N	N	N	Y	Y	Y	N
Nonassociative Shear Flow Rule	N	N	N	N	Y	Y	N	Y
Critical State at Large γ	N	N	Y	Y	Y	Y	Y	Y
Strain Softening	N	N	N	N	N	N	N	Y

Notation:

- Y = yes
- N = no
- E = easy
- D = difficult

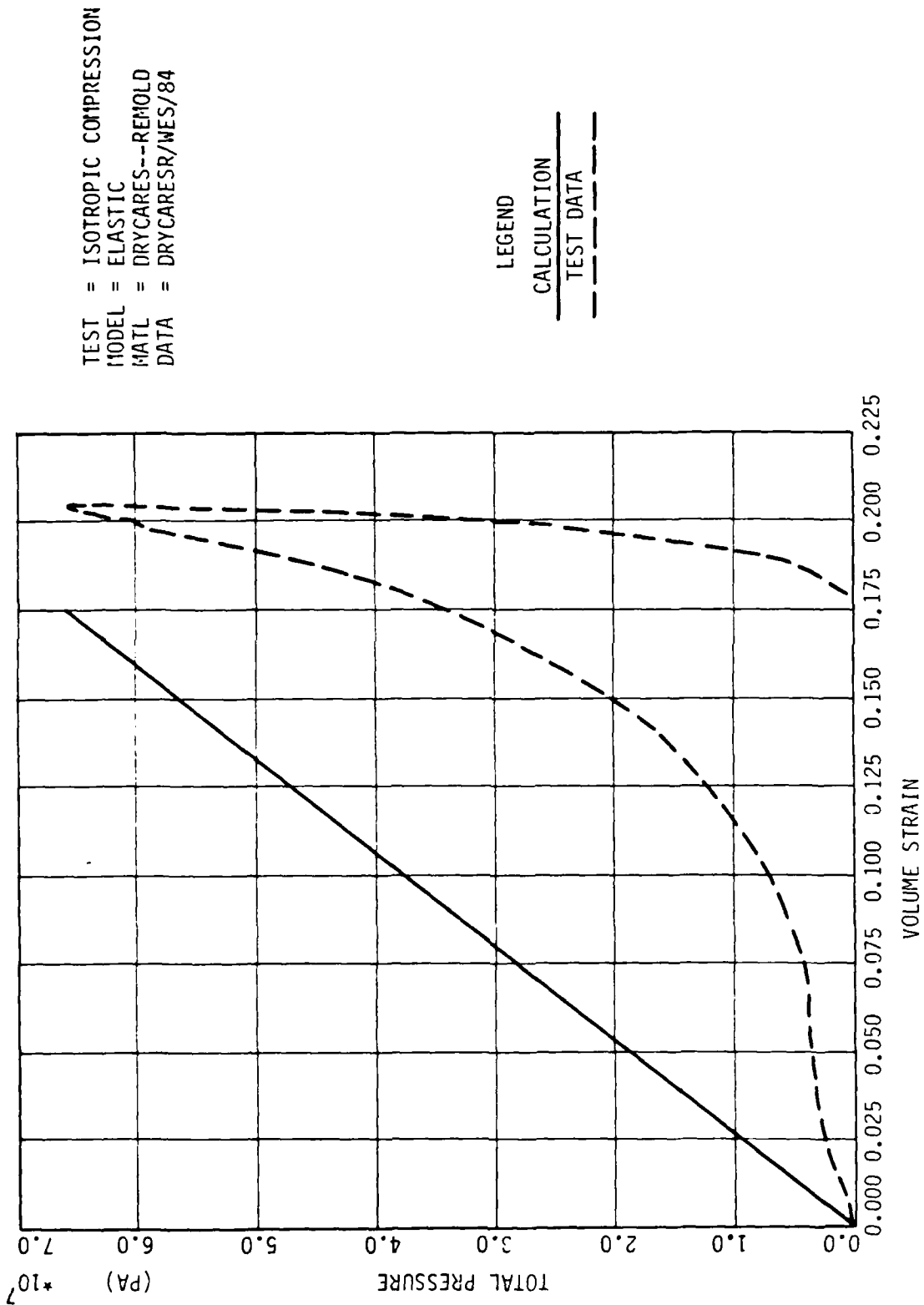
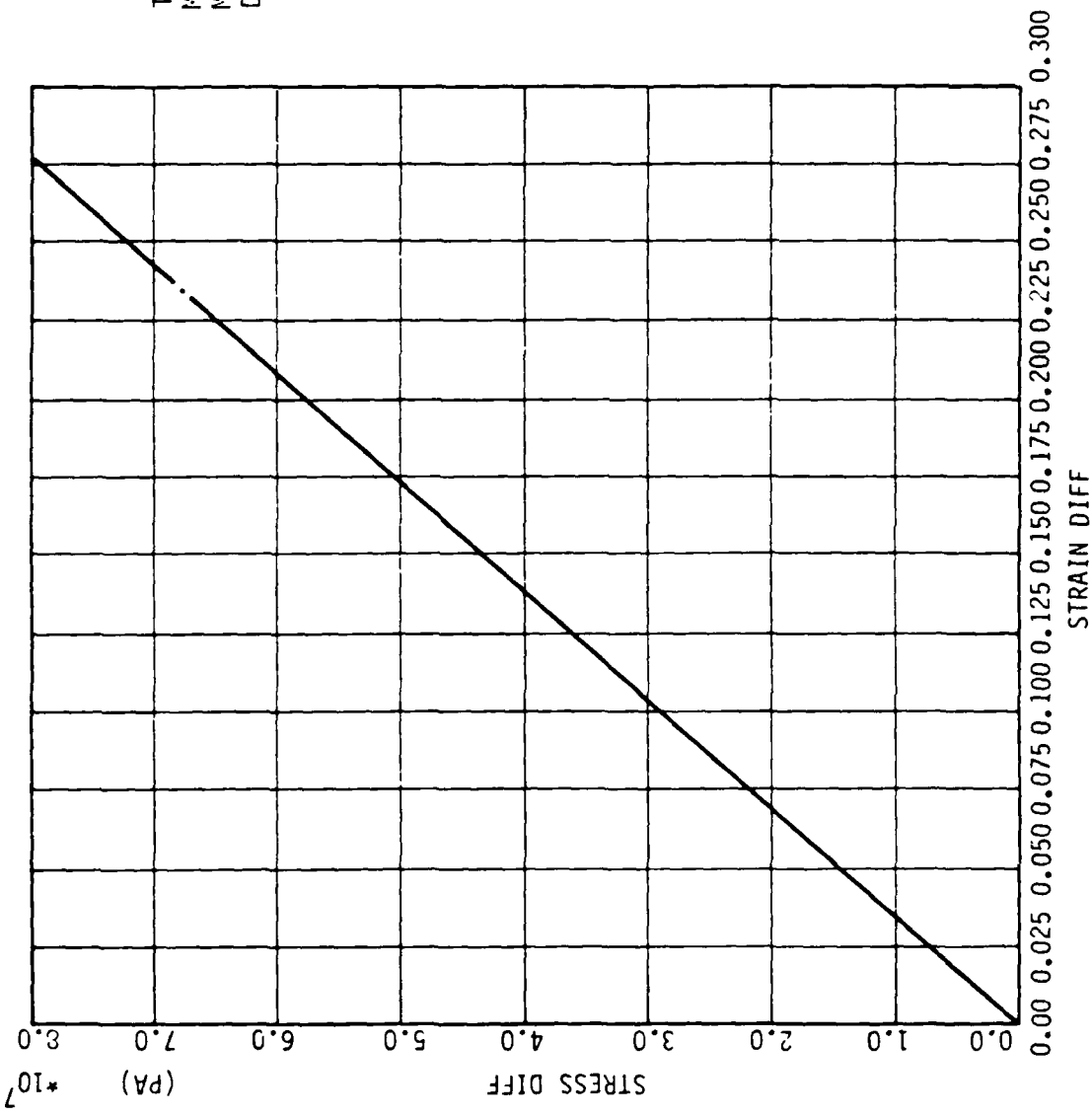


Figure 3.1. Elastic Model Exercise--Isotropic Comp.--Pressure vs. Volumetric Strain

shear behavior. Similarly, the relation between each computed deviatoric stress component and the corresponding deviatoric strain component shown in Figure (3.2) is unique and independent of the volumetric response and all other deviatoric responses. Figures (3.1) and (3.2) are a complete characterization of a linear elastic material at particular constant volumetric and deviatoric strain rates, and all other responses can be obtained from them. The detailed evaluation of the linear elastic model is presented in Appendix V.1.

The main advantages of the linear viscoelastic model are ease of parameter determination, the availability of closed form solutions and proven, stable, numerical solution techniques, and the model's ability to dissipate energy. It does not accurately represent soil stress-strain behavior at all strain rates, and predicts complete strain recovery upon unloading. Volumetric and deviatoric responses are also uncoupled for a linear viscoelastic material, although each is rate dependent as shown in Figures (3.3) and (3.4). Figures (3.3) and (3.4) are a complete characterization of a linear viscoelastic material at particular constant volumetric and deviatoric strain rates, and all other responses at those strain rates can be obtained from them. The detailed evaluation of the linear viscoelastic model is presented in Appendix V.2.

The hyperbolic model is a simple, practical procedure for representing the nonlinear, stress-dependent, inelastic stress-strain behavior of soils, under approximately axisymmetric stress conditions well below the failure level. Model parameter determination is straightforward. *The hyperbolic model is an incremental elastic model, in which the incremental elastic constants depend on the current stress state but not on stress or strain history.* Thus, residual strains can result if



TEST = STANDARD TRIAXIAL
 MODEL = ELASTIC
 MATL = DRYCARES--RENOLO
 DATA = DRYCARES/RES/84

LEGEND

SIGMA3C= 3.4E6

 SIGMA3C= 7.0E6

 SIGMA3C= 58.8E6

 SIGMA3C=101.0E6

Figure 3.2. Elastic Model Exercise--Triaxial Comp(CTC)--Stress Diff. vs. Strain Diff.

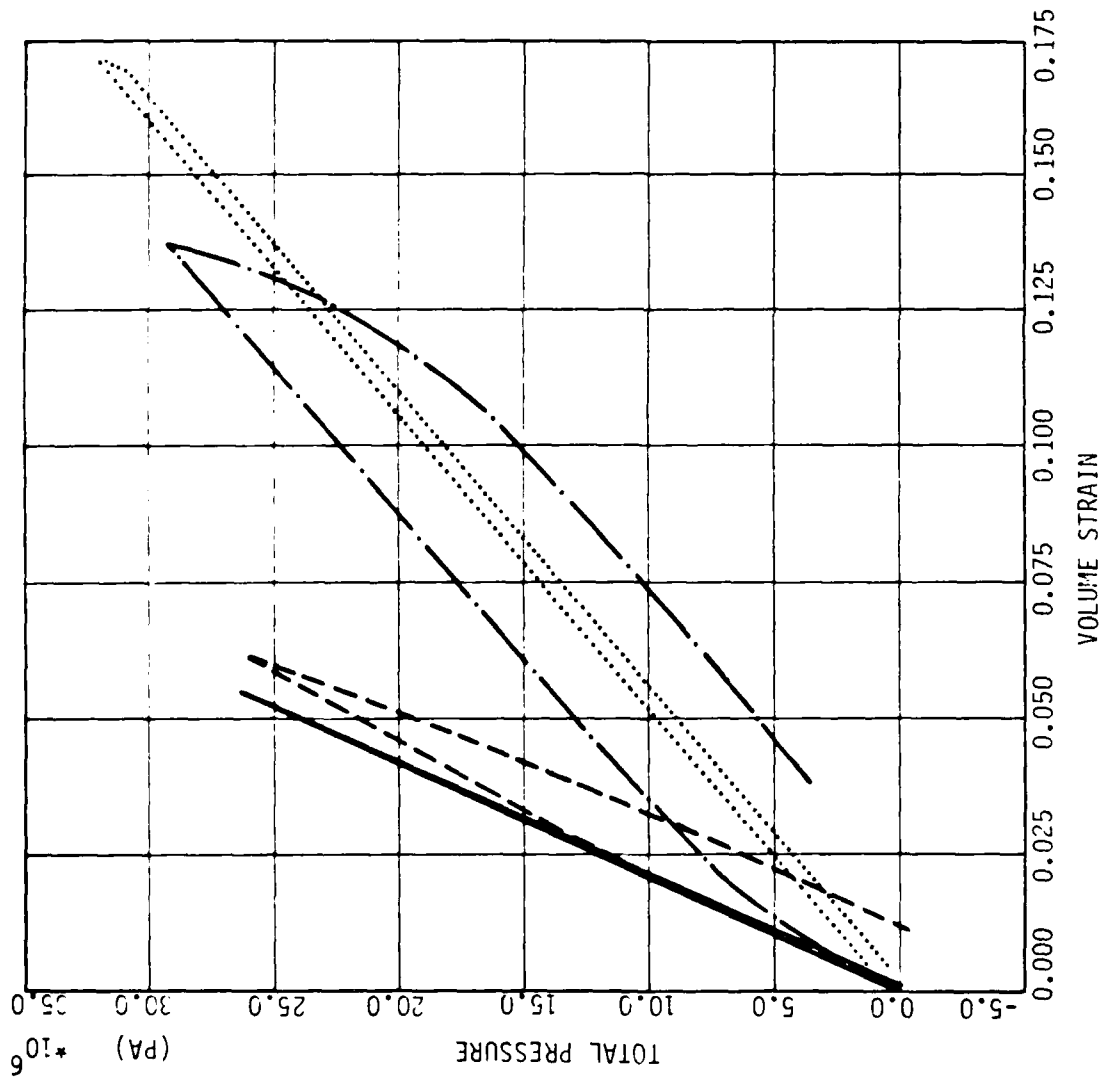


Figure 3.3. Visco Model Exercise--Uniaxial Strain--Pressure vs. Volumetric Strain

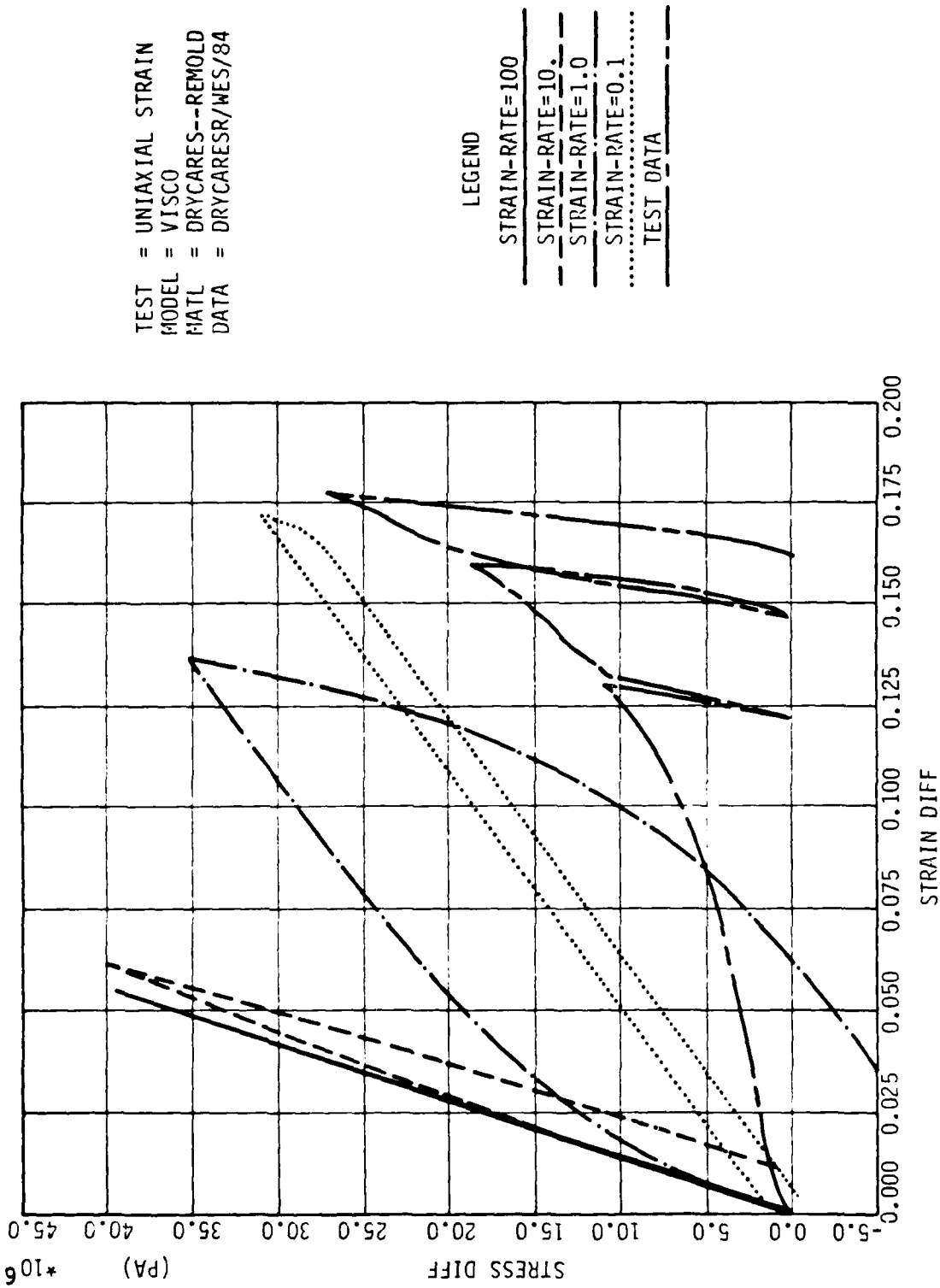


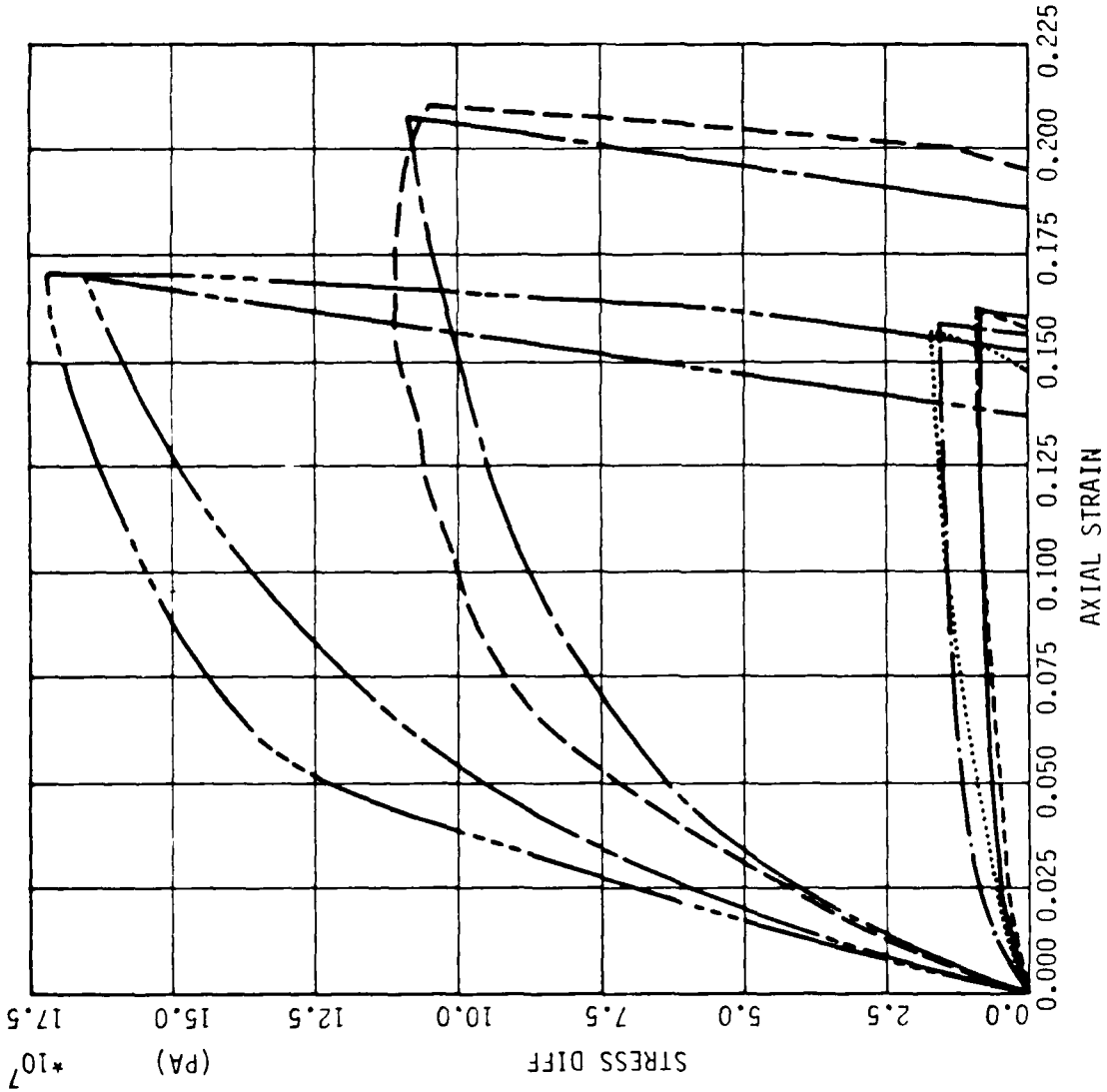
Figure 3.4. Visco Model Exercise--Uniaxial Strain--Stress Diff. vs. Strain Diff.

the unloading stress path does not retrace the loading stress path, but there is no guarantee against energy generation over a closed stress path. The hyperbolic model does not fully account for stress path effects on strength, stiffness, or dilatancy. To improve agreement between calculated and measured behavior during detailed evaluation of the hyperbolic model reported in Appendix V.3, several model modifications were made:

- a) The unloading elastic constants were made functions of maximum past axial strain.
- b) A Mohr-Coulomb shear failure criterion was added.
- c) When the computed stress point violated the Mohr-Coulomb shear failure surface, the stress point was corrected back to the failure surface along a radial line in the octahedral plane.
- d) Negative values of mean normal stress were prohibited. Whenever tensile failure (net volumetric expansion) occurred, all stresses were set to zero.

Figures (3.5) and (3.6) show the hyperbolic model's shear and volumetric response in triaxial compression. Agreement between computed and measured shear response is good, but the volumetric response agreement is not good. The problem with the hyperbolic model's volumetric response is lack of dilatancy. As noted above, the detailed evaluation of the hyperbolic model is presented in Appendix V.3.

The main advantages of the Pyke cyclic simple shear model are ease of parameter determination, and the ability to accurately describe irregular cyclic simple shear response, including limiting the peak shear stress to a fixed value independent of the cyclic loading history. It is not a



TEST = STANDARD TRIAXIAL
 MODEL = HYPER
 MATL = DRYCARES--REMOLD
 DATA = DRYCARES/WES/84

LEGEND

SIGMA3C= 3.4E6

TEST DATA

SIGMA3C= 7.0E6

TEST DATA

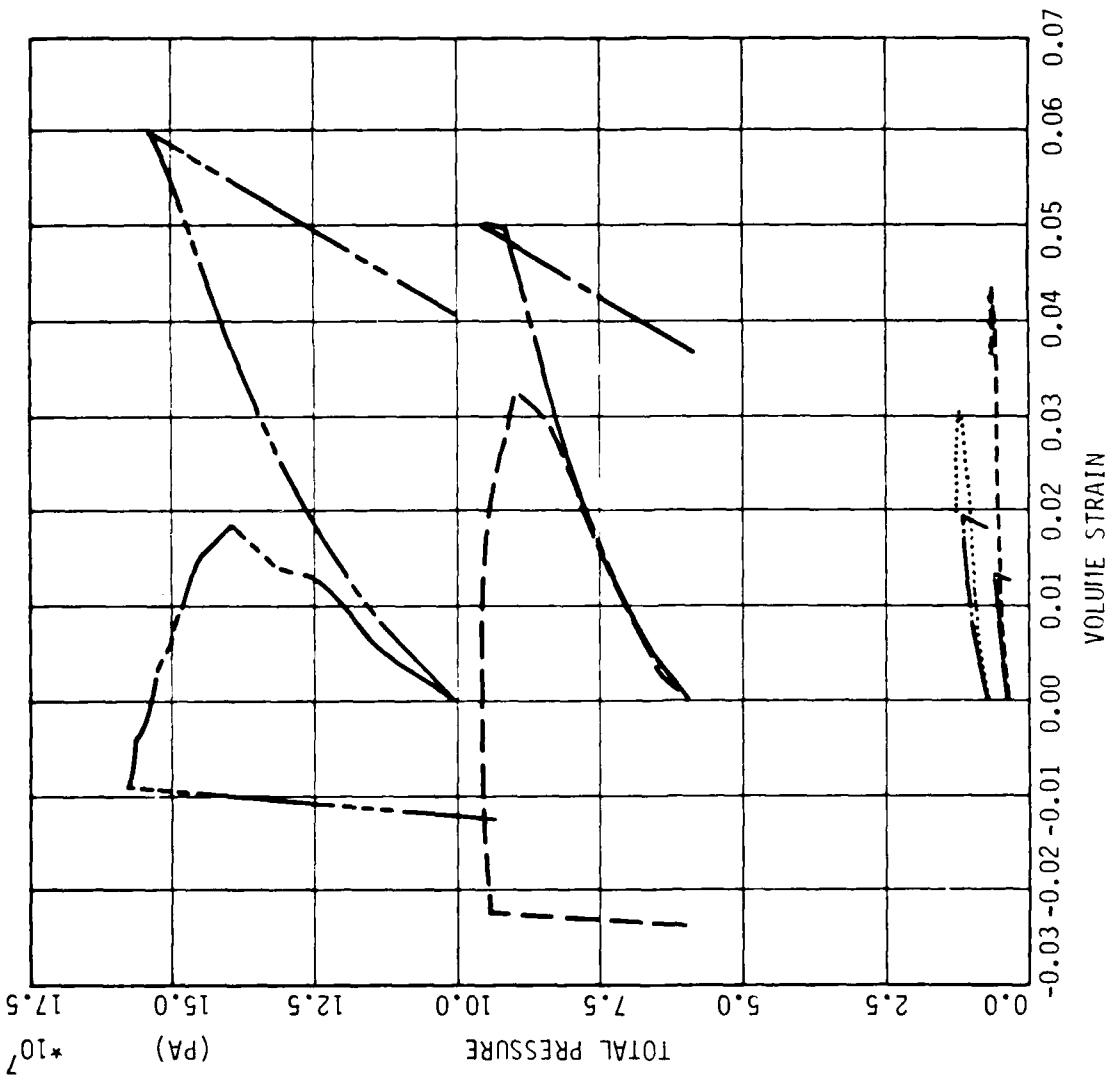
SIGMA3C= 58.8E6

TEST DATA

SIGMA3C= 100.0E6

TEST DATA

Figure 3.5. Hyper Model Exercise--Triaxial Comp(CTC)--Stress Diff. vs. Axial Strain



TEST = STANDARD TRIAXIAL
 MODEL = HYPER
 MATL = DRYCARES--REMOLD
 DATA = DRYCARES/WES/84

LEGEND
 SIGMA3C= 3.4E6
 TEST DATA
 SIGMA3C= 7.0E6
 TEST DATA
 SIGMA3C= 58.8E6
 TEST DATA
 SIGMA3C=100.0E6
 TEST DATA

Figure 3.6. Hyper Model Exercise--Triaxial Comp(CTC)--Pressure vs. Volumetric Strain

general stress-strain model, and therefore cannot be evaluated for a general triaxial stress or strain path. The model's response under irregular cyclic simple shear is shown in Figure (3.7). The detailed evaluation of the Pyke cyclic simple shear model is presented in Appendix V.4.

The main advantages of the elastic-perfectly plastic model are ease of parameter determination, incorporation of stress state limits observed in laboratory strength tests, and production of inelastic strains when a limiting stress state is reached. The main disadvantages are that nonlinear, inelastic, dilatant behavior does not occur until the failure surface is reached, and with an associative flow rule predicted plastic volume increases at failure are frequently too large. Figures (3.8) and (3.9) show the elastic-perfectly plastic model's shear and volumetric response in triaxial compression. Agreement between computed and measured shear response is fair at the two lower confining pressures, but poor at the two higher confining pressures. This is because Young's modulus, which determines the initial slope of the stress difference versus axial strain curve, has been assumed independent of confining pressure. A higher assumed value for E would have improved the agreement between computed and measured shear response at higher confining pressure, but would have worsened the agreement at lower confining pressure. Had an associative flow rule been used, the computed volumetric response shown in Figure (3.9) would have exhibited considerable dilatancy. In fact, the reason the non-associative flow rule was used (which corrects the stress point back to the failure surface along an octahedral plane radial) was that previous elastic-perfectly plastic model calculations using the

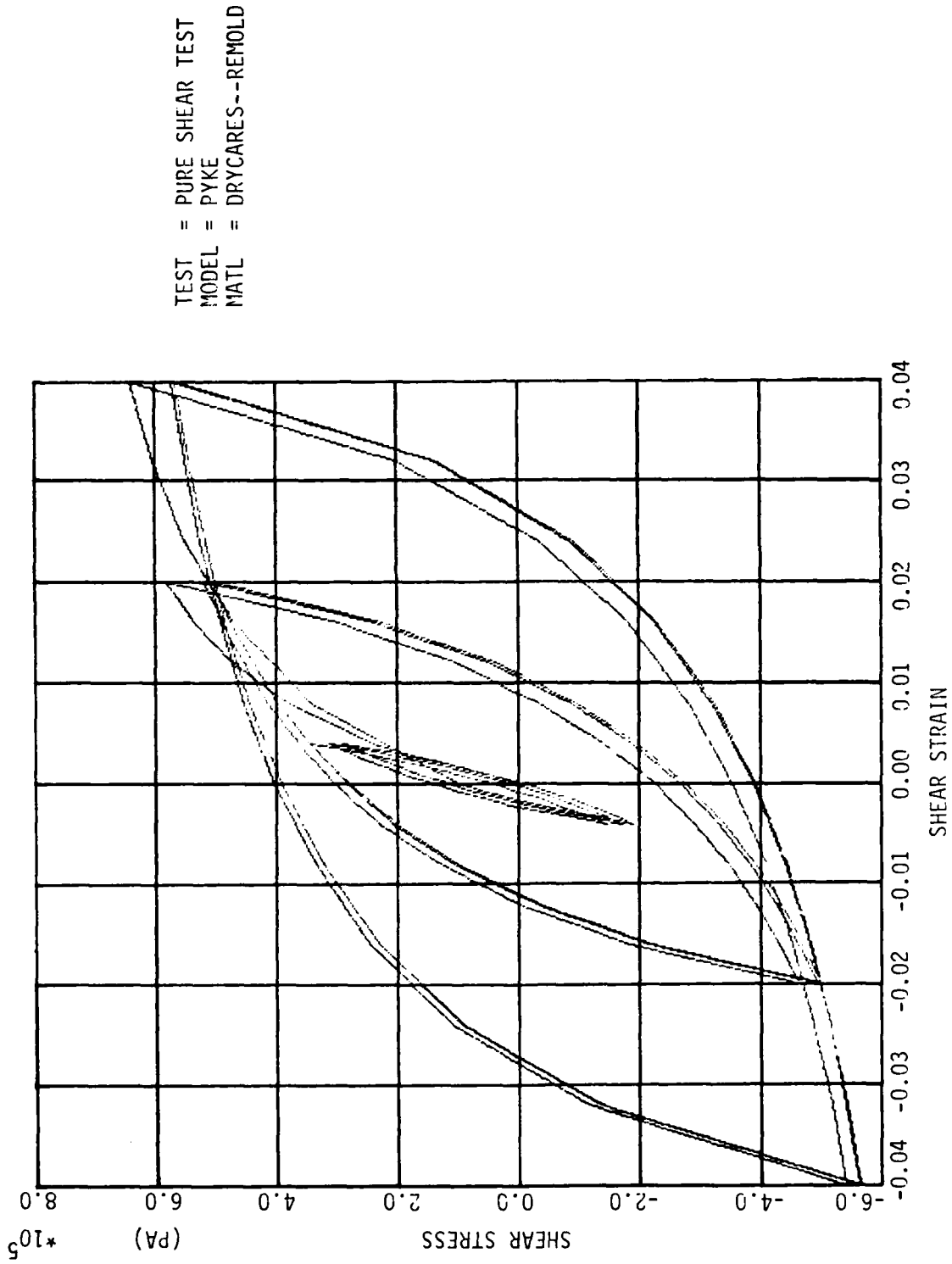
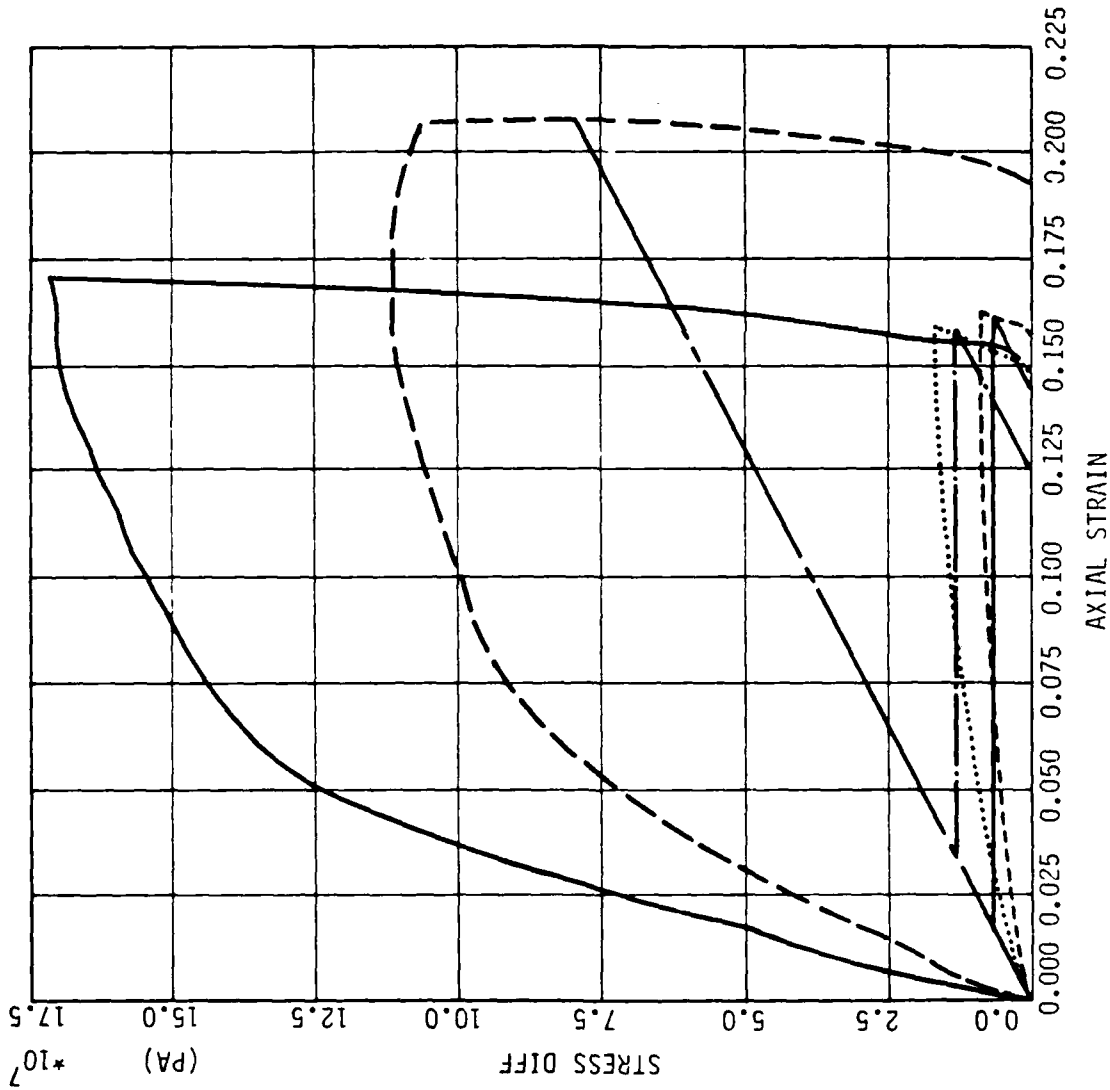


Figure 3.7. PYKE Model Exercise--Cyclic Shear--Shear Stress vs. Shear Strain

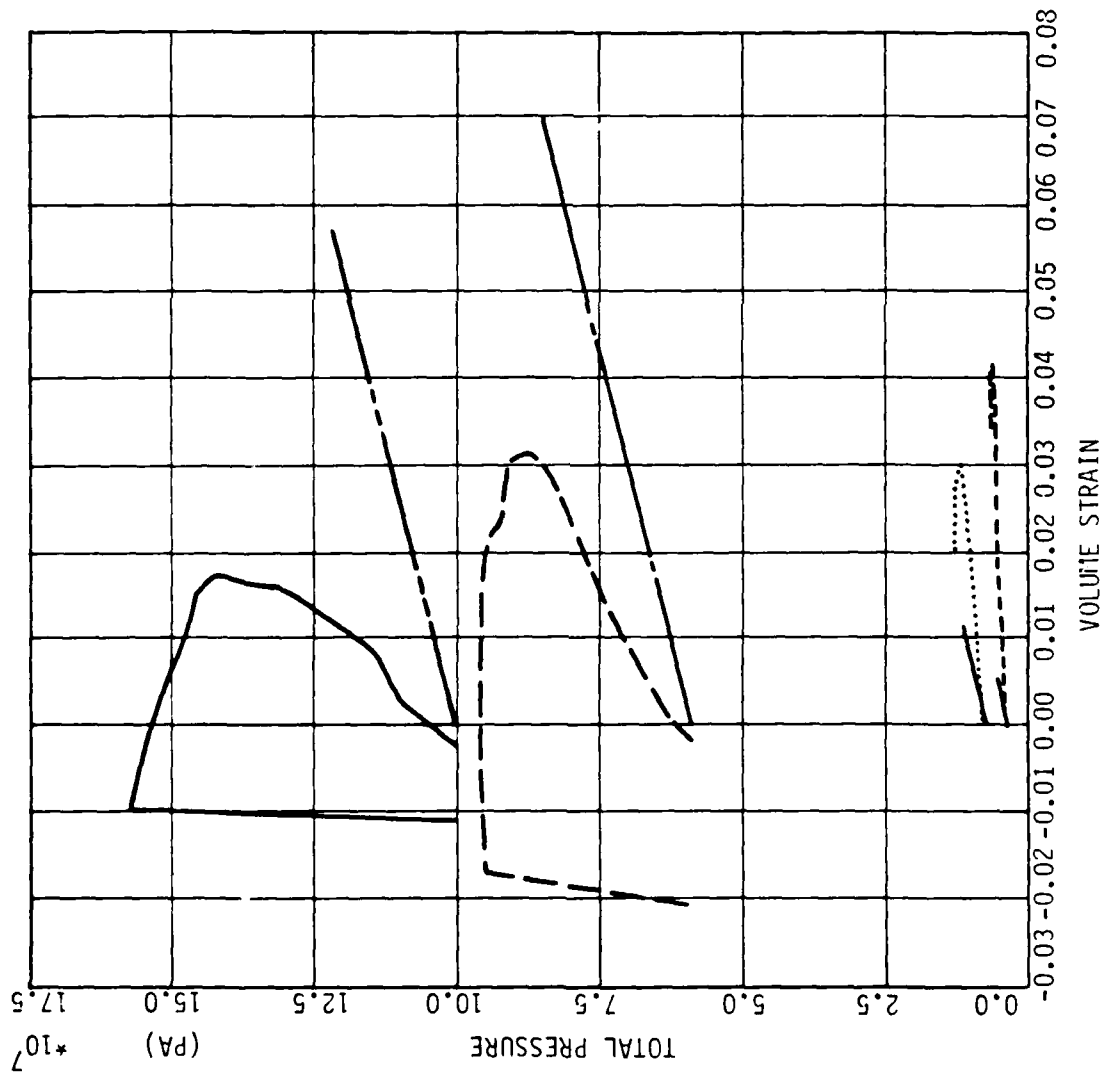


TEST = STANDARD TRIAXIAL TEST
 MODEL = ELPLA
 MATL = DRYCARES--REMOLD
 DATA = DRYCARES/R/WES/84

LEGEND

SIGMA3C= 3.4E6
TEST DATA
SIGMA3C= 7.0E6
TEST DATA
SIGMA3C= 58.8E6
TEST DATA
SIGMA3C=100.0E6
TEST DATA

Figure 3.8. Elpla Model Exercise--Triaxial Comp(CTC)--Stress Diff. vs. Axial Strain



TEST = STANDARD TRIAXIAL TEST
 MODEL = ELPLA
 MATL = DRYCARES--REMOLD
 DATA = DRYCARES/WES/84

LEGEND
 _____ SIGMA3C= 3.4E6
 - - - - - TEST DATA
 - - - - - SIGMA3C= 7.0E6
 TEST DATA
 SIGMA3C= 58.8E6
 - - - - - TEST DATA
 - - - - - SIGMA3C=100.0E6
 _____ TEST DATA

Figure 3.9. Elpla Model Exercise--Triaxial Comp(CTC)--Pressure vs. Volumetric Strain

associative flow rule had often produced excessive dilatancy. The detailed evaluation of the elastic-perfectly plastic model is presented in Appendix V.5.

The main advantages of the modified AFWL engineering model are ease of fitting to laboratory and in-situ test data, simplicity of the shear plasticity formulation, and the fact that the model exhibits compressive hysteresis, which most soils do but many elastic-perfectly plastic models do not. Its main disadvantages are lack of pure shear hysteresis at constant volume below the failure surface, and lack of dilatancy. The lack of dilatancy at failure arises because when a computed stress point violates the shear failure surface, the stress point is corrected back to the failure surface along an octahedral plane radial. Figures (3.10) and (3.11) show the modified AFWL engineering model's shear and volumetric response in triaxial compression. Agreement between computed and measured shear response is good at the two lower confining pressures, and fair at the two higher confining pressures. The reason the modified AFWL engineering model shows slightly better agreement between computed and measured triaxial compression shear response than does the elastic-perfectly plastic model is that in the modified AFWL engineering model the segmental elastic constants were determined by fits to uniaxial compression stress-strain and stress path data, whereas in the elastic-perfectly plastic model the elastic constants are fixed [cf. Figures (V.6.1) and (V.5.1)]. The poor agreement between computed and measured triaxial compression volumetric response for the modified AFWL engineering model is caused by the assumption that the volumetric response

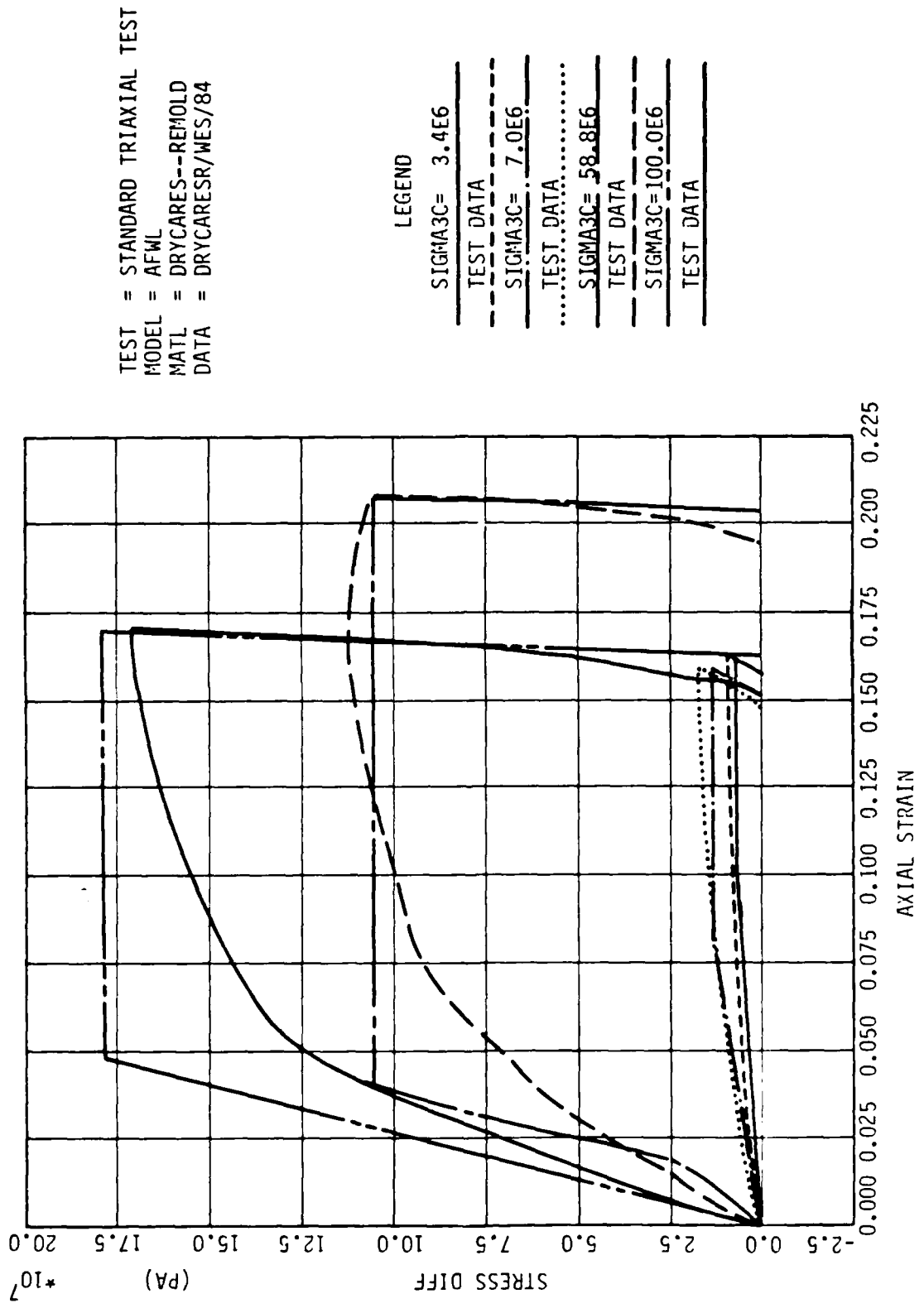
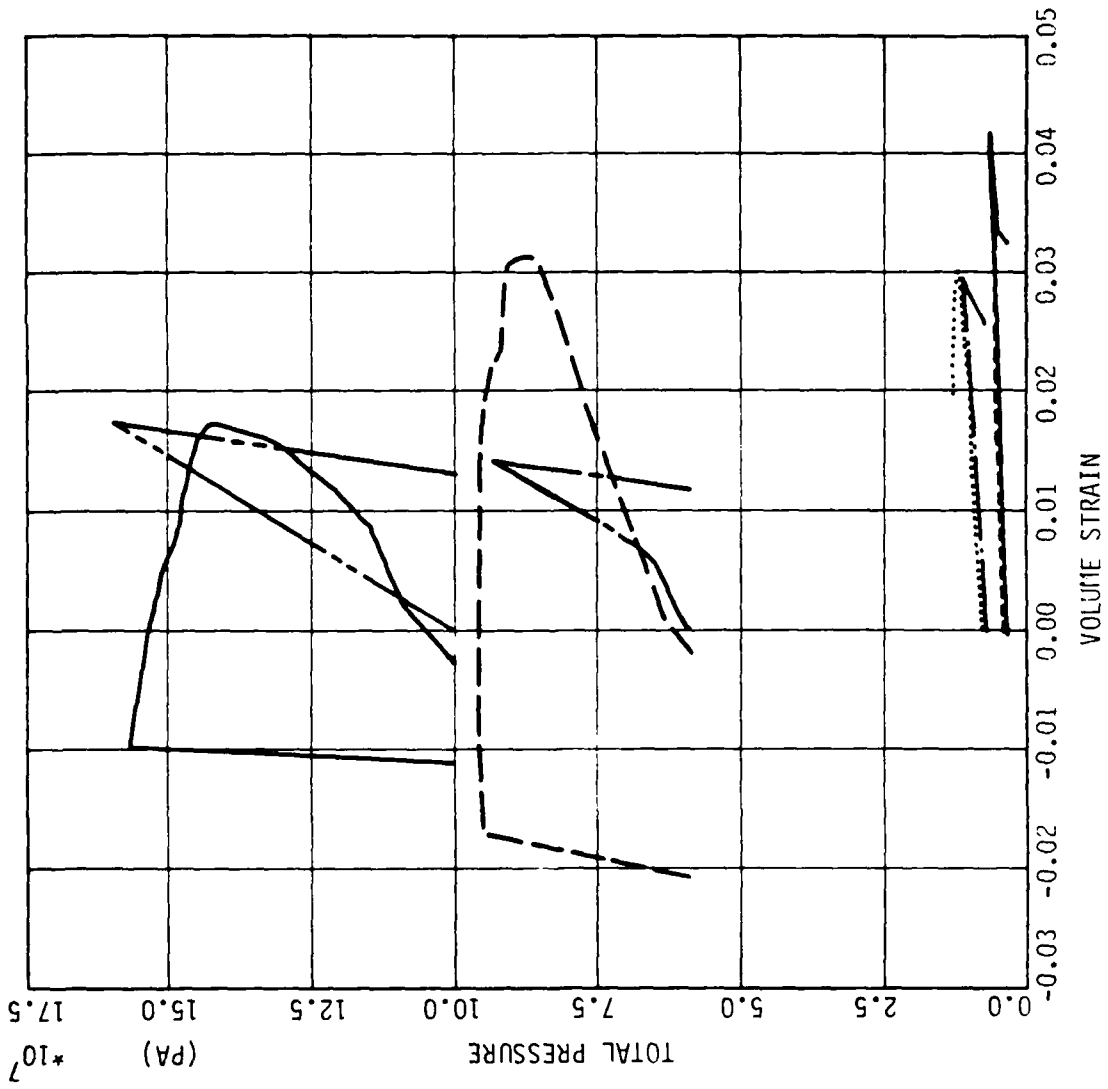


Figure 3.10. AFWL Model Exercise--Triaxial Comp(CTC)--Stress Diff. vs. Axial Strain



TEST = STANDARD TRIAXIAL TEST
 MODEL = AFWL
 MATL = DRYCARES--REMOLD
 DATA = DRYCARES/R/WES/84

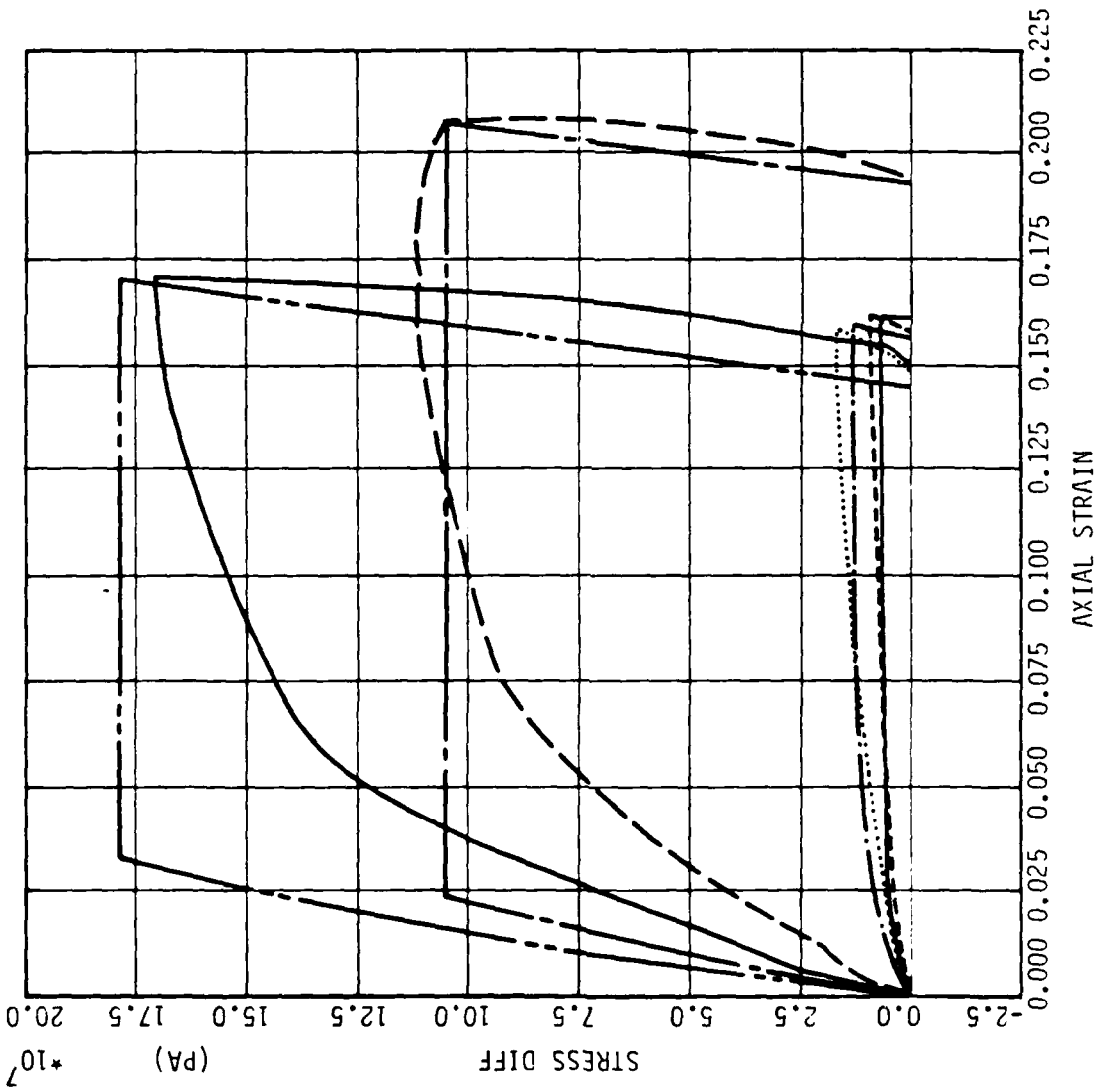
LEGEND

SIGMA3C= 3.4E6
 TEST DATA
 SIGMA3C= 7.0E6
 TEST DATA
 SIGMA3C= 58.8E6
 TEST DATA
 SIGMA3C= 100.0E6
 TEST DATA

Figure 3.11. AFWL Model Exercise--Triaxial Comp (CTC)--Pressure vs. Volumetric Strain

is independent of shear. The detailed evaluation of the modified AFWL engineering model is presented in Appendix V.6.

The effective stress cap model sacrifices some analytical and computational simplicity for a more accurate representation of soil behavior than provided by simpler models. The main advantage of the cap model is accuracy in representing most aspects of soil stress-strain behavior. The main disadvantages are mathematical complexity, the large number of material parameters required, the amount of trial and error based on experience needed to determine the parameters, inability to predict dilatancy prior to shear failure, and an oversimplified approach to undrained response analysis. Figures (3.12) and (3.13) show the cap model's shear and volumetric response in triaxial compression. Agreement between computed and measured shear response is good at the two lower confining pressures, and fair at the two higher confining pressures. Below the shear failure surface the hypoelastic-plastic volumetric response depends only on the octahedral normal stress, and the hypoelastic shear response depends only on the octahedral shear stress. These two relations determine the value of Young's modulus in Figure (3.12), and therefore strongly influence the degree of agreement between computed and measured triaxial compression shear response prior to shear failure. Because the hypoelastic-plastic volumetric stress-strain curve is independent of shear strain, the cap model predicts no dilatancy prior to shear failure, and therefore the agreement between computed and measured triaxial compression volumetric response is not good. The detailed evaluation of the cap model is presented in Appendix V.7.

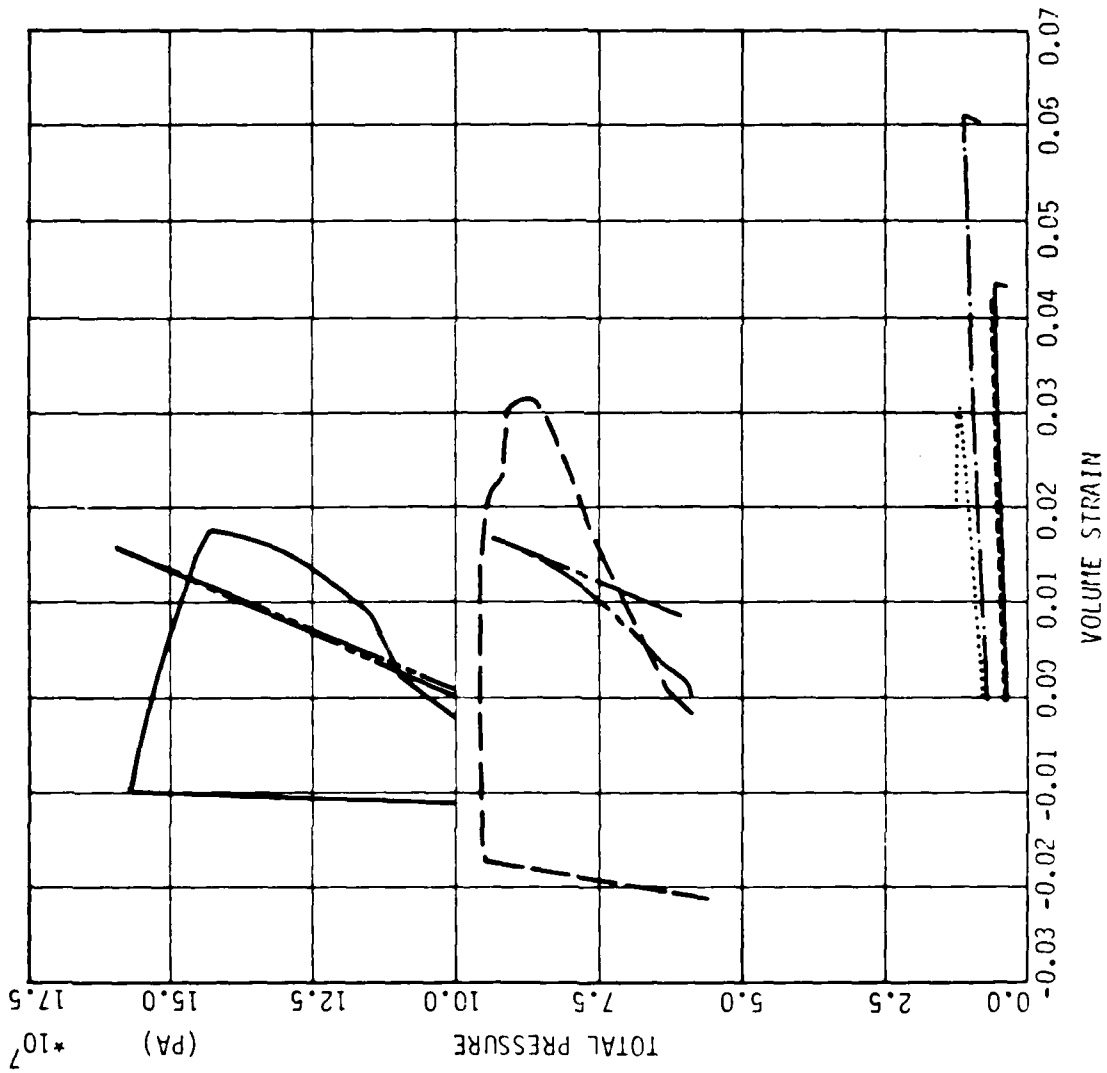


TEST = STANDARD TRIAXIAL TEST
 MODEL = CAP
 MATL = DRYCARES--REMOLD
 DATA = DRYCARES/WES/84

LEGEND

SIGMA3C= 3.4E6
TEST DATA
SIGMA3C= 7.0E6
TEST DATA
SIGMA3C= 58.8E6
TEST DATA
SIGMA3C=100.0E6
TEST DATA

Figure 3.12. Cap Model Exercise--Triaxial Comp(CTC)--Stress Diff. vs. Axial Strain



TEST = STANDARD TRIAXIAL TEST
 MODEL = CAP
 MATL = DRYCARES--REMOLD
 DATA = DRYCARES/WES/84

LEGEND

SIGMA3C= 3.4E6
 TEST DATA

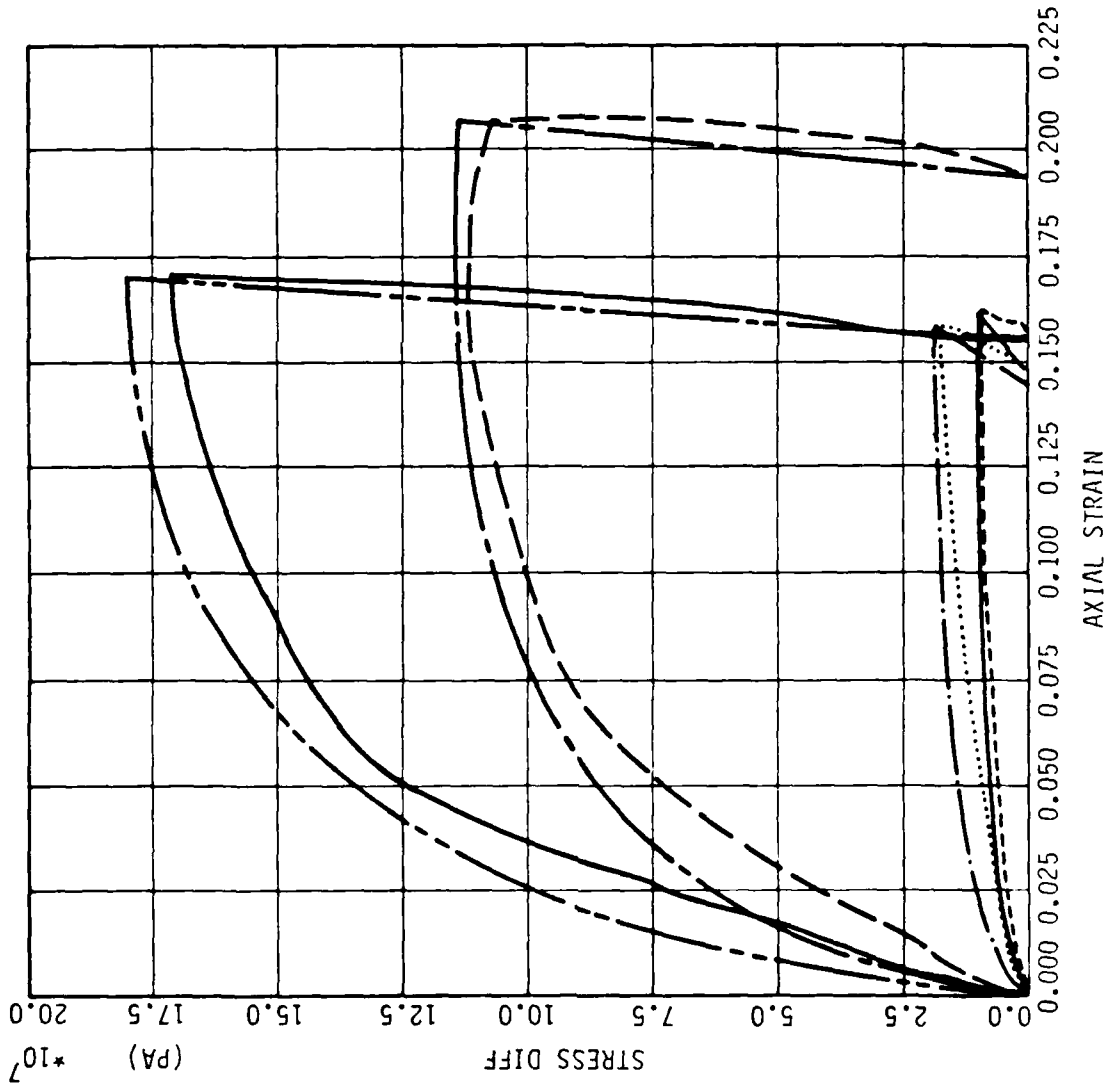
 SIGMA3C= 7.0E6
 TEST DATA

 SIGMA3C= 58.8E6
 TEST DATA

 SIGMA3C=100.0E6
 TEST DATA

Figure 3.13. Cap Model Exercise--Triaxial Comp(CTC)--Pressure vs. Volumetric Strain

The Lade model is an elastoplastic model with two yield surfaces. One, called the expansive yield surface, is bullet shaped with its nose at the origin in stress space. The other, called the collapse yield surface, is spherical with its center at the origin. Both yield surfaces harden in response to the corresponding plastic work, and the expansive yield surface also softens when the corresponding plastic work exceeds a certain value. The collapse yield surface is associative and the expansive yield surface nonassociative. The main advantage of the Lade model is accuracy in representing most aspects of soil stress-strain behavior. The model exhibits nonlinear, inelastic, dilatant behavior in both shear and compression even at small strains, and the expansive yield surface has a non-circular octahedral cross-section. The main disadvantages of the Lade model are possible underprediction of compressibility under the influence of shear at small strains, overprediction of dilatancy at large strains, lack of flexibility in matching true triaxial shear strength data in the octahedral plane, lack of a device to prevent negative plastic work, and possible instability and lack of uniqueness due to strain softening of the expansive yield surface. Figures (3.14) and (3.15) show the Lade model's shear and volumetric response in triaxial compression. Agreement between computed and measured shear response is excellent. Agreement between computed and measured volumetric response is good at the highest confining pressure, but dilatancy overprediction worsens as the initial confining pressure decreases. The detailed evaluation of the Lade model is presented in Appendix V.8. Inspection of Table 3.1 reveals the Lade model to have the highest number of favorable ratings in the ten evaluation areas.

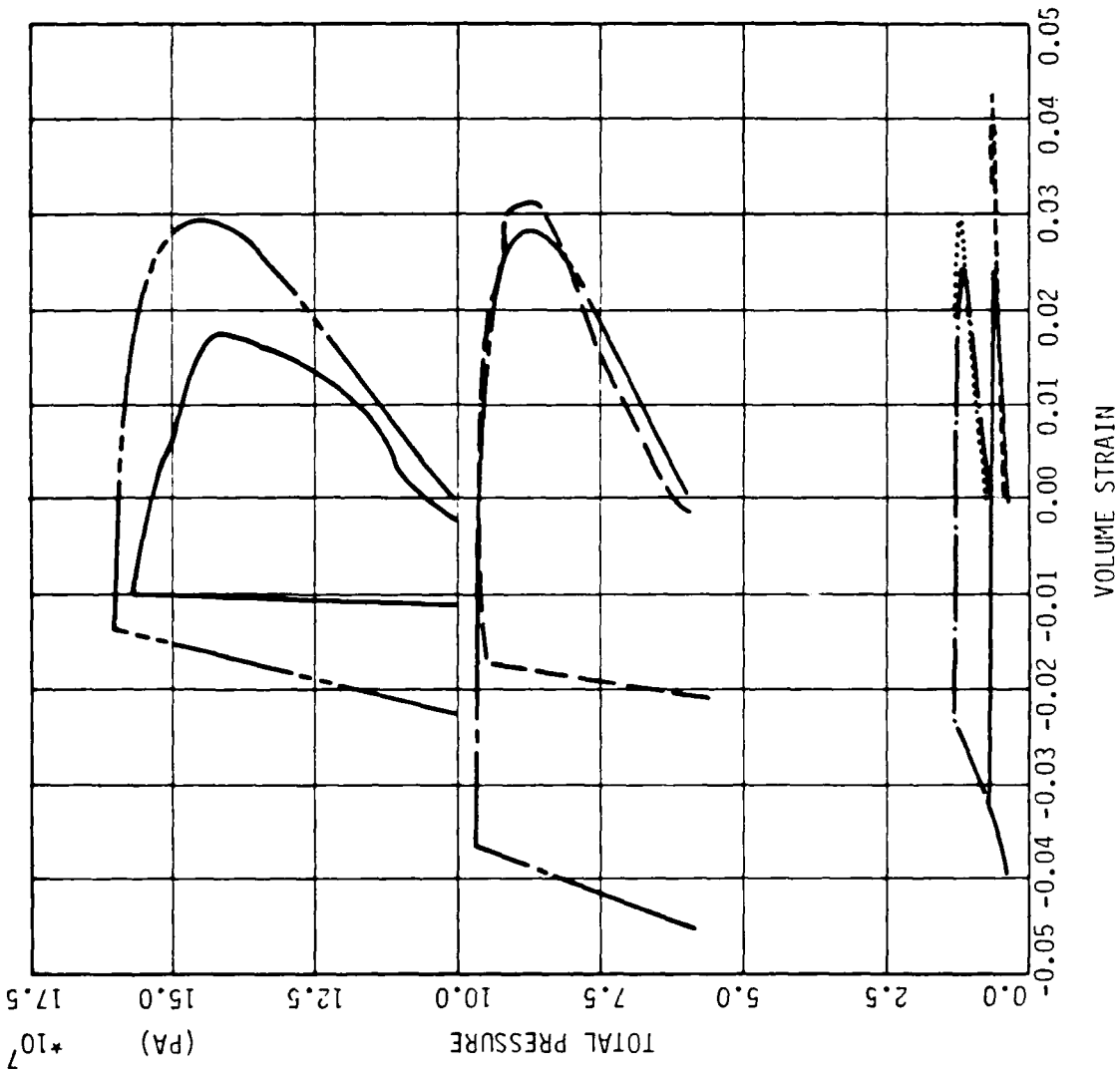


TEST = STANDARD TRIAXIAL TEST
 MODEL = LADE
 MATL = DRYCARES--REMOLD
 DATA = DRYCARES/WES/84

LEGEND

SIGMA3C= 3.4E6
 TEST DATA
 LADE
 SIGMA3C= 7.0E6
 TEST DATA
 LADE
 SIGMA3C= 58.8E6
 TEST DATA
 LADE
 SIGMA3C=100.0E6
 TEST DATA
 LADE

Figure 3.14. Lade Model Exercise--Triaxial Comp(CTC)--Stress Diff. vs. Axial Strain



TEST = STANDARD TRIAXIAL TEST
 MODEL = LADE
 MATL = DRYCARES--REMOLED
 DATA - DRYCARES/RWES/84

LEGEND
 SIGMA3C= 3.4E6
 TEST DATA
 SIGMA3C= 7.0E6
 TEST DATA
 SIGMA3C= 58.8E6
 TEST DATA
 SIGMA3C=100.0E6
 TEST DATA

Figure 3.15. Lade Model Exercise--Triaxial Comp(CTC)--Pressure vs. Volumetric Strain

3.4 Comparative Evaluation

The ten evaluation criteria used in Table 3.1 consider general, but not detailed stress-strain response, and the brief discussions of stress-strain response in Section 3.3 focus mainly on triaxial compression. This is because the triaxial compression test is well understood and involves both deformation and strength response. However, it is also necessary to compare the detailed stress-strain response of several existing models over a wide range of loading conditions, because the purpose of the models is to yield accurate detailed stress-strain response for a wide range of complex dynamic loading conditions of interest to the Air Force.

Figures (3.16) through (3.22) show the axial stress versus axial strain response in uniaxial compression of the elastic, viscoelastic, hyperbolic, elastic-perfectly plastic, AFWL engineering, cap, and Lade models. The uniaxial compression test data curve was used to determine some of the AFWL engineering and cap model parameters, so it is not surprising that the AFWL engineering model gives the best fit, the cap model the next best, and the Lade model the next best. After shear failure, the Lade model's response is unreasonable because of too rapid strain softening. The other four models yield generally unreasonable uniaxial compression stress-strain responses, which could probably be improved somewhat by fitting them to the uniaxial compression curve, but at the expense of reasonableness of some other response.

Figures (3.23) through (3.28) show eight axially symmetric stress path responses for the elastic, hyperbolic, elastic-perfectly plastic, AFWL engineering, cap, and Lade models. The eight stress paths enforce

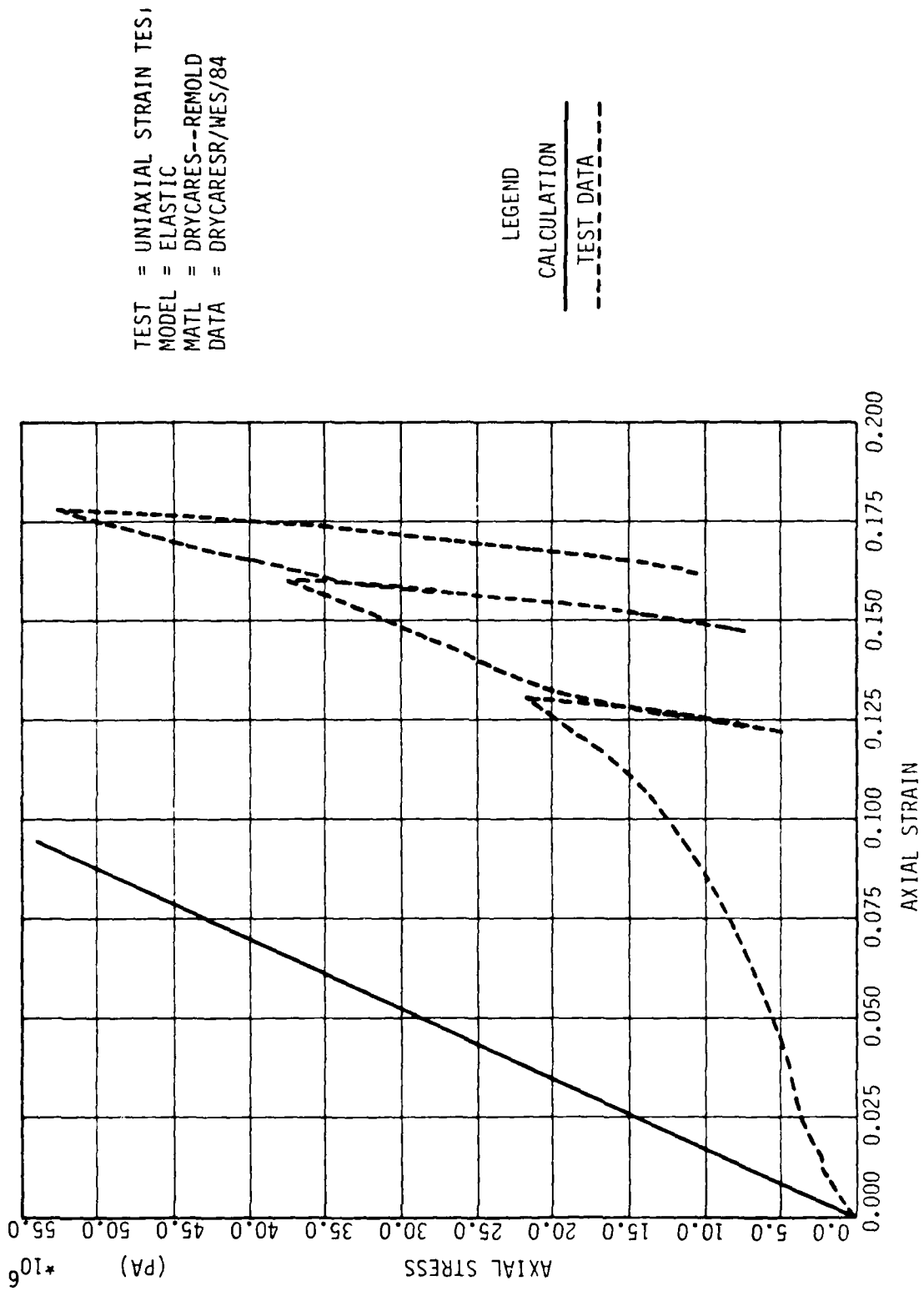
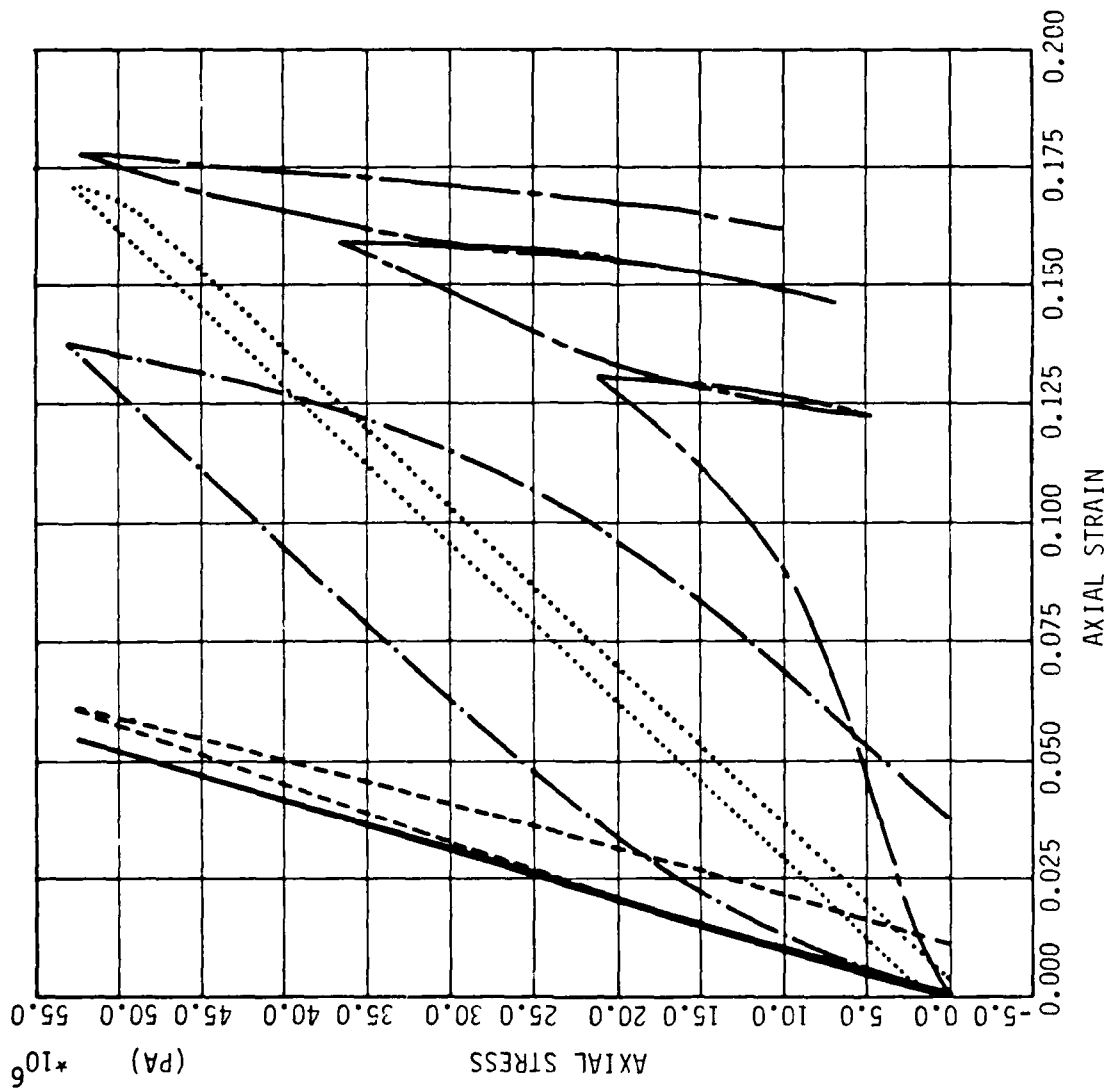


Figure 3.16. Elastic Model Exercise--Uniax Strain(UXC)--Tot Ax1 Stress vs. Ax1 Strain



TEST = UNIAXIAL STRAIN
 MODEL = VISCO
 MATL = DRYCARES--REMOLD
 DATA = DRYCARES/WE/84

LEGEND

- STRAIN-RATE=100
- STRAIN-RATE=10.
- STRAIN-RATE=1.0
- STRAIN-RATE=0.1
- TEST DATA

Figure 3.17. Visco Model Exercise--Uniaxial Strain--Tot Ax1 Stress vs. Ax1 Strain

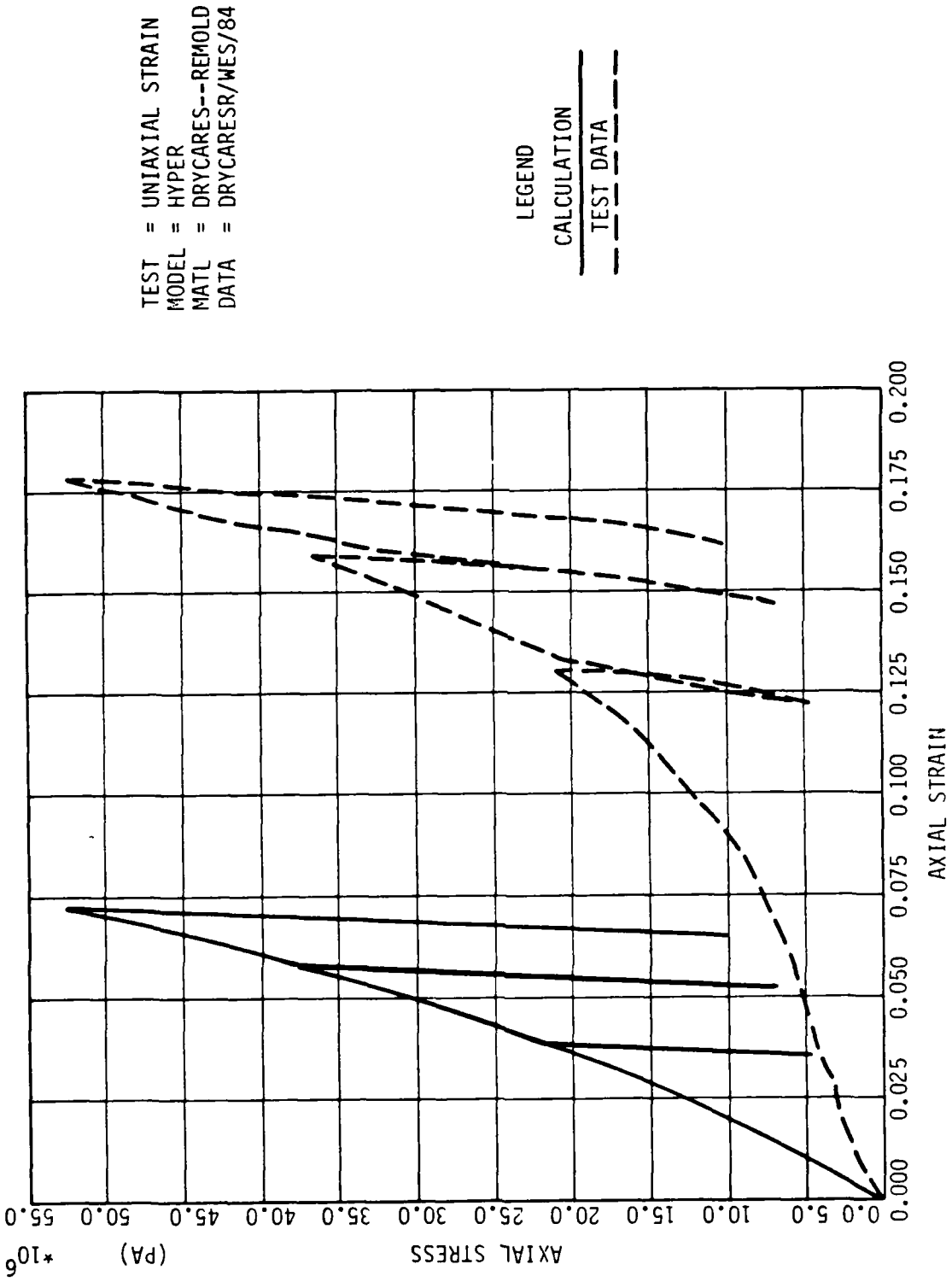
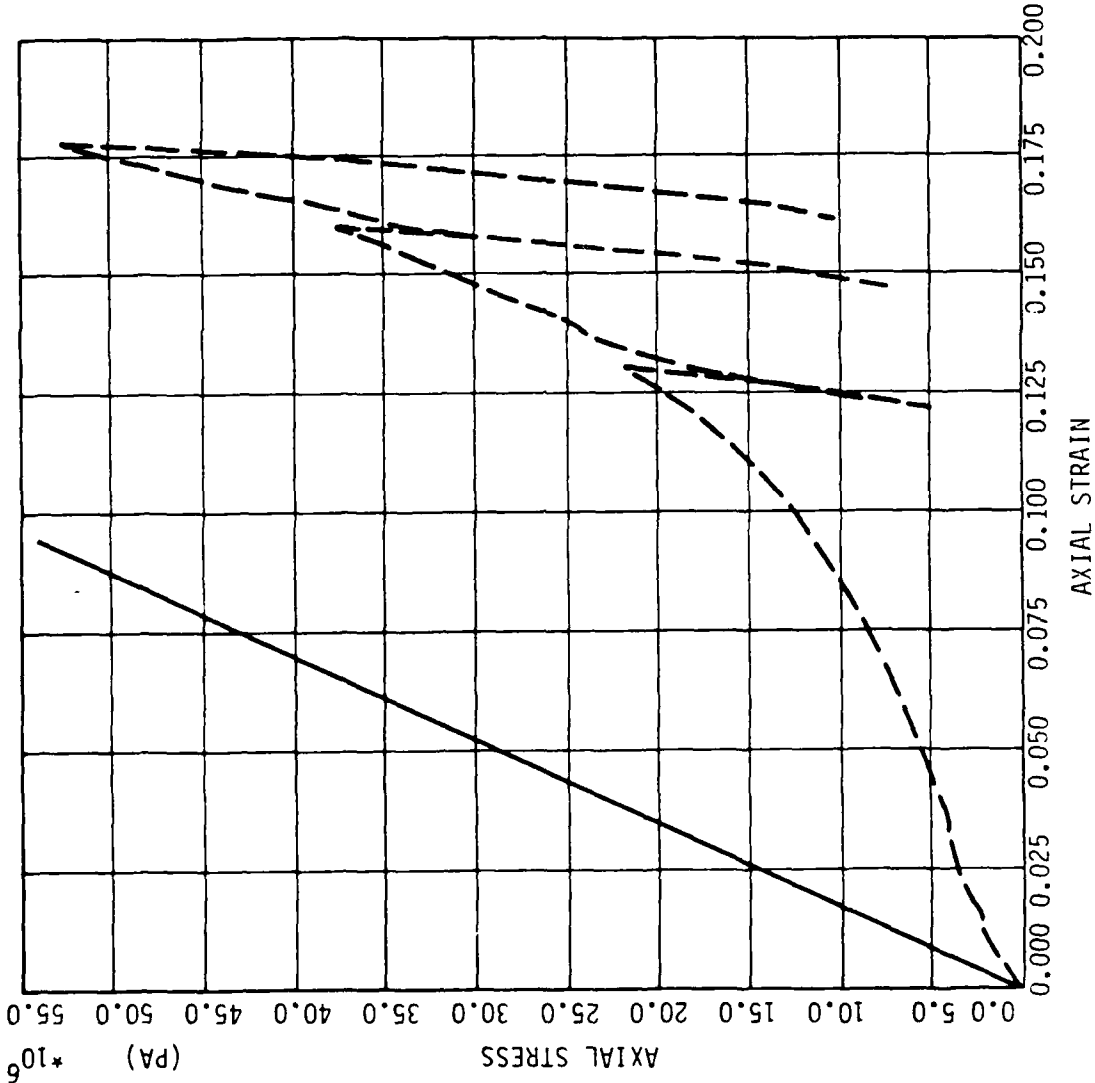


Figure 3.18. Hyperbolic Model--Uniaxial Strain(UXC)--Tot Ax1 Stress vs. Ax1 Strain



TEST = UNIAXIAL STRAIN TEST
 MODEL = ELPLA
 MATL = DRYCARES--REMOLD
 DATA = DRYCARES/WES/84

LEGEND
 _____ CALCULATION
 - - - - - TEST DATA

Figure 3.19. Elpla Model Exercise--Uniaxial Strain(UXC)--Tot Axl Stress vs. Axl Strain

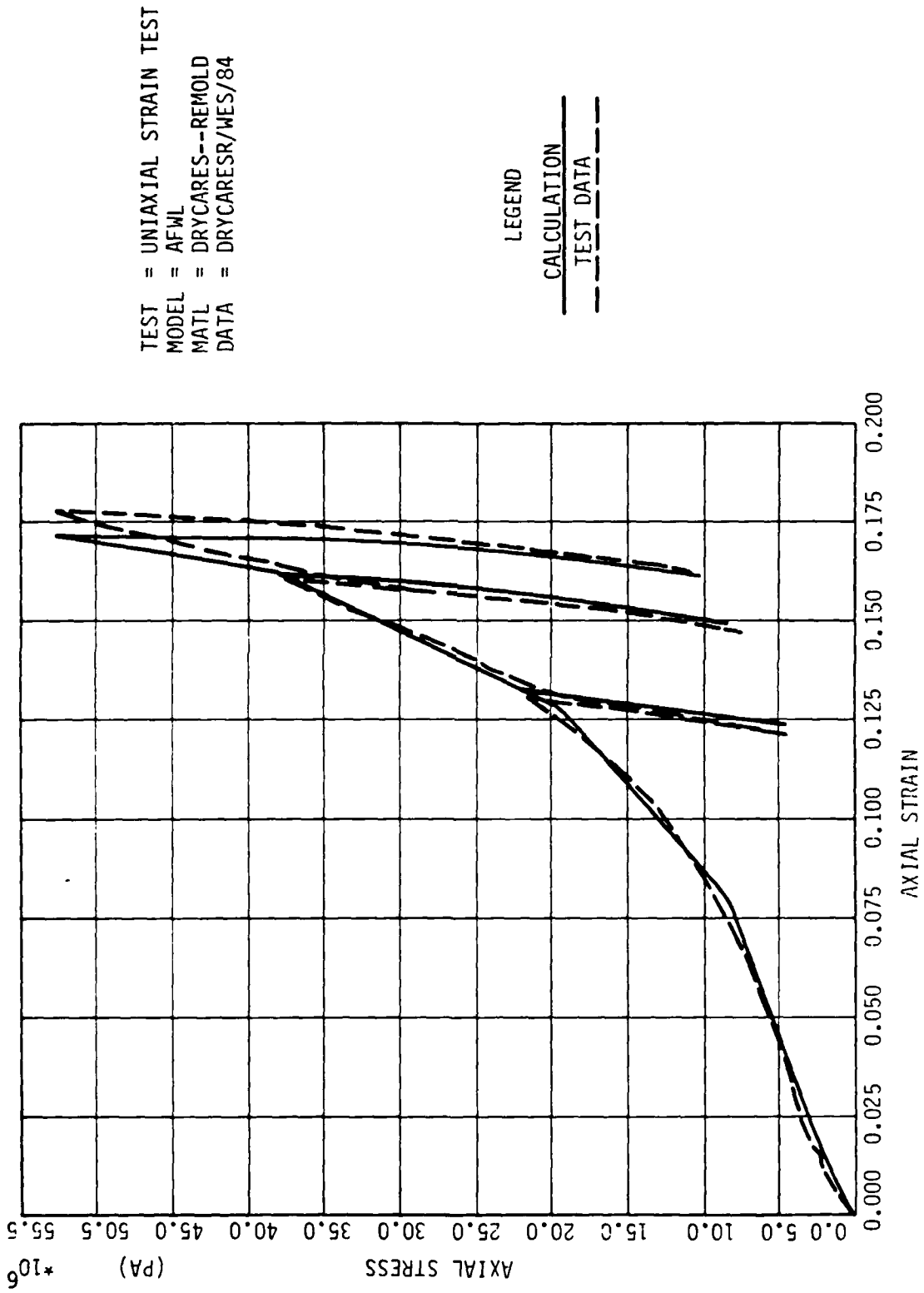


Figure 3.20. AFWL Model Exercise--Uniax Strain(UXC)--Tot Ax1 Stress vs. Ax1 Strain

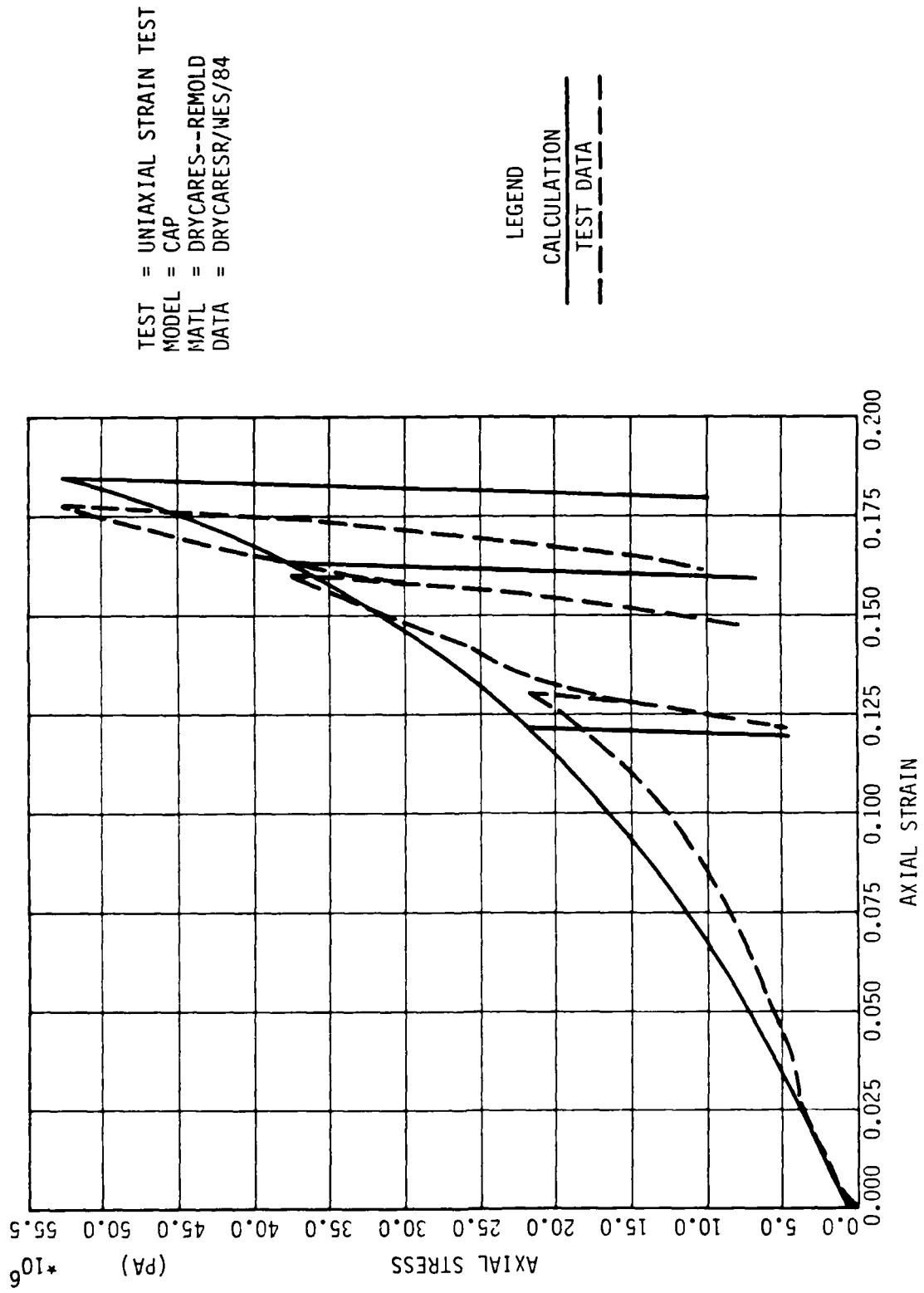


Figure 3.21. Cap Model Exercise--Uniax Strain(UXC)--Tot Ax1 Stress vs. Ax1 Strain

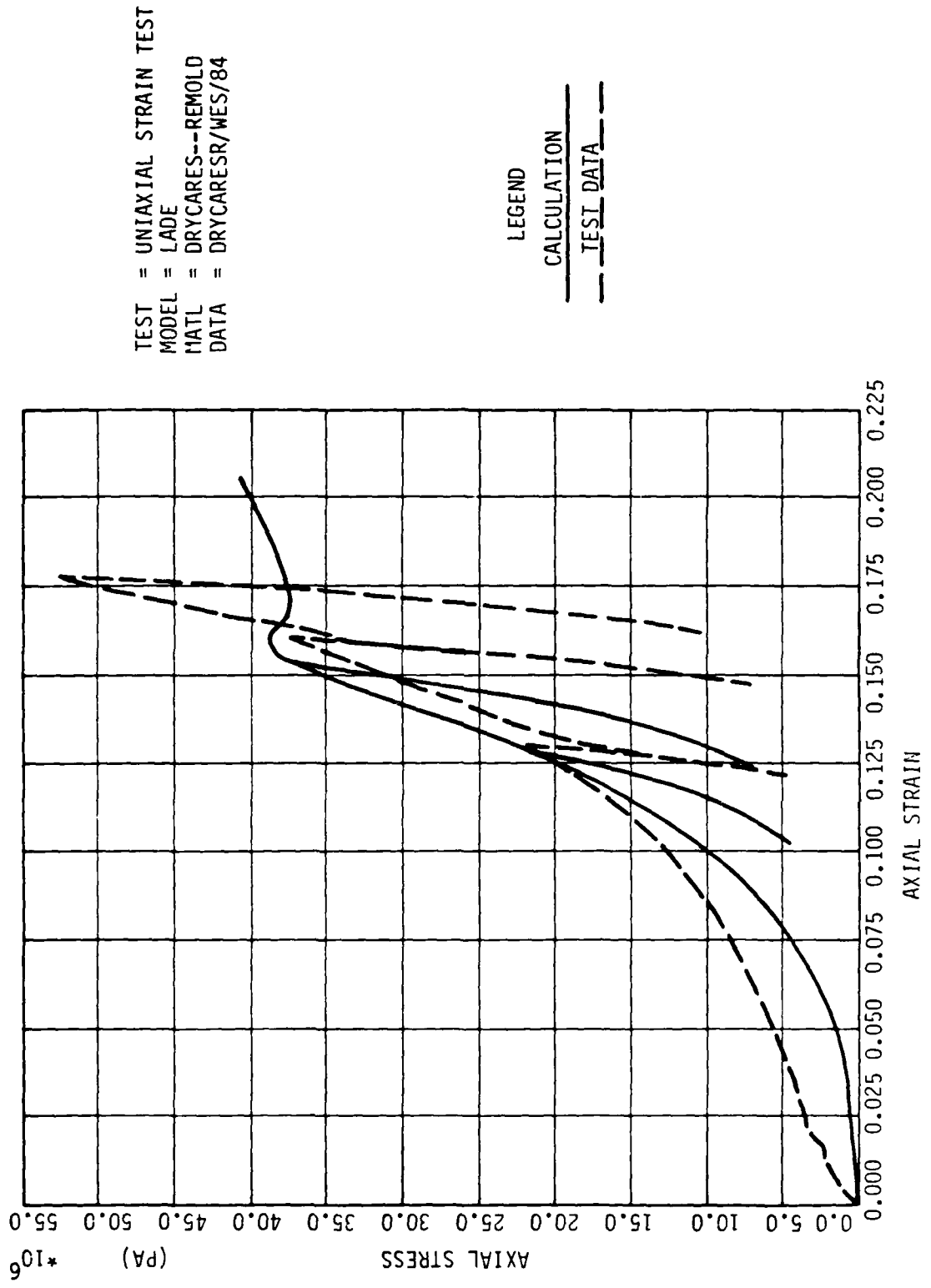


Figure 3.22. Lade Model Exercise--Uniax Strain(UXC)--Tot Ax1 Stress vs. Ax1 Strain

TEST = STANDARD TRIAXIAL
 MODEL = ELASTIC
 MATL = DRYCARES--REMOLD

LEGEND

ISO EXTEN	---
RTC	---
PSC	---
CTC	---
ISO COMP	---
RTE	---
PSE	---
CTE	---

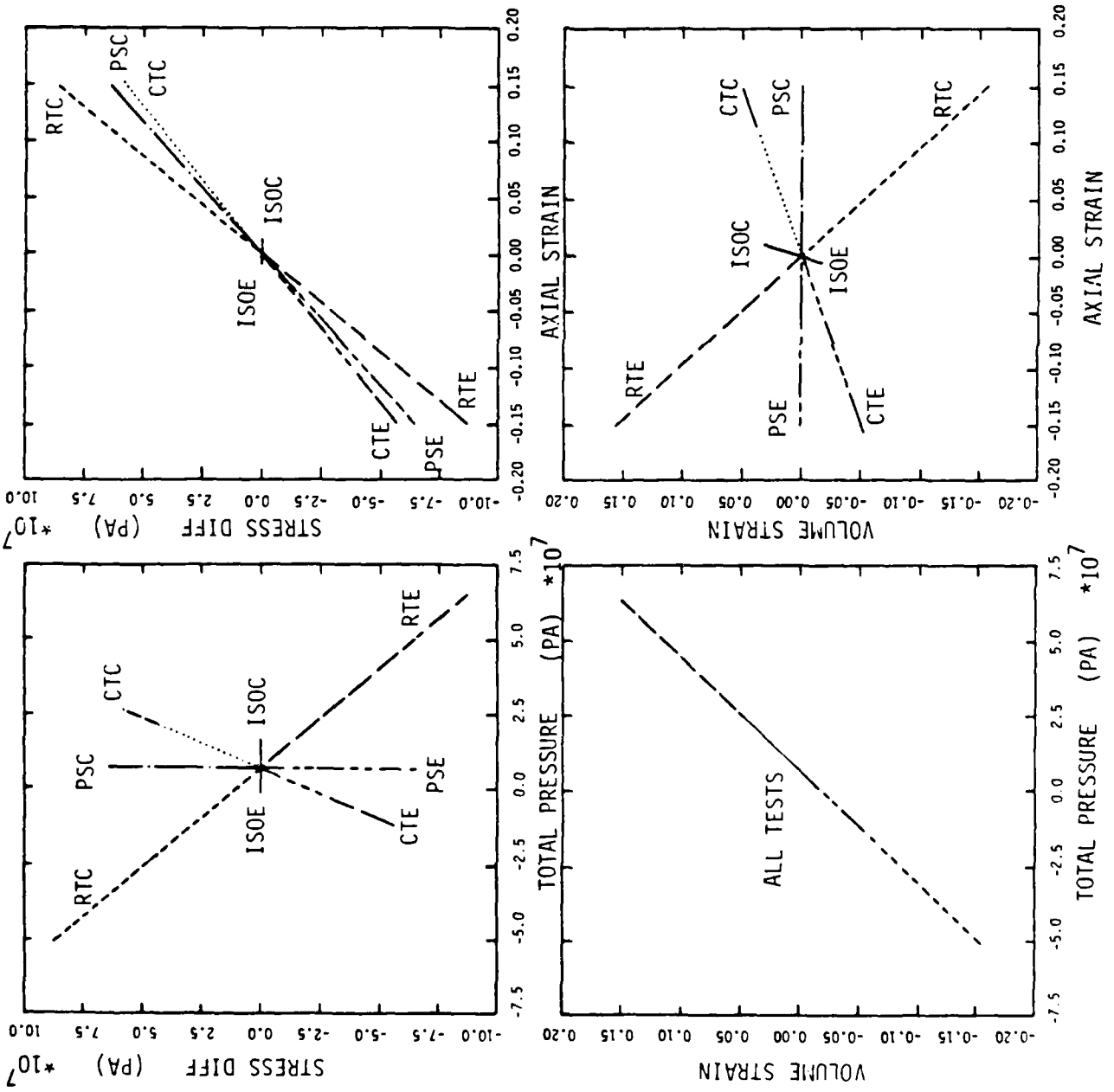
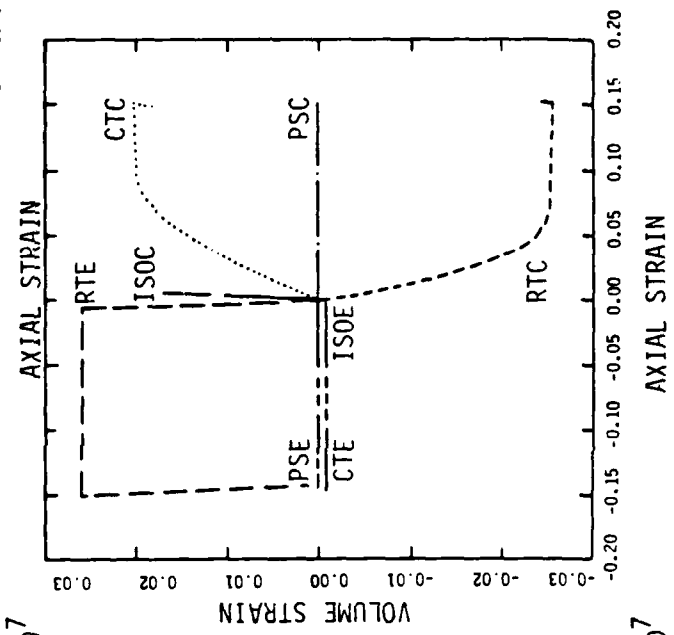
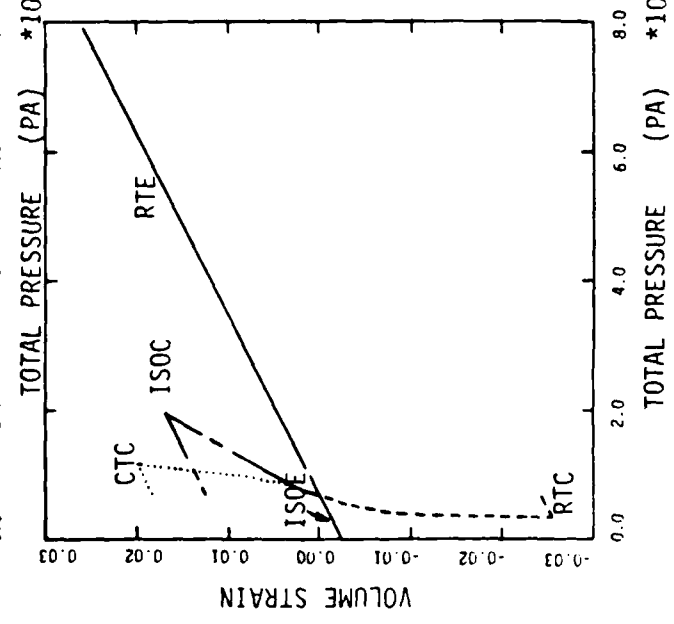
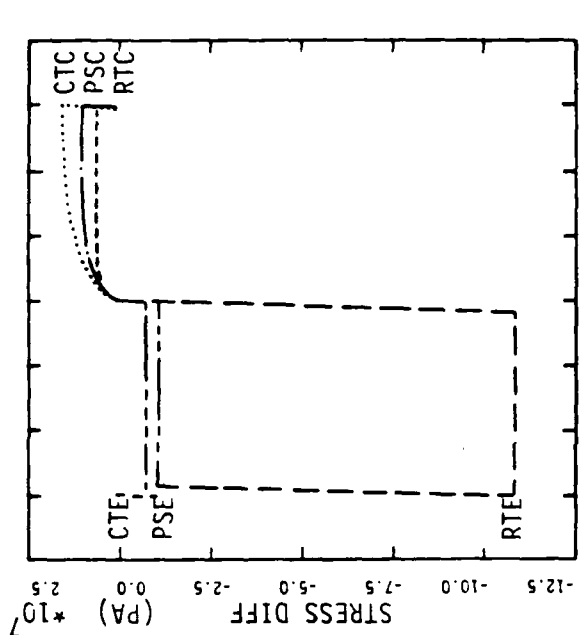
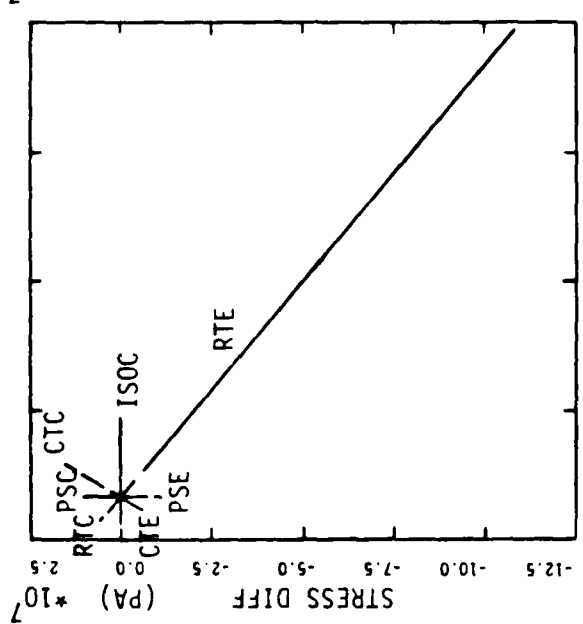


Figure 3.23. Elastic Model Behavior Summary (S3C=7.1MIPA) --SDIFF/P/ EV/EA ANALYSIS



TEST = STANDARD TRIAXIAL
 MODEL = HYPER
 MATL = DRYCARES--REMOLD
 DATA = DRYCARES/R/WES/84

LEGEND

ISO_EXTEN
 RTC ---
 PSC ---
 CTC
 ISO_COMP
 RTE ---
 PSE ---
 CTE ---

Figure 3.24. Hyperbolic Model Behavior Summary (7.1MPa)--SDIFF/P/EV/EA ANALYSIS

TEST = STANDARD TRIAXIAL
 MODEL = ELPLA
 MATL = DRYCARES--REMOLD

LEGEND
 ISO_EXTEN
 RTC
 PSC
 CTC
 ISO_COMP
 RTE
 PSE
 CTE

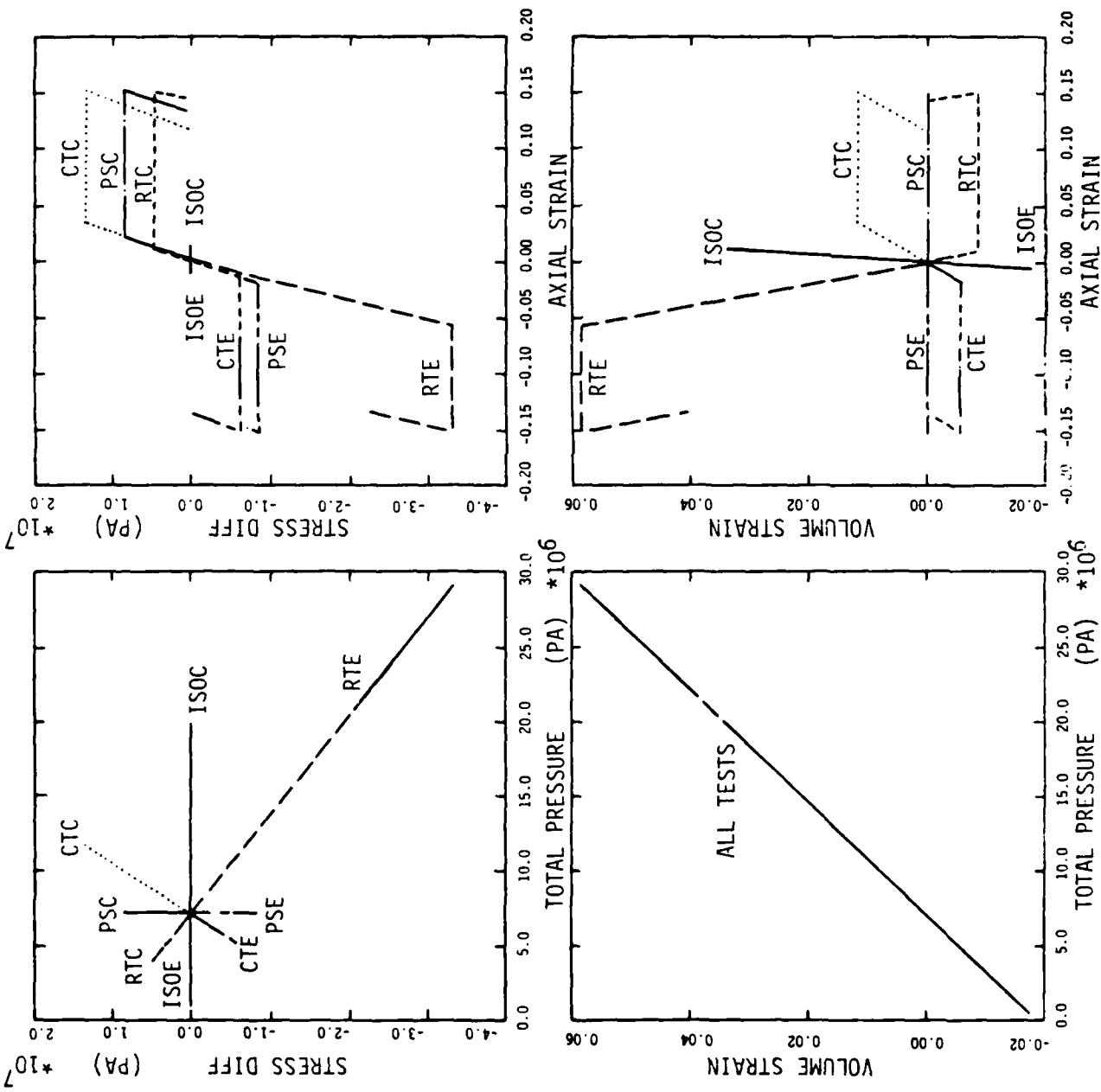


Figure 3.25. Elastic-Plastic Model Behavior Summary (S3C=7.1MPa) DRYCARES--REMOLD--SDIFF/P/EV/EA

TEST = STANDARD TRIAXIAL
 MODEL = AFWL
 MATL = DRYCARES--REMOLD

LEGEND

ISO EXTEN
RTC
PSC
CTC
ISO COMP
RTE
PSE
CTE

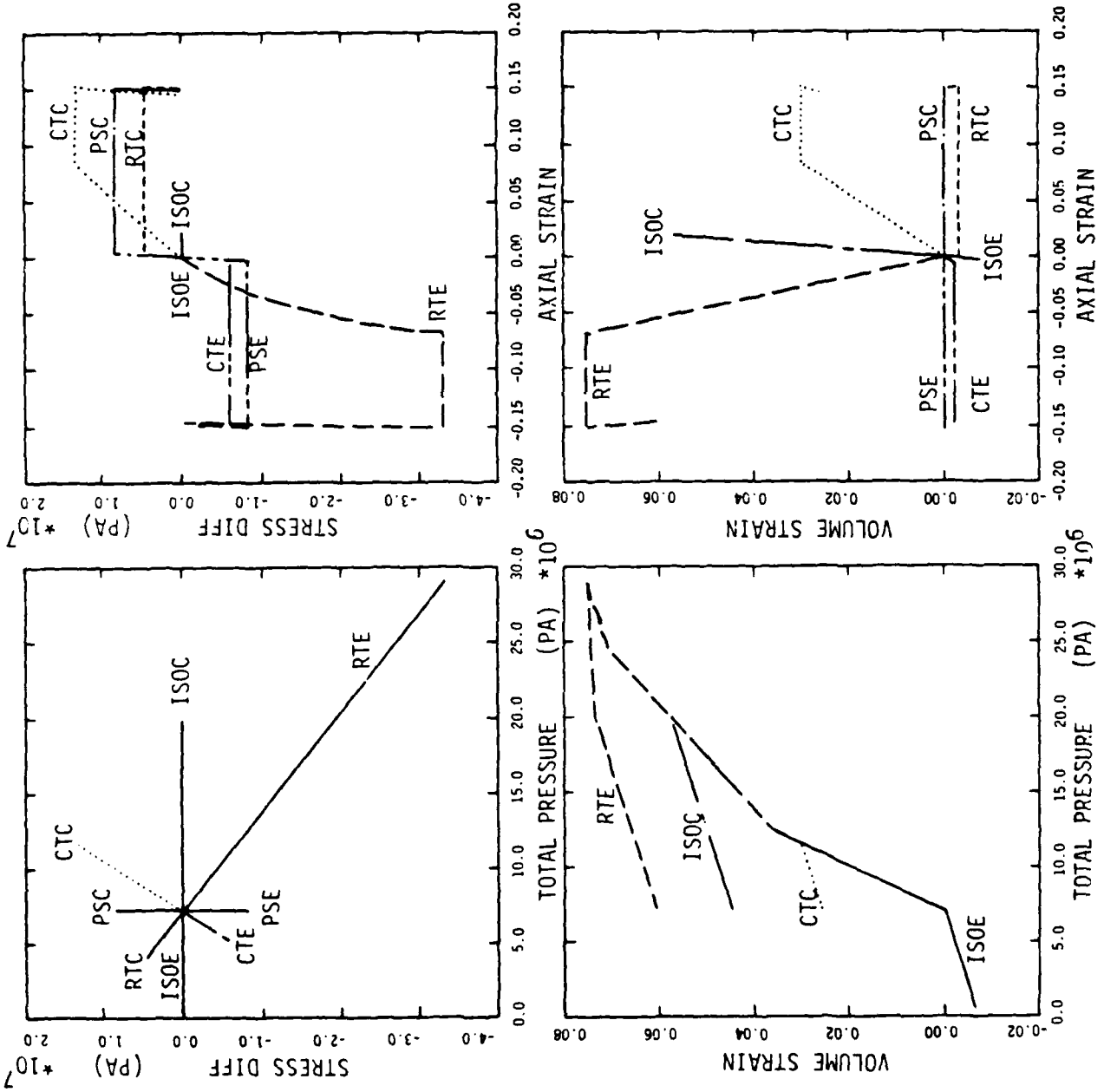
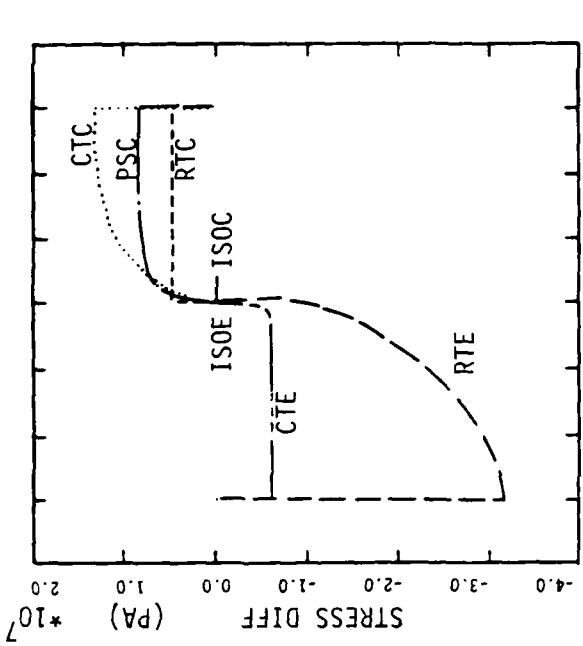
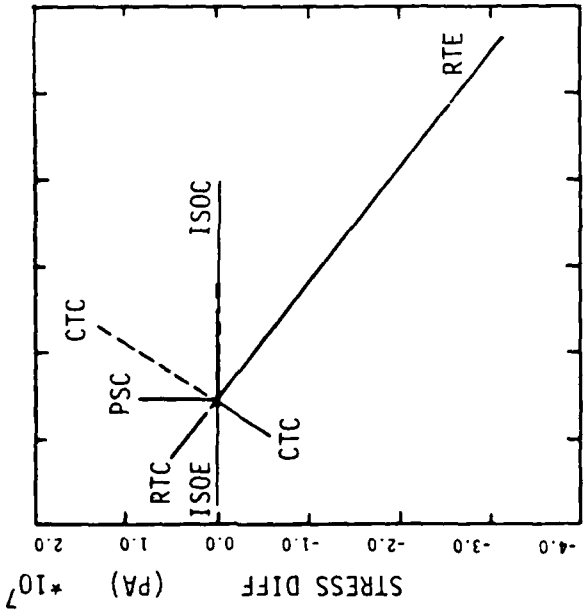


Figure 3.26. AFWL Eng Model Behavior Summary (S3C=7.1MPA)--SDIFF/P/EV/EA ANALYSIS



TEST = STANDARD TRIAXIAL
 MODEL = CAP
 MATL = DRYCARES--REMOLD

LEGEND

ISO EXTEN	---
RTC	----
PSC	-.-.-
CTC
ISO COMP	----
RTE	----
CTE	----

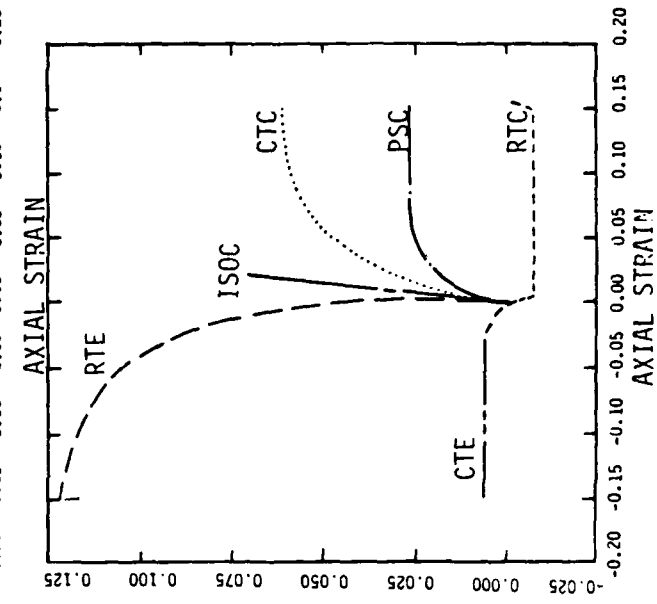
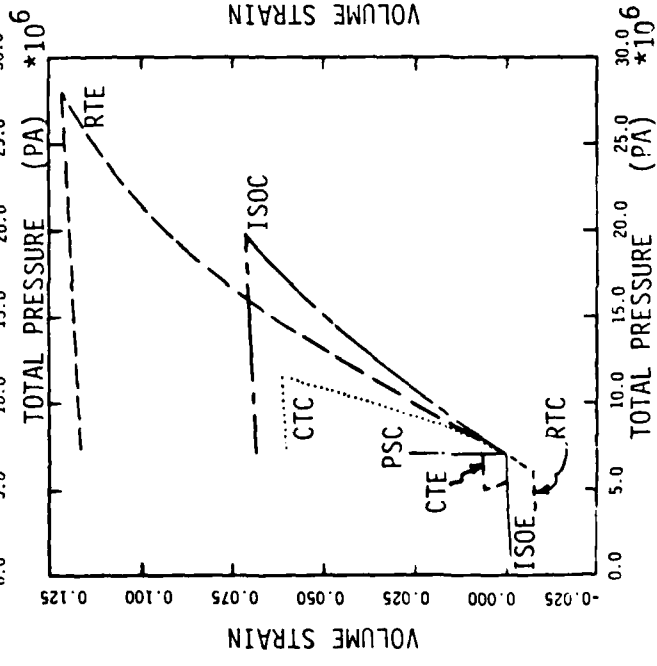


Figure 3.27. Cap Model Behavior Summary (S3C=7.1MPa)--SDIFF/P/EV/EA ANALYSIS

TEST = STANDARD TRIAXIAL
 MODEL = LADE
 MATL = DRYCARES--REMOLD
 DATA = DRYCARES/R/WES/84

LEGEND

ISO EXTEN	---
RTC	---
PSC	---
CTC	---
ISO COMP	---
RTE	---
PSE	---
CTE	---

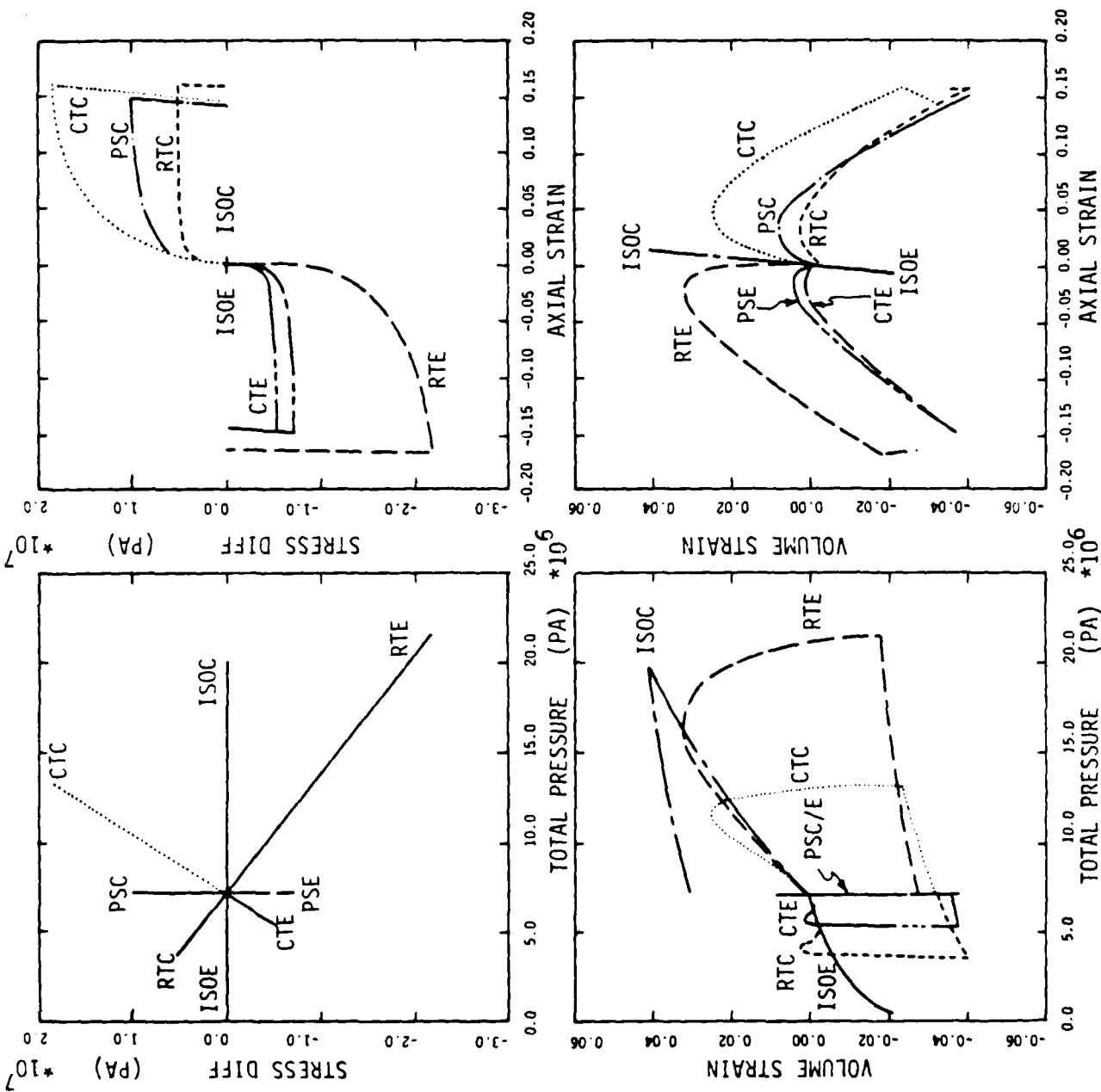


Figure 3.28. Lade Model Behavior Summary (S3C=7.1MPa)--SDIFF/P/EV/EA ANALYSIS

constant stress difference, constant mean stress, constant radial stress, and constant axial stress, in either axial compression or axial extension. These eight stress paths are shown in the upper left hand quadrant of each figure. The only model which shows a reversal of volumetric strain without a reversal of axial strain is the Lade model. Inspection of Figure (V.8.22) shows that such a reversal did occur for remolded CARES-DRY sand in triaxial compression. The multilinear character of the AFWL engineering model stress-strain plots is unsatisfying for situations other than those in which a multilinear curve has been fit to measured data. The cap model yields smooth curves, but the volumetric response is so different from measured data in triaxial compression that it might prove unreliable in a genuine two phase calculation.

Because it received the greatest number of favorable ratings with respect to the ten evaluation criteria in Table 3.1, and on the basis of the above comparative evaluation of detailed stress-strain behavior including the many plots in Appendix V, the Lade model was selected as the most promising point of departure for developing a new soil dynamic stress-strain model.

4.0 ARA CONIC MODEL

4.1 Introduction

Of the eight soil constitutive models examined in Section 3 and Appendix V, the Lade model is most appealing from three important standpoints:

- a) favorable rating with respect to seven of the ten evaluation criteria in Table 3.1;
- b) accuracy and flexibility in representing soil stress-strain behavior; and
- c) ease of developing intuition for parameter physical significance and accuracy.

Consequently ARA elected to modify the Lade model rather than create a completely new one, to develop a soil constitutive model suitable for analyzing the response of soil masses to complex dynamic loadings.

The modifications were designed to achieve the following additional desirable features:

- a) better volumetric strain response under non-isotropic loading;
 - b) greater flexibility in matching shear strength data, in both the triaxial and octahedral planes;
 - c) correct plastic mode selection based on the thermodynamically related dissipation condition that a positive plastic work increment accompany yielding;
 - d) finite, reasonable friction angle at low confining pressure;
 - e) essentially constant shear strength at high confining pressure;
- and

- f) direct (noniterative) shear strength calculation in both the triaxial and octahedral planes.

Several Lade model features have been retained:

- a) the basic model construction, i.e., two yield surfaces, one compressive and one expansive, both strain hardening, the compressive yield surface associative and the expansive yield surface nonassociative;
- b) both the compressive and expansive work hardening formulations; and
- c) the unloading/reloading elastic modulus formulation.

New features include:

- a) an ellipsoidal compressive yield surface to increase compressibility in the presence of shear deformation;
- b) a hyperbolic expansive yield surface with a triple ellipsoidal octahedral cross section, possessing a finite, adjustable slope (friction angle) at low confining pressure, essentially constant shear strength at high confining pressure, flexibility in matching both compression and extension shear strength data, a completely smooth octahedral cross section, and directly computable shear strength;
- c) enforcement of the dissipation condition;
- d) development of a polar mode check based on the dissipation condition, to determine uniquely and without trial and error which yield surfaces are active under a given state of stress and prescribed total strain increment; and

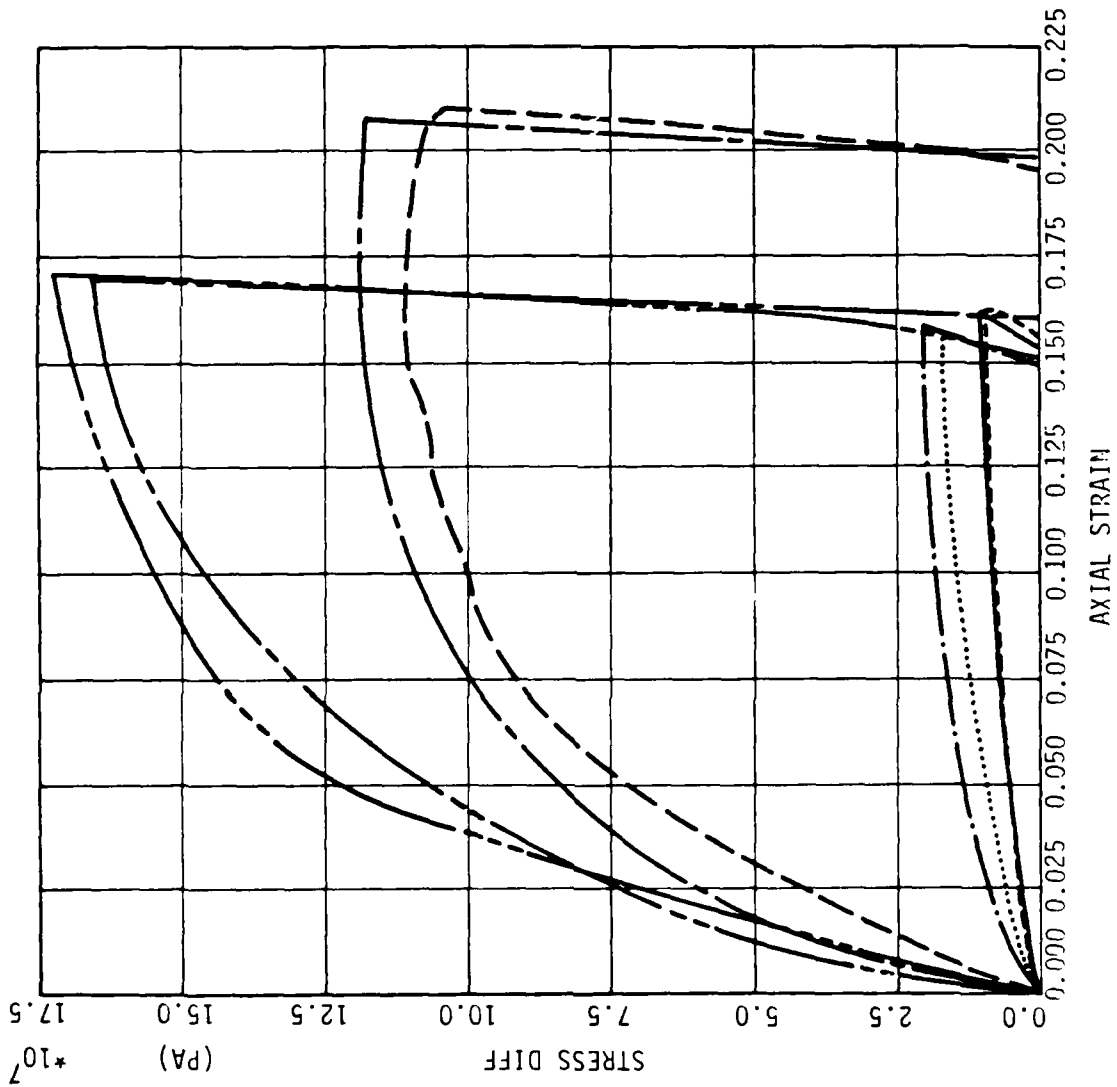
- e) determination of compressive yield surface parameters by fitting the plastic hydrostat directly (using a linear transformation) rather than having to compute compressive plastic work.

In addition, the work softening feature of the expansive hardening function may be modified or deleted in future versions of the conic model to insure uniqueness and stability, and to achieve a finite, constant shear strength at large shear strain (a non zero critical state). An unloading/reloading hysteresis feature has also been formulated but not yet coded. The model is called a conic model because all three controlling surfaces in principal stress space have both triaxial and octahedral cross-sections which are conic sections. It is also called a three invariant model because the expansive yield and potential surfaces involve three independent stress invariants: the first total stress invariant and the second and third deviator stress invariants. The ARA conic model rates favorably with respect to all ten evaluation criteria in Table 3.1.

At present the conic model uses the incremental stiffness formulation developed in Appendix G, rather than a trial and error yield surface violation correction procedure such as that discussed in Appendix S for the cap model. However, the initial strain increments needed for numerical stability of the conic model are very small (of the order of 10^{-6}), and a trial and error correction procedure may be an economic necessity when using it to solve dynamic or static boundary value problems.

4.2 Individual Evaluation

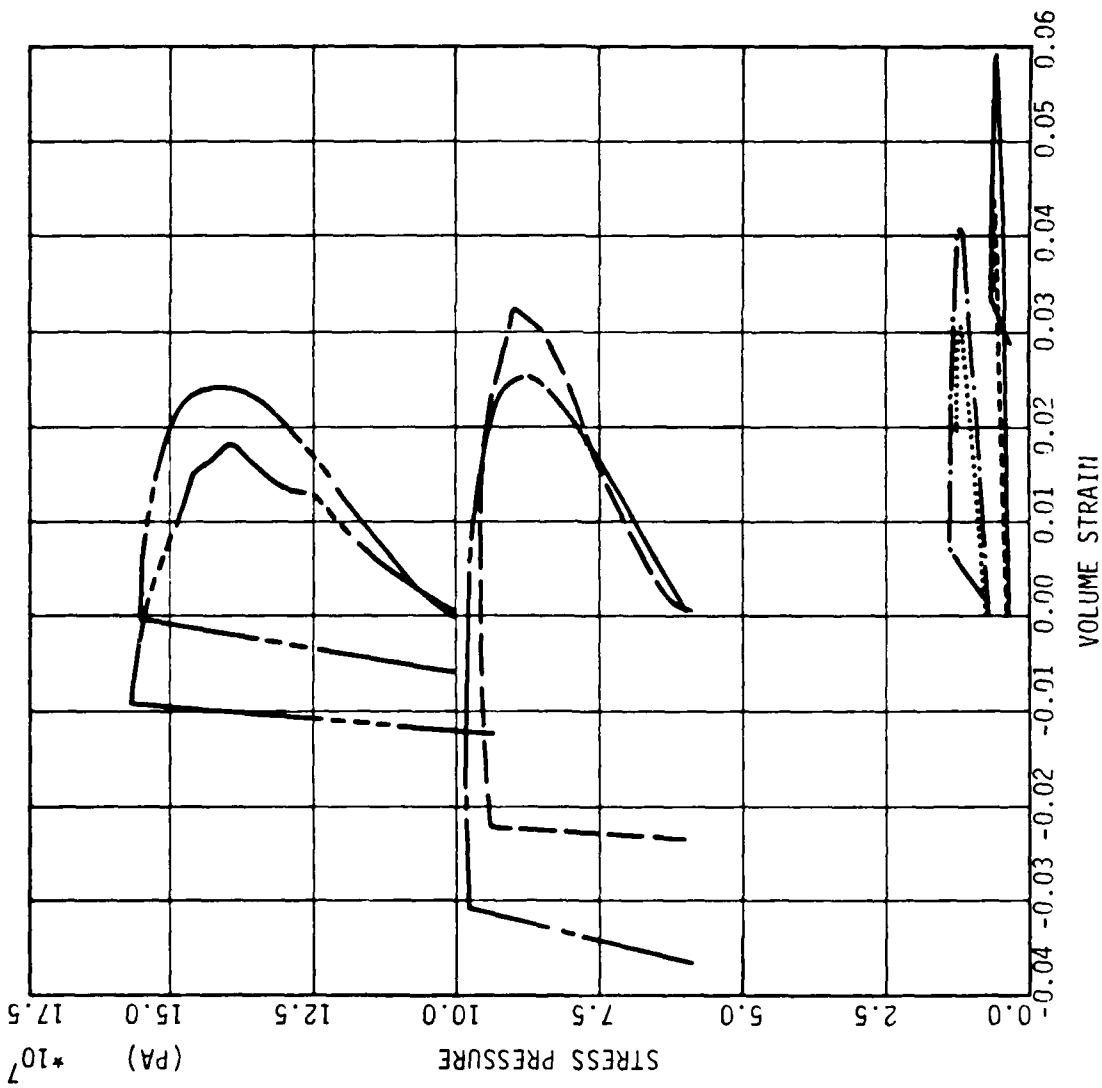
Figures (4.1) and (4.2) show the ARA conic model's shear and volumetric response in triaxial compression. Agreement between computed and measured shear response is excellent, and agreement between computed



TEST = STANDARD TRIAXIAL
 MODEL = ARA1
 MATL = DRYCARES---REMOLD
 DATA = DRYCARES/WES/84

LEGEND
 _____ SIGMA3C= 3.4E6
 - - - - - TEST DATA
 _____ SIGMA3C= 7.0E6
 TEST DATA
 _____ SIGMA3C= 58.8E6
 - - - - - TEST DATA
 _____ SIGMA3C=100.0E6
 - - - - - TEST DATA

Figure 4.1. ARA Model Exercise--Triaxial Comp(CTC)--Stress Diff vs. Axial Strain



TEST = STANDARD TRIAXIAL
 MODEL = ARA1
 MATL = DRYCARES--REMOLD
 DATA = DRYCARES/R/WES/84

LEGEND

SIGMA3C= 3.4E6
 TEST DATA
 SIGMA3C= 7.0E6
 TEST DATA
 SIGMA3C= 58.8E6
 TEST DATA
 SIGMA3C= 100.0E6
 TEST DATA

Figure 4.2. ARA Model Exercise--Triaxial Comp(CTC)--Pressure vs. Volumetric Strain

and measured volumetric response is better than that for the Lade model, because the ARA conic model overpredicts dilatancy at low confining pressure, and underpredicts it at high confining pressure. Figure (4.3) shows the ARA conic model's axial stress versus axial strain response in uniaxial compression. The ARA conic model does not have the same shear failure/strain softening problem displayed by the Lade model in Figure (3.22) and (V.8.38), and agreement between computed and measured uniaxial response is comparable to that of the cap model but not as good as that of the AFWL engineering model. Note that the CARES DRY uniaxial compression tests involved unloading to an isotropic stress condition rather than to a zero axial stress condition. Therefore, the test data do not show the rapid decrease of axial strain as axial stress approaches zero which characterizes some uniaxial test data. Consequently, no special attention was given to this aspect of stress-strain response when formulating the ARA conic model. The detailed development of the ARA conic model is presented in Appendix W.

4.3 Comparative Evaluation

Figures (4.4) through (4.11) compare the ARA conic model's stress-strain response with that of the AFWL engineering, cap, and Lade models, for various simple and complex load paths. Figure (4.4) shows the models' triaxial compression and extension responses. The ARA conic model shows the highest compression and next lowest extension strength, dilates less in compression than does the Lade model, and shows the greatest volumetric compression in extension. The test data in Figure (W.28) shows more volumetric compression in triaxial extension than does any of the nine models. Figure (4.5) shows the models' constant axial stress

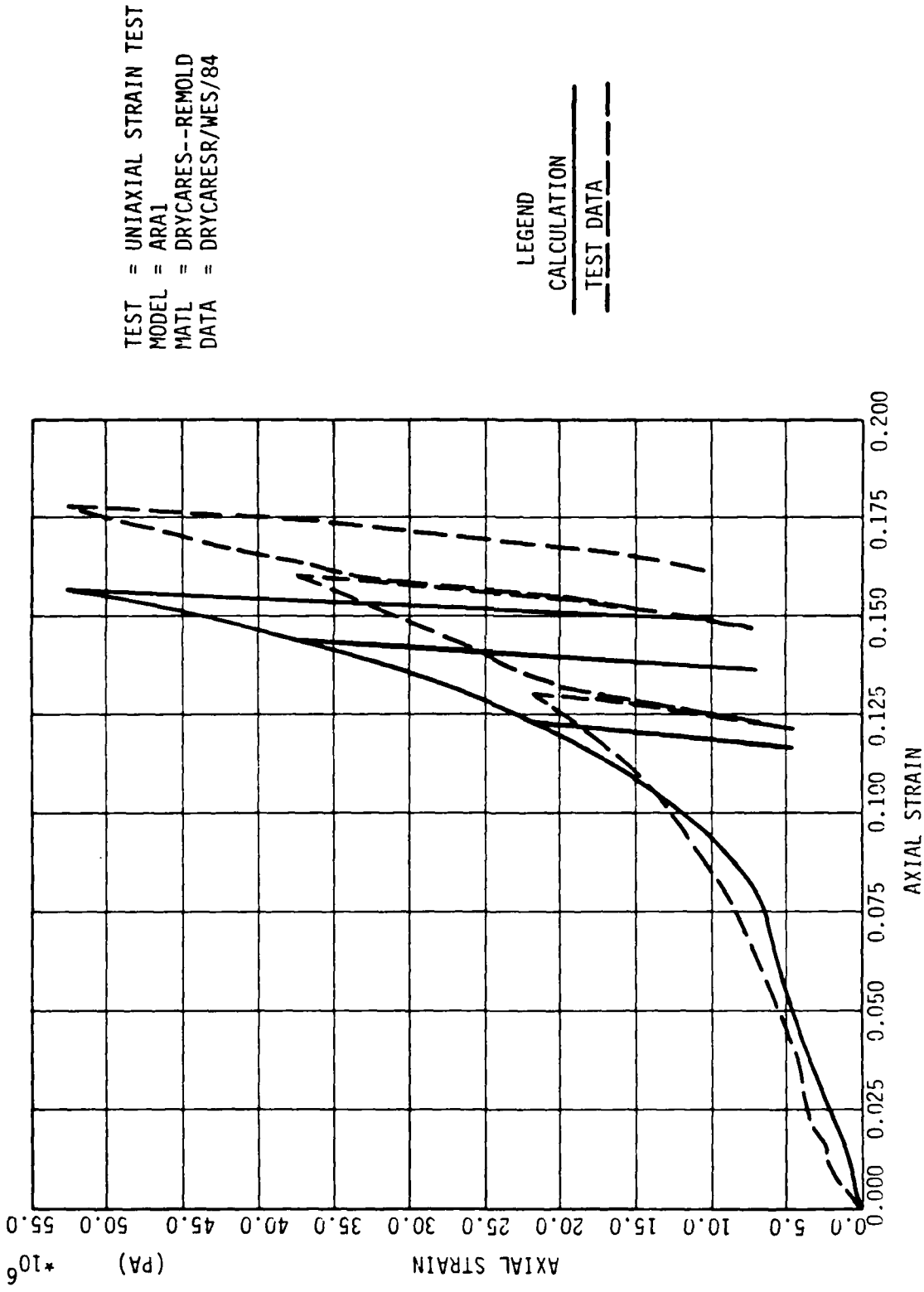
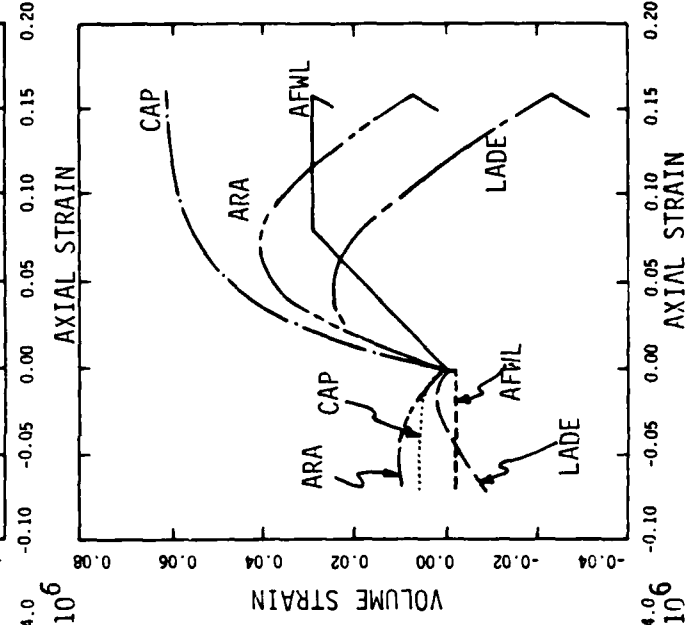
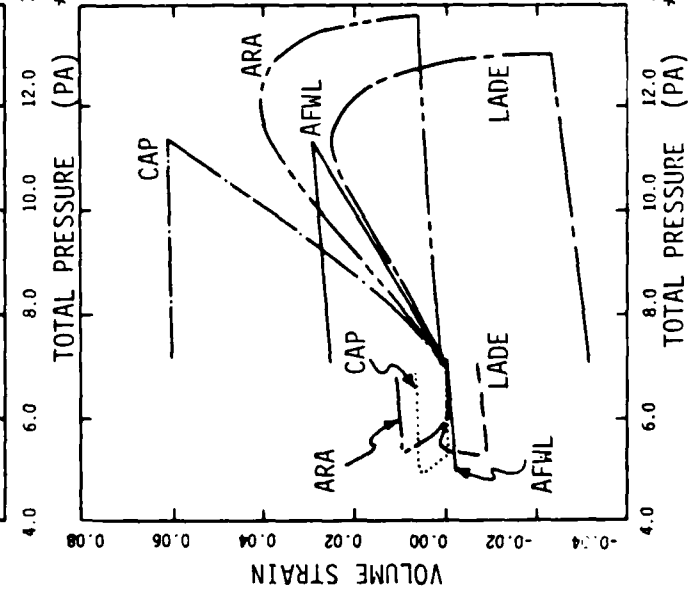
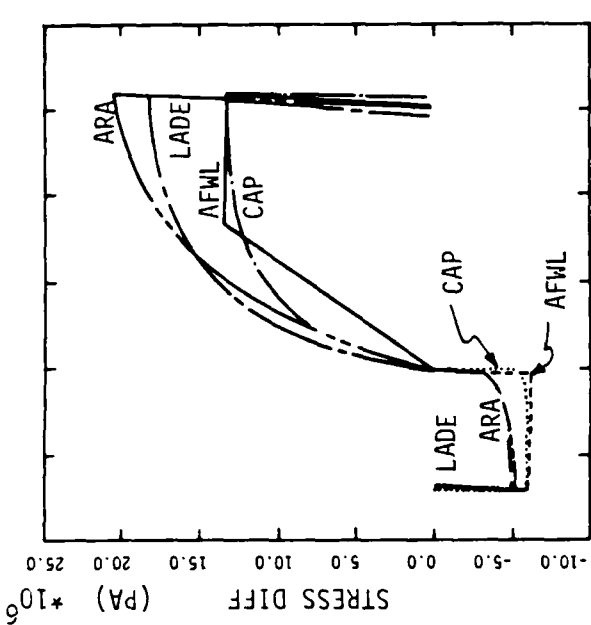
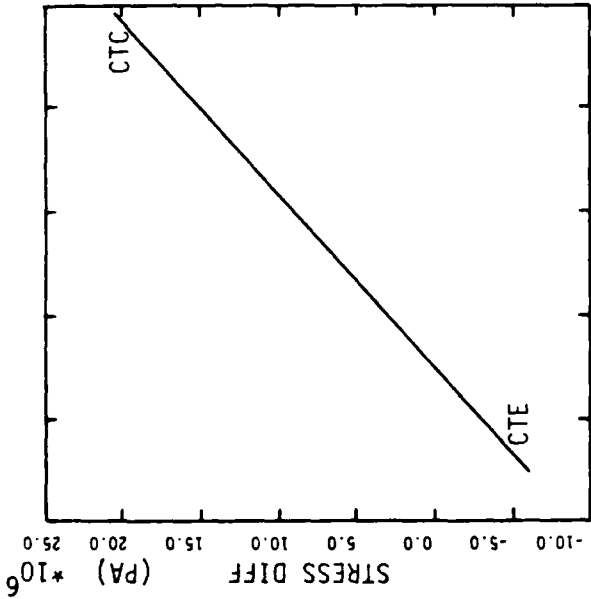


Figure 4.3. ARA Model Exercise--Uniaxial Strain (UXC)--Tot Ax1 Stress vs. Ax1 Strain



TEST = STANDARD TRIAXIAL
 MATL = DRYCARES--REMOLO

LEGEND

AFWL/CTC	---
AFWL/CTE	---
CAP/CTC	---
CAP/CTE	---
LADE/CTC	---
LADE/CTE	---
ARA/CTC	---
ARA/CTE	---

Figure 4.4. Model Comparison--Const S3C=7MPA TRIAX--SDIFF/P/EV/EA ANALYSIS

TEST = STANDARD TRIAXIAL
 MATL = DRYCARES--REMOULD

LEGEND

AFWL/RTC	_____
AFWL/RTE	-----
CAP/RTC	_____
CAP/RTE	-----
LADE/RTC	_____
LADE/RTE	-----
ARA/RTC	_____
ARA/RTE	-----

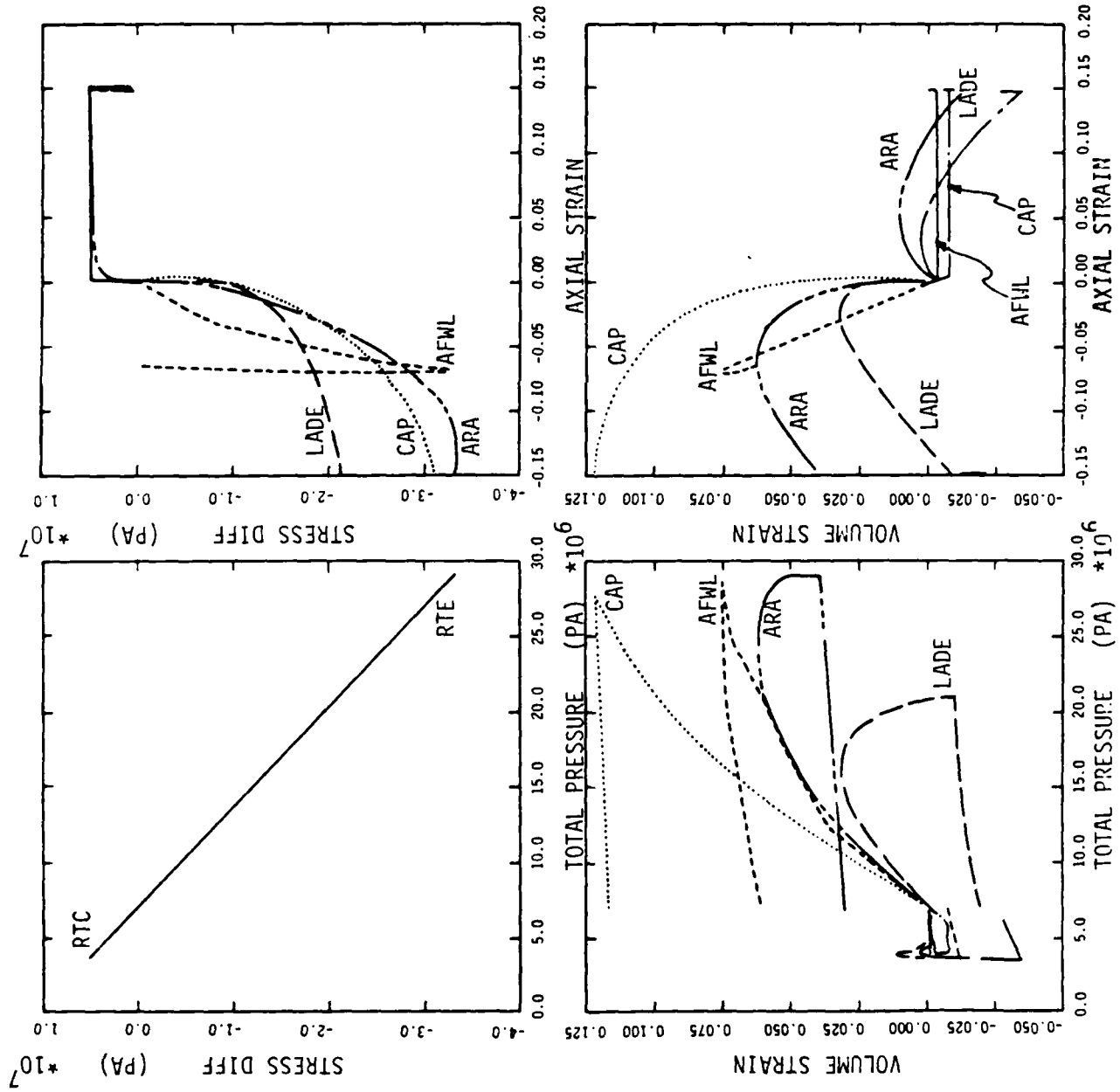
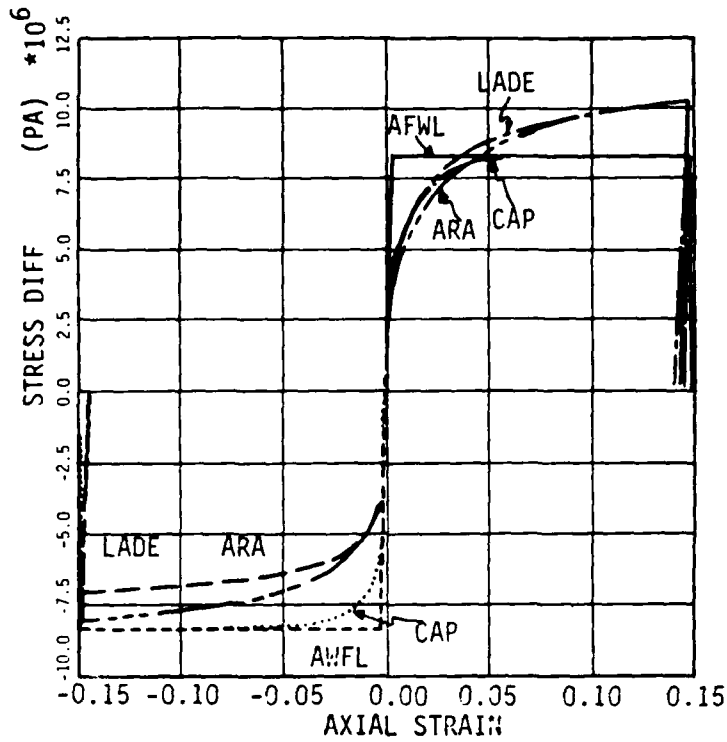


Figure 4.5. Model Comparison--RTC/E S3C=7MPA TRIAX--SDIFF/P/EV/EA ANALYSIS

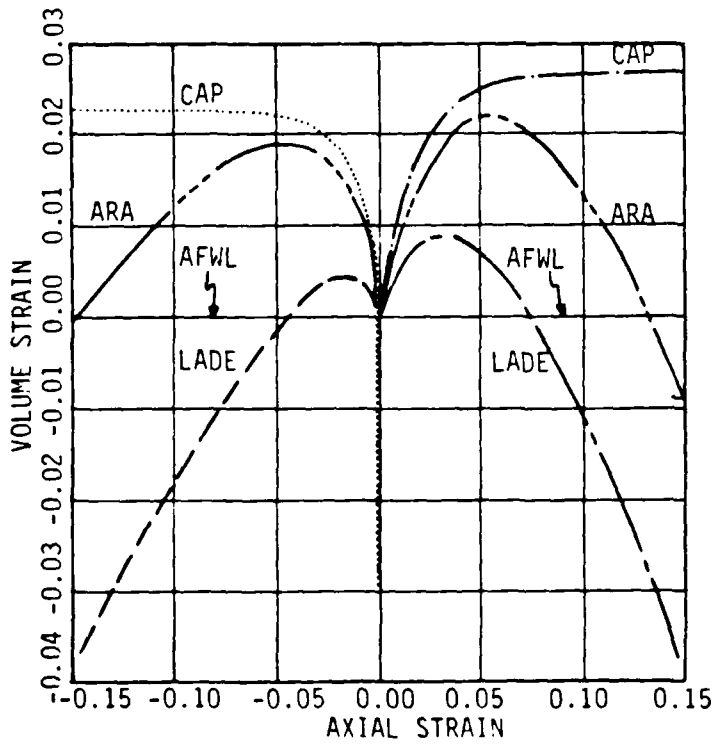
compression and extension responses. All four models show equal compression strengths, and the ARA conic model shows the highest extension strength. The ARA conic model shows the greatest volumetric compression in compression and less dilation than the Lade model, and its volumetric response in extension is midway between that of the cap and Lade models. The AFWL engineering model's extension response is peculiar and not at all similar to that of the other three models. Figure (4.6) shows the models' pure shear compression and extension responses. All four models show similar stress difference versus axial strain responses, although both the AFWL engineering and cap model curves break abruptly. The ARA conic model's volumetric response lies midway between that of the cap and Lade models, while the AFWL engineering model shows no volumetric response at all. Figure (4.7) shows the models' uniaxial compression response. Below about 15 MPa the ARA conic model shows an axial stress about midway between that of the Lade and cap models, and very close to the AFWL engineering model. At 50 MPa the ARA model shows the highest axial stress. The ARA stress path is similar in shape to that of the AFWL and cap models, while that for the Lade model is peculiarly different because of its strain softening problem. Figure (4.8) shows the models' uniaxial extension response. The ARA conic model stress path is similar to that of the Lade model, and considerably different from those of the AFWL engineering and cap models, which are virtually identical but unrealistically linear, and break abruptly. The ARA conic model is the only one which reaches zero axial stress, and in this respect its response seems more reasonable than that of the other three models. Figure (4.9) shows the models' response to WES strain path 3C. The ARA conic and AFWL



(a) STRESS DIFF VS. AXIAL STRAIN

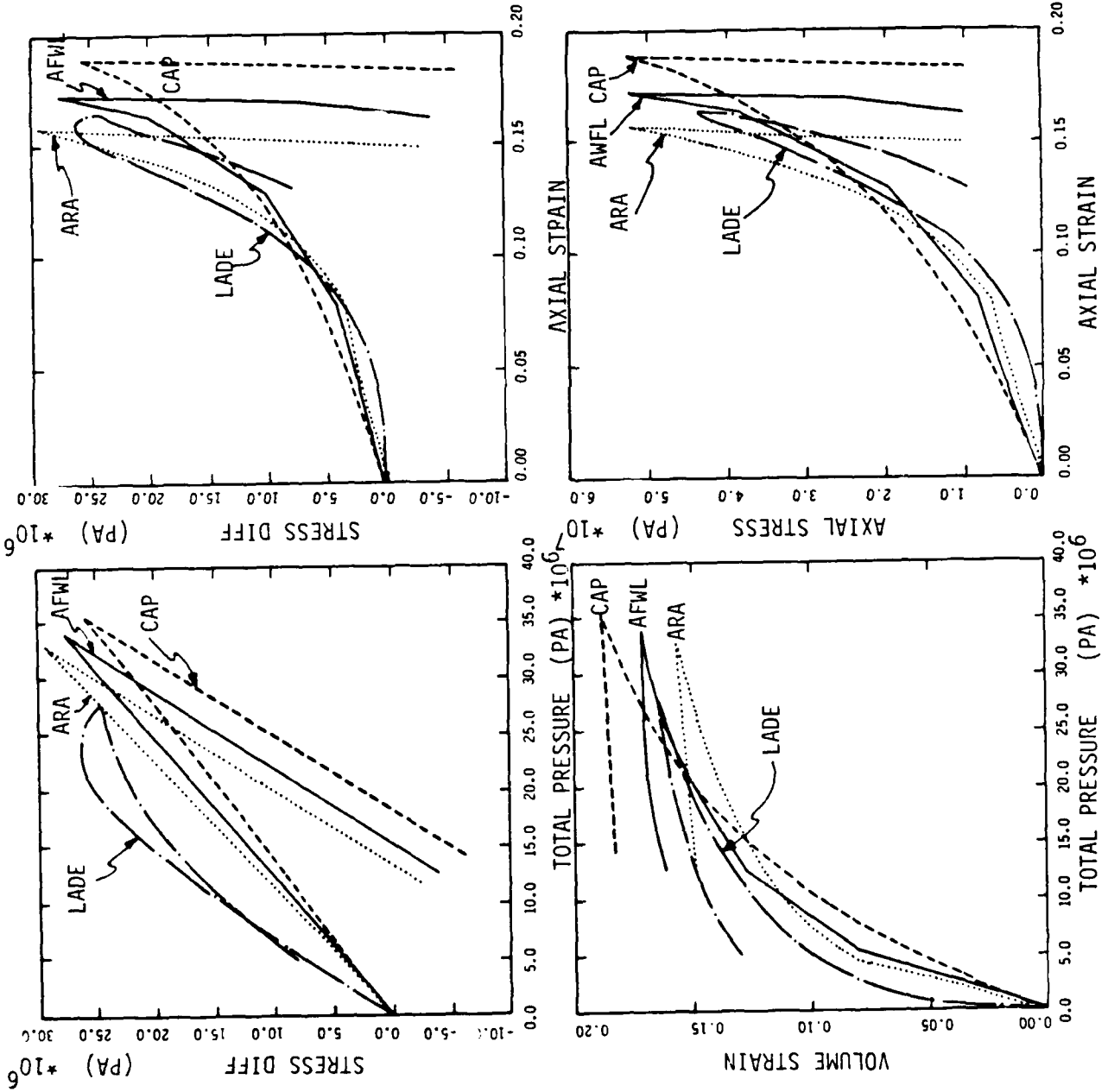
LEGEND

AFWL/PSC
AFWL/PSE
CAP/PSC
CAP/PSE
LADE/PSC
LADE/PSE
ARA/PSC
ARA/PSE



(b) AXIAL STRAIN VS. VOLUMETRIC STRAIN

Figure 4.6. Model Comparison--Pure Shear (SC3=7MPA)



TEST = UNIAXIAL STRAIN
 MATL = DRYCARES--REMOLD

LEGEND

- AFWL MODEL
- CAP MODEL
- LADE MODEL
- ARA MODEL

Figure 4.7. Model Comparison--Uniaxial Strain Compression--SDIFF/P/EV/E11/S11 ANALYSIS

TEST = UNIAXIAL STRAIN
 MATL = DRYCARES--REMOLD

LEGEND
 AFWL MODEL
 CAP MODEL
 LADE MODEL
 ARA MODEL

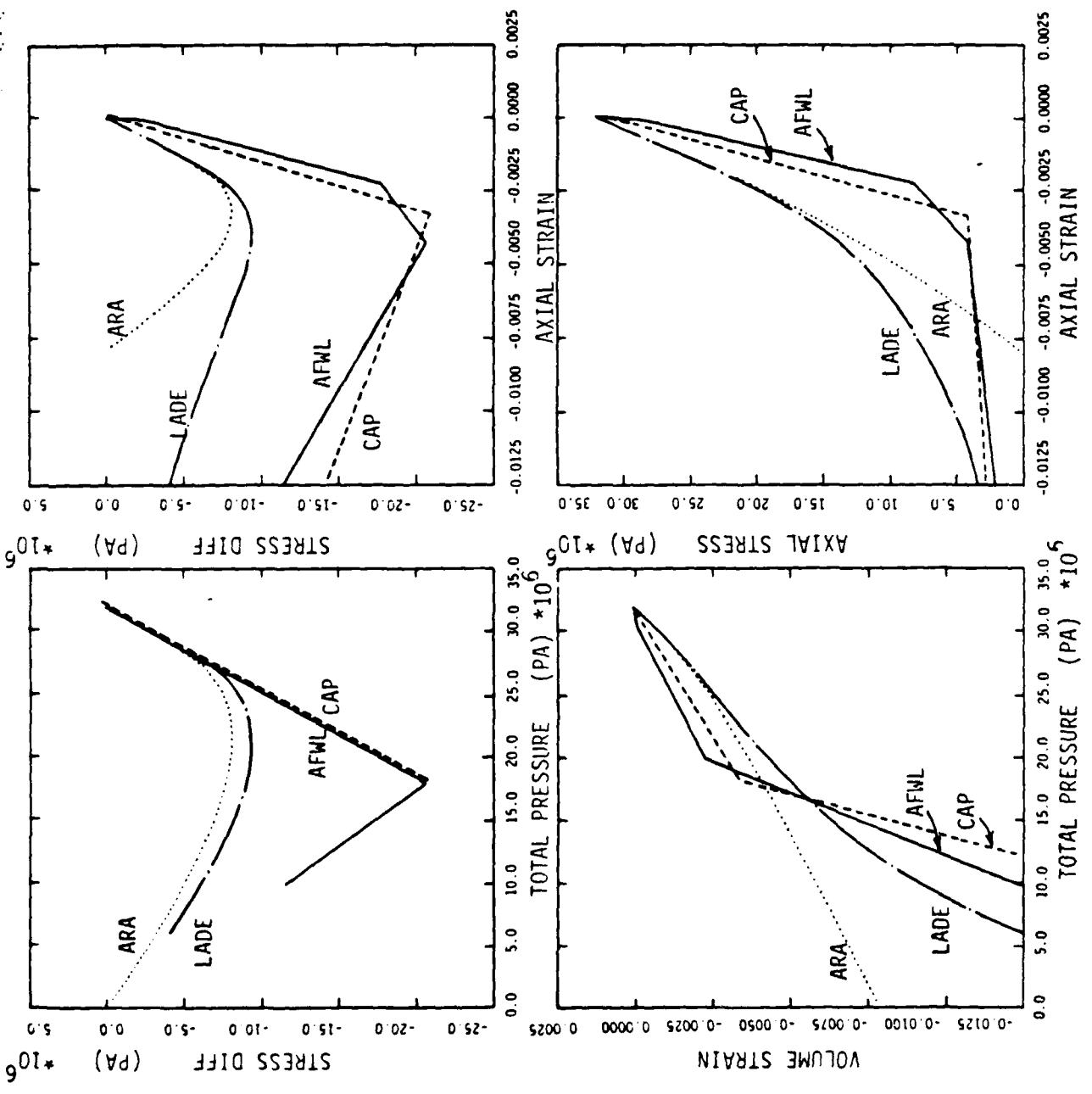


Figure 4.8. Model Comparison--Uniaxial Strain Extension--SDIFF/P/EV/C11/S11 ANALYSIS

TEST = STRAIN PATH
 MATL = DRYCARES--REMOLD

LEGEND
 AFWL MODEL
 CAP MODEL
 LADE MODEL
 ARA MODEL

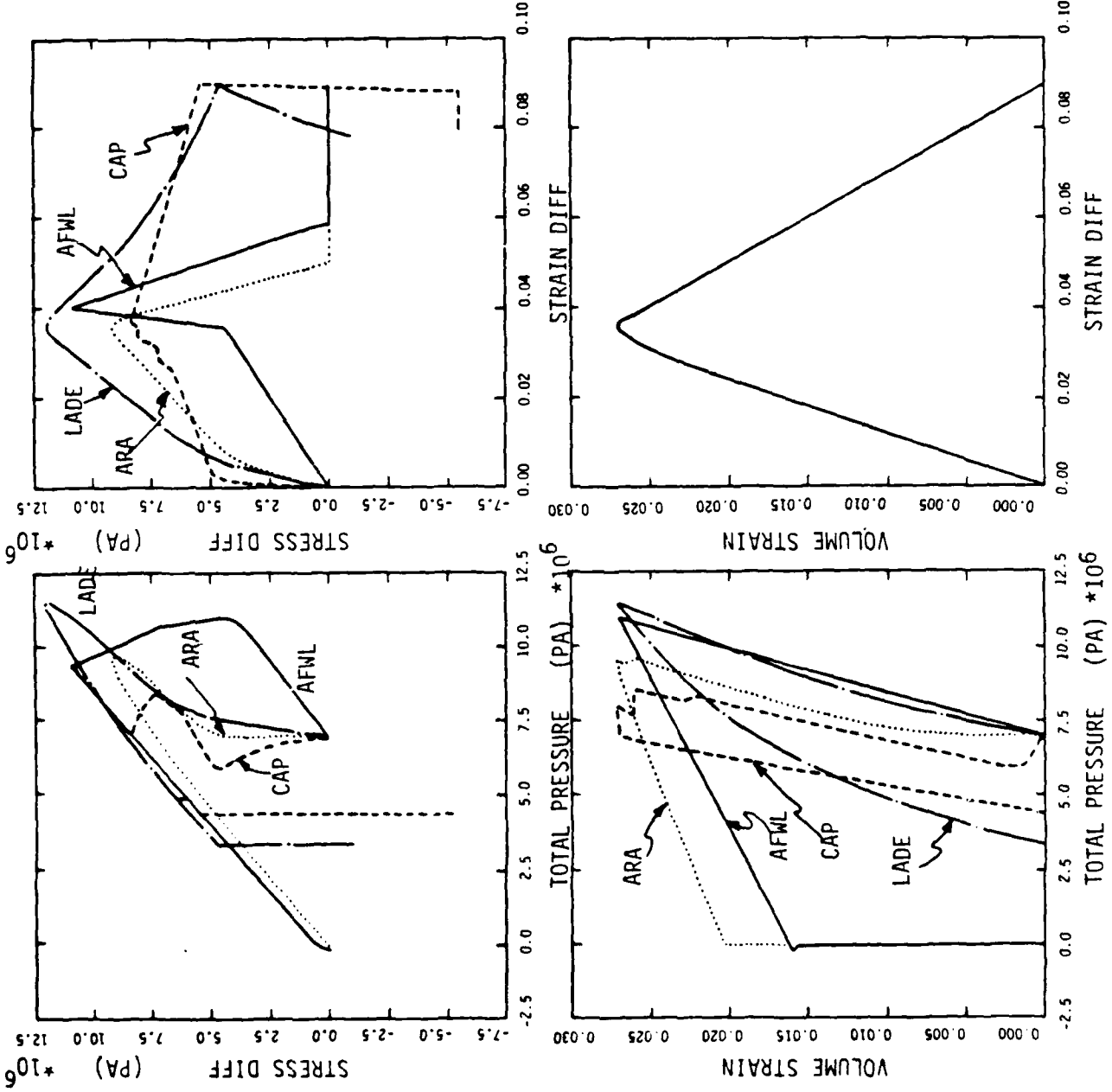


Figure 4.9. Model Comparison--WES AXISYM EPATH3C--SDIFF/EV/EDIFF ANALYSIS

engineering model stress paths follow the failure surface back to the origin, but the cap and Lade model stress paths do not, and neither does the measured stress path shown in Figure (W.43). The cap and Lade models clearly give the best response for this strain path because the stress difference for the ARA conic and AFWL engineering models decreases too sharply with axial strain after the onset of dilation. Figures (4.10) and (4.11) show the models' stress path and volumetric responses along the true triaxial strain path shown in Figure (2.13). The ARA conic and AFWL engineering models both match the measured σ_{22} versus σ_{33} stress path well, while the cap and Lade models do not. The ARA conic model shows good to excellent agreement with the measured σ_{11} versus σ_{33} stress path shown in Figure (W.46), the AFWL engineering model shows fair agreement, and the other two models show poor agreement. The ARA conic model shows good agreement with the measured volumetric response shown in Figure (W.47), while the other models show fair to poor agreement.

Overall, of the four models considered (AFWL engineering, cap, Lade, and ARA conic), the ARA conic model shows the best agreement with measured stress-strain data, for a wide range of simple and complex stress and strain paths.

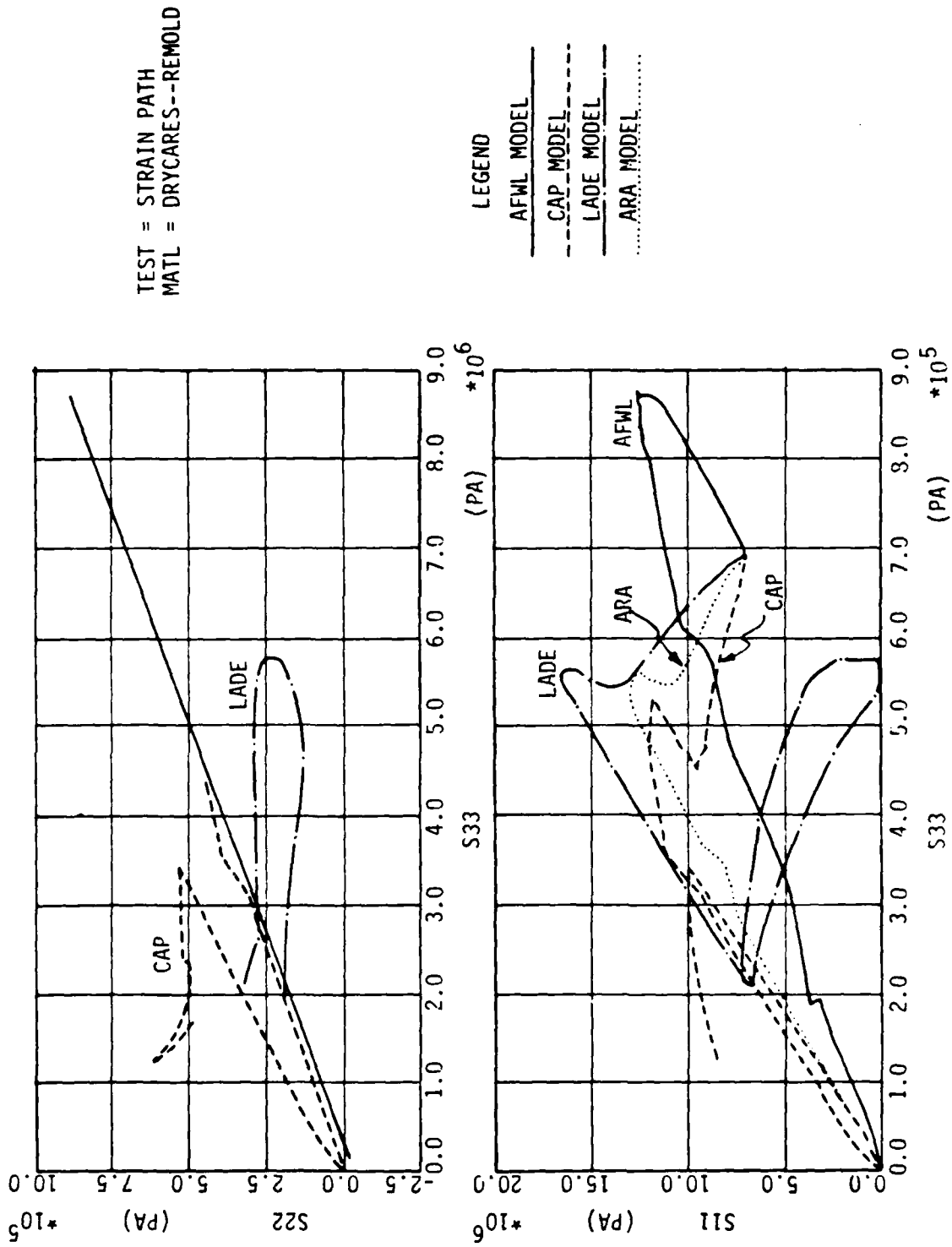


Figure 4.10. Model Comparison--True Triaxial Strain Path--Principal Stress Path

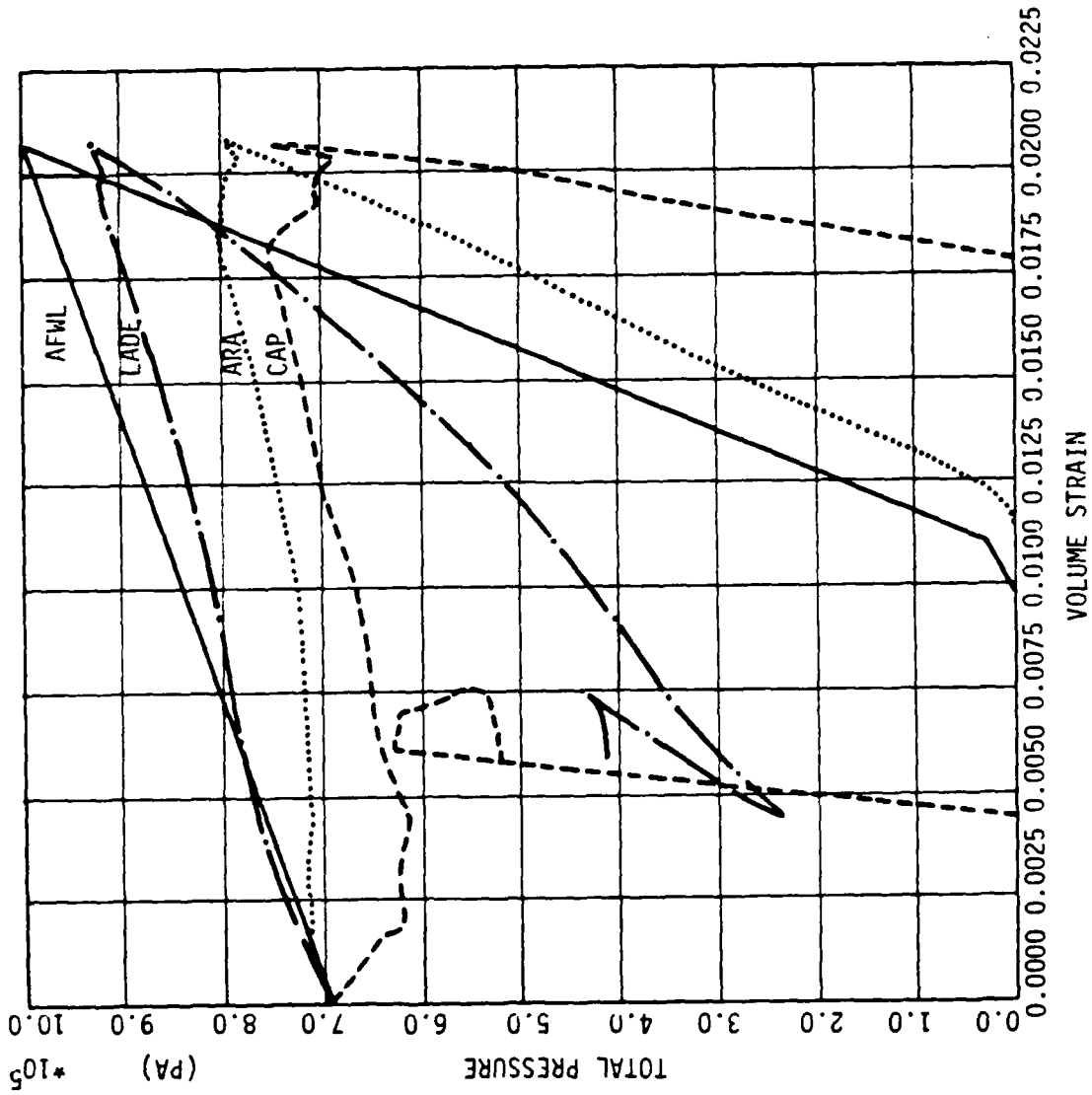


Figure 4.11. Model Comparison--True Triaxial Strain Path--Pressure vs. Volumetric Strain

5.0 SUMMARY

As stated in the Introduction, the objective of the research reported herein was to develop a general soil stress-strain model which can be used to solve a wide range of soil dynamics problems of interest to the Air Force. Requirements of a useful soil constitutive model are categorized in Section 1, and discussed in detail in Section 2. Eight existing models were studied:

- a) Linear elastic
- b) Linear viscoelastic
- c) Hyperbolic
- d) Pyke cyclic simple shear
- e) Elastic-perfectly plastic
- f) Modified AFWL engineering
- g) Effective stress cap
- h) Lade

For each model, five attributes were examined:

- a) motivation
- b) assumptions
- c) basic equations
- d) parameter determination
- e) computed behavior

Each model was exercised, insofar as possible, under the following eleven conditions:

- a) isotropic compression
- b) triaxial compression at constant cell pressure
- c) triaxial extension at constant cell pressure

- d) triaxial compression at constant axial stress
- e) triaxial extension at constant axial stress
- f) triaxial compression at constant mean normal stress
- g) triaxial extension at constant mean normal stress
- h) constrained compression
- i) constrained extension
- j) axisymmetric strain path
- k) true triaxial strain path

Each of the eight existing soil constitutive models was evaluated individually and the results summarized in Table 3.1. A comparative evaluation of stress-strain response was also performed and the results reported in Section 3. Based on both evaluations the Lade model was selected as the best point of departure for developing an improved model. The new model is called the ARA conic model because all its principal surfaces in stress space happen to be conic sections. It is also called a three invariant model because its shear yield surface depends on three independent stress invariants. The ARA conic model was also examined with respect to the above same five attributes, and exercised under the above same eleven stress and strain path conditions. The computer code used to exercise all nine soil constitutive models under all eleven stress and strain path conditions is called the Soil Element Model (SEM). It can be incorporated in large finite difference or finite element codes for analyzing the response of soil masses to complex dynamic loads.

The principal conclusions of this study are:

a) Ease of model parameter determination, without help from the model originator other than published instructions, is a paramount model attribute. If a model cannot be easily understood, and is not convenient to use it will not win wide acceptance.

b) The intermediate principal effective stress can have a significant effect on soil shear strength. Of the nine models studied, only the ARA model has sufficient flexibility to match measured strength values in triaxial compression and extension.

c) Shear deformation often has a strong influence on the relation between mean normal stress and volumetric strain, and can cause the volumetric strain at a given mean normal stress to be greater or less than that obtained in an isotropic compression test. None of the nine models studied deals with this problem in an entirely satisfactory way, but the ARA model does the best job.

d) The thermodynamic requirement that plastic deformation dissipate energy rather than create it must be enforced as a separate condition. Neither the yield criterion nor the flow rule, even for an associative material, guarantees plastic energy dissipation. Fortunately, enforcement of the dissipation condition leads to convenient uniqueness criteria for dual yield surface elastoplastic models under strain control.

e) Strain softening under strain control is an observed fact, but can lead to theoretical difficulties. A strain softening formulation is needed which matches peak stress, strain at peak stress, and the ratio of ultimate stress to peak stress.

f) Keeping the stress point inside the yield surface(s) is an important numerical problem. If overlooked, erratic and unrealistic computed behavior can result.

g) Of the nine models evaluated, the ARA conic model shows the best overall agreement with measured stress-strain response for a wide range of simple and complex stress and strain paths.

h) Of the nine models evaluated, only the ARA model rates favorably with respect to all ten evaluation criteria in Table 3.1.

i) The ARA model should now be thoroughly checked out in a continuum code, so that it can be used with confidence to predict soil mass response under a wide range of complex dynamic loads. That work is currently under way.

REFERENCES

- Akers, S.A., "Axisymmetric Strain Path Tests on CARES-DRY Clayey Sand," U.S. Army Waterways Experiment Station report (in preparation, 1985).
- Akers, S.A., "Axisymmetric Strain Path Tests on Nellis Baseline Sand," U.S. Army Waterways Experiment Station report, (Oct. 1983).
- Baladi, G.Y. and S.A. Akers, "Constitutive Properties and Material Model Development for Marine Sediments in Support of the Subseabed Disposal Program," U.S. Army Waterways Experiment Station report to Sandia National Laboratories, (Mar. 1981).
- Bell, J.M., "Stress Strain Characteristics of Cohesionless Granular Materials Subjected to Statically Applied Homogeneous Loads in an Open Stress System," Ph.D. Thesis, Cal Tech., (1965).
- Bland, D.R., THE THEORY OF LINEAR VISCOELASTICITY, Pergamon Press, (1960).
- Cargile, J.D., "Geotechnical Investigation for the CARES-DRY Site: Laboratory Test Results," U.S. Army Waterways Experiment Station report, (Feb. 1984).
- Casagrande, A., "Characteristics of Cohesionless Soils Affecting the Stability of Slopes and Earth Fills," JOURNAL OF THE BOSTON SOCIETY OF CIVIL ENGINEERS, Vol. 23, (Jan. 1936), pp. 13-32; reprinted in CONTRIBUTIONS TO SOIL MECHANICS 1925-1940, BSCE, (1940), pp. 257-276.
- Dass, W.C., J.L. Bratton and C.J. Higgins, "Fundamental Properties of Soils for Complex Dynamic Loadings," Applied Research Associates report to the Air Force Office of Scientific Research, AFOSR-TR-82-0101, ADA 111901 (30 Sep. 1981), 166 pp.
- Dass, W.C., D.H. Merkle and J.L. Bratton, "Fundamental Properties of Soils for Complex Dynamic Loadings: Dynamic Constitutive Modeling of Sandy Soils," Annual Technical Report No. 2, Applied Research Associates report to the Air Force Office of Scientific Research, AFOSR-TR-83-0653, ADA 131284, (Apr. 1983), 107 pp.
- Desai, C.S. and J.F. Abel, INTRODUCTION TO THE FINITE ELEMENT METHOD, A NUMERICAL METHOD FOR ENGINEERING ANALYSIS, Van Nostrand Reinhold, (1972).
- DiMaggio, F.L. and I.S. Sandler, "A Material Model for Granular Soils," ASCE PROC., Vol. 97, No. 3, (Jun. 1971), pp. 935-950.
- Duncan, J.M. and C.Y. Chang, "Nonlinear Analysis of Stress and Strain in Soils," ASCE PROC., Vol. 96, No. SM5, (Sep. 1970), pp. 1629-1653; disc. Vol. 97, No. SM4, (Apr. 1971), pp. 702-704; Vol. 97, No. SM5, (May 1971), pp. 815-820; Vol. 97, No. SM7, (Jul. 1971), pp. 1037-1038; errata Vol. 97, No. SM11, (Nov. 1971), p. 1597; closure Vol. 98, No. SM5, (May 1971). pp. 495-498.

REFERENCES (continued)

- Ehrgott, J.Q., "Calculation of Stress and Strain from Triaxial Test Data on Undrained Soil Specimens," U.S. Army Waterways Experiment Station Miscellaneous Paper S-71-9, (May 1971).
- Fung, Y.C., FOUNDATIONS OF SOLID MECHANICS, Prentice-Hall, (1965).
- Green, G.E. and A.W. Bishop, "A Note on the Strength of Sand Under Generalized Strain Conditions," GEOTECHNIQUE, Vol. 19, No. 1, (Mar. 1969), pp. 144-149.
- Gregory, M.S., "The Use of Measured Strains to Obtain Critical Loads," CIVIL ENGINEERING AND PUBLIC WORKS REVIEW, Vol. 55, No. 642, (Jan. 1960), pp. 80-82.
- Gregory, M.S., "The Use of the Southwell Plot on Strains to Determine the Failure Load of a Lattice Girder When Lateral Buckling Occurs," AUSTRALIAN JOURNAL OF APPLIED SCIENCE, Vol. 10, No. 4, (Dec. 1959), pp. 371-376.
- Hart, R. D., "A Fully Coupled Thermo-Mechanical-Fluid Flow Model for Nonlinear Geologic Systems," Ph.D. thesis, University of Minnesota, (1981).
- Janbu, N., "Soil Compressibility as Determined by Oedometer and Triaxial Tests," PROC. EUROPEAN CONF. ON SOIL MECHANICS AND FOUNDATION ENGINEERING, (Wiesbaden, Germany, 1963), Vol. I, pp. 19-25.
- Ko, H.Y. and R.W. Meier, "Cubical Test Data and Strain Path Testing on Nellis Baseline Sand," University of Colorado report, (Jan. 1983).
- Kondner, R.L., "Hyperbolic Stress-Strain Response: Cohesive Soils," ASCE PROC. Vol. 89, No. SM1, (Feb. 1963), pp. 115-143.
- Kondner, R.L. and R.J. Krizek, "Correlation of Load Bearing Tests on Soils," HRB PROC., Vol. 41, (1962), pp. 557-590.
- Kondner, R.L. and J.S. Zelasko, "A Hyperbolic Stress-Strain Formulation for Sands," PROC. OF THE 2ND PAN AMERICAN CONFERENCE ON SOIL MECHANICS AND FOUNDATION ENGINEERING, (Brazil, Jul. 1963), Vol. I, pp. 289-324.
- Kondner, R.L. and J.S. Zelasko, "Void Ratio Effects on the Hyperbolic Stress-Strain Response of a Sand," in ASTM STP 361, LABORATORY SHEAR TESTING OF SOILS, (1964), pp. 250-257.
- Kulhawy, F.H., telephone conversation with D.H. Merkle, (19 Sep. 1984).
- Kulhawy, F.H., J.M. Duncan, and H.B. Seed, "Finite Element Analysis of Stresses and Movements in Embankments During Construction," University of California at Berkeley report to the U.S. Army Waterways Experiment Station 5-69-8, (Nov. 1969).

REFERENCES (continued)

- Lade, P.V., "Strain Path Tests on Yuma Soil," report to Applied Theory, Inc., (Oct. 1983).
- Lade, P.V. and R.B. Nelson, "Incrementalization Procedure for Elasto-Plastic Constitutive Model With Multiple, Simultaneous Yield Surfaces," in IMPLEMENTATION OF COMPUTER PROCEDURES AND STRESS-STRAIN LAWS IN GEOTECHNICAL ENGINEERING, edited by C.S. Desai and S.K. Saxena, Vol. II, Acorn Press, (Durham, NC, Aug. 1981), pp. 503-518.
- Lambe, T.W. and R.V. Whitman, SOIL MECHANICS, Wiley, (1969).
- Lee, E.L., H.C. Hornig and J.W. Kury, "Adiabatic Expansion of High Explosive Detonation Products," Lawrence Radiation Laboratory Report UCRL-50422, (May 1968).
- Merkle, D.H., "Influence of σ_2 on Soil Shear Strength," in ENGINEERING MECHANICS IN CIVIL ENGINEERING, edited by A.P. Boresi and K.P. Chong, ASCE, (1984), Vol. 2, pp. 1296-1299.
- Merkle, D.H., "The Effective Stress Mechanics of Undrained Shear Strength," Ph.D. thesis, MIT, (1971); published as Air Force Weapons Laboratory report AFWL-TR-71-85, (Jul. 1971), 802 pp.
- Merkle, D.H. and W.C. Dass, "Fundamental Properties of Soils for Complex Dynamic Loadings: Dynamic Constitutive Model Fundamentals," Annual Technical Report No. 3, Applied Research Associates report to the Air Force Office of Scientific Research, AFOSR-TR-84-0166, ADA 139358, (Dec. 1983), 117 pp.
- Nadai, A., THEORY OF FLOW AND FRACTURE OF SOLIDS, Vol. I, 2nd Edition, McGraw-Hill, (1950).
- Nelson, I., M.L. Baron and I. Sandler, "Mathematical Models for Geological Materials for Wave-Propagation Studies," Chapter 13 in SHOCK WAVES AND THE MECHANICAL PROPERTIES OF SOLIDS, edited by J.J. Burke and V. Weiss, Syracuse University Press, (1971), pp. 289-351; now available from Plenum Publishing Corp.
- Pyke, R.M., "Nonlinear Soil Models for Irregular Cyclic Loadings," ASCE PROC., Vol. 105, No. GT6, (Jun, 1979), pp. 715-726.
- Running, T.R., EMPIRICAL FORMULAS, No. 19 in the MATHEMATICAL MONOGRAPHS series edited by M. Merriman and R.S. Woodward, Wiley, (1917).
- Saxelby, F.R., A COURSE IN PRACTICAL MATHEMATICS, 5th Edition, Longman's Green, (London, 1913).
- Sokolnikoff, I.S. and R.M. Redheffer, MATHEMATICS OF PHYSICS AND MODERN ENGINEERING, 2nd Edition, McGraw-Hill, (1966).

REFERENCES (concluded)

Southwell, R.V., AN INTRODUCTION TO THE THEORY OF ELASTICITY, Oxford University Press, (1936); reprinted by Dover (1969).

Southwell, R.V., "On the Analysis of Experimental Observations in Problems of Elastic Stability," PROC. ROY. SOC., Series A, Vol. 135, No. A828, (1 Apr. 1932), pp. 601-616.

Terzaghi, K., THEORETICAL SOIL MECHANICS, Wiley, (1943).

Timoshenko, S.P., STRENGTH OF MATERIALS, Part II, ADVANCED THEORY AND PROBLEMS, 3rd Edition, (1956).

Timoshenko, S.P. and J.M. Gere, THEORY OF ELASTIC STABILITY, 2nd Edition, McGraw-Hill, (1961).

Timoshenko, S.P. and J.N. Goodier, THEORY OF ELASTICITY, 3rd Edition, McGraw-Hill, (1970).

Uspensky, J.V., THEORY OF EQUATIONS, McGraw-Hill, (1948).